Composite bone cements based on PMMA loaded with a ferrimagnetic bioactive glass-ceramic for the treatment of bone tumour

POLITECNICO DI TORINO

PhD in Biomedical Engineering- Cycle XXXVII°

PhD Thesis

Composite bone cements based on PMMA loaded with a ferrimagnetic bioactive glass-ceramic for the treatment of bone tumour

Matteo Bruno

Tutor

prof. Enrica Vernè

Co-tutor

prof. Roberto Gerbaldo

Phd Coordinator

prof. Cristina Bignardi

Febbraio 2015

Ringraziamenti

Vorrei ringraziare tutte le persone che mi hanno seguito e aiutato nell'attività sperimentale e nella stesura di questo elaborato.

In particolare la Prof.ssa Enrica Vernè per aver coordinato l' intero progetto di ricerca , l'Ing. Marta Miola per il supporto nell'attività sperimentale in laboratorio , il gruppo di ricerca del Prof. Roberto Gerbaldo e della Prof.ssa Lia Rimondini che hanno collaborato nella caratterizzazione del materiale non solo sotto l'aspetto ingegneristico ma anche fisico e biologico.

Summary

Chapter 1

Bone tumor and hyperthermia treatment

Introduction

Before the presentation of the problem, it is very useful to remember that human body is made up of various organ systems such as: musculoskeletal system (bones and muscles), respiratory system (lungs), cardiovascular system (heart and blood vessels), gastrointestinal system, integumentary system (skin), nervous system (brain, spinal cord and nerves) and urinary system (kidneys, bladder). Each system is made up of individual organs that function together to ensure that the total system works. Each organ is built up of tissues such as muscle, nerves, connective tissue, bone, epithelial tissue. Each individual tissue is made up of specific types of cells. The cell is the smallest building block of the body. The body is made up of billions of cells. The cell contains genetic material in its nucleus that determines the function and characteristics of the cell and therefore of the all body . The genetic material order the cell when to grow, divide and replicate. As cells age, they eventually die and are replaced by other cells that divide to replenish the aging cells. It may happen that an alteration occurs in a cell's genetic material or some other alteration occurs in the cell and it begins to grow, divide and replicate itself, uncontrollably. The body's immune system may detect this and destroy the abnormal cells. If the body does not detect this abnormality, then the cell continues to divide and form a tumor.[1]

1.1. Bone tumor classification

Tumors can be classified as benign or malignant. Depending upon the type of cell that the tumor is derived from, a malignant tumor can be classified as a sarcoma or a carcinoma. Malignant tumors can also be considered primary or secondary. In terms of bone tumors, a primary bone tumor arises directly from a particular bone. Secondary bone tumors are tumors that involve the bone but they originates from a cancer in another part of the body. Primary malignant bone tumors are sarcomas. Secondary bone tumors are called metastatic bone tumors or metastatic bone cancers and most are carcinomas that have traveled from other primary tumors such as breast cancer, lung cancer, prostate cancer, kidney cancer, thyroid cancer and gastrointestinal cancer. For instance, breast cancer that spreads to the bone; the breast cancer is the primary cancer and the breast cancer that is in the bone is a secondary cancer or a metastatic cancer.[1]
In table 1.1 , there is a bone tumor classification divided in benign and malignant pathology.

Category	Benign	Malignant
Osseous	Osteoma Osteoid Osteoma Osteoblastoma	Osteosarcoma
Cartilaginous	Enchondroma Osteochondroma Chondroblastoma Chondromyxofibroma	Chondrosarcoma
Fibrous	Fibrous dysplasia Fibrocartilaginous Dysplasia Histiocytoma Osteofibrous Dysplasia Fibroma Benign Fibrous Desmoplastic Fibroma	Fibrosarcoma Malignant Fibrous Histiocytoma
Small Round Blue Cell	Eosinophilic Granuloma Infection	Ewing's Sarcoma/PNET Lymphoma Multiple Myeloma
Giant Cell	Giant Cell Tumor	

Table 1.1: Classifications of bone tumors[1]

Bone tumor generally refers to any abnormal growth from bone or in the bone. It can be a primary malignant tumor like an osteosarcoma, Ewing's sarcoma or chondrosarcoma. It can also be a metastatic carcinoma such as a breast cancer, lung cancer, prostate cancer, kidney cancer and thyroid cancer. It is important to differentiate between the various types of cancers that affect the bone because each has its own type of treatment and care. [1]

Sarcomas and carcinomas are two different types of malignant tumors that can affect bones. They are derived from different cells. Sarcomas are derived from mesodermal (mesenchymal cells) and carcinomas are derived from epithelial types of cells. Sarcomas and carcinomas grow and spread differently.[2]

1.1.1. Sarcoma

Sarcomas grow like "ball-like" masses and tend to push adjacent structures like arteries, nerves, veins away. They compress adjacent muscles into a pseudocapsule that contains microscopic projections of the tumor referred to as satellite nodules. The local growth of sarcomas like a ball enables resection in most instances. Sarcomas tend to arise primarily (directly) from bone. Sarcomas rarely spread to lymph nodes. It is derived from a particular type of cell referred to as a pluripotential mesenchymal cell. Under normal situations, mesenchymal cells in the body form bones, muscles, cartilage, connective tissue, blood vessels, blood cells, and nerves. Pluripotential means that cell has the ability to differentiate or grow along different pathways and form these various types of tissues. Under cancerous conditions, the mesenchymal cells that form a sarcoma can grow along a specific pathway and form tissue that looks like bone, cartilage, muscle, connective tissue, blood vessels as presented in table 1.1. Thus, it can have a bone sarcoma (malignant tumor of bone made up of mesenchymal cells) that is actually producing bone. The name given to this type of tumor is osteosarcoma (osteo means bone; thus osteosarcoma is a bone forming sarcoma). A patient can have a malignant bone tumor that produces cartilage. This is called a chondrosarcoma (chondro means cartilage). Malignant tumors that arise directly from bone are called sarcomas. Sarcoma is greek for "fleshy". The name was given to these types of tumors because of their appearance. They have a fleshy appearance when cut open and examined. Sarcomas are rare cancers and constitute about 1% of all cancers. [1]

1.1.2. Carcinoma

Carcinomas grow in an infiltrative manner and grow through infiltration or invasion of adjacent structures. They more easily invade adjacent nerves, blood vessels and muscles. They do not form a pseudocapsular layer and therefore it is difficult to determine its exact anatomic extent during surgery. This makes it more difficult to remove entirely with surgery. Carcinomas spread to lymph nodes, lungs, bones and many other organs depending on the type of carcinoma. Carcinomas involve bone secondarily, that is by spreading from another site such as the breast to the bone. A patient can have the primary site removed and treated (ie. the breast cancer removed) and years later develop a bone tumor/metastasis from the old breast cancer.

Carcinomas are distinctly different from sarcomas. They are derived from cells that look like epithelial cells or glandular cells. These cells do not form bone, muscle, nerve, etc. They do not

have this ability. If a carcinoma is growing from a bone, it has usually come from a primary cancer in another part of the body. It is always considered cancerous and malignant because it has spread from another body part or another cancer. Breast cancer, lung cancer, kidney cancer, prostate cancer, thyroid cancer and gastrointestinal cancer are the most common carcinomas that travel or metastasize to bone. They can result in extensive destruction of the bone and can cause the bone to break/fracture. In some areas such as the pelvis and scapula, they can form large tumors that can involve the major nerves and blood vessels to the extremities. This is a serious situation. It can lead to uncontrollable pain and loss of the arm or extremity. The tumor in the bone is the same type of tumor as the primary carcinoma. For instance, if breast cancer has spread to the bone, the tumor in the bone is exactly the same as the breast cancer under the microscope. This is considered metastatic breast cancer to the bone. Carcinomas are much common and make up the majority of the cancers that occur yearly.[1]

These large two family of cancer are characterized by similar symptoms:

1. Manifestation of pain without any traumatological event that does not decrease with the assumption of an anti-inflammatory drug. Pain in the early stages can be contained but it will gradually increase with time
2. Swelling that increases over time and in size
3. Presence of pathologic fracture occurred without trauma of the affected bone segment[2].

1.2. Primary malignant bone tumors

Primary malignant bone tumors include:

- Osteosarcoma
- Ewing's sarcoma
- Chondrosarcoma

The three main forms of primary bone sarcoma are osteosarcoma and Ewing's sarcoma, both of which primarily affect children and adolescents, and chondrosarcoma tend to affect middle-aged and elderly patients.[2]

1.2.1. Osteosarcoma

Conventional osteosarcoma usually arises in the medulla of long bones within the metaphysis, and over half are in the distal femur and proximal tibia, at the sites of greatest skeletal growth. Proximal humerus and femur and distal radius are also often involved, and no bone is exempt.

Osteosarcoma spreads between the medullary trabeculae (figure 1.1), and penetrates and partially destroys the cortex to extend beneath and elevate the periosteum.

Figure1.1 :Surgical specimen of distal femur containing an osteosarcoma which involve the medullary canal of the methaphisis [2]

Effects of preoperative chemotherapy may modify both the progression and microscopic appearances by inducing necrosis and hemorrhage. This is important in assessing the response to therapy and informs the choice of postoperative regimen.

Modern therapy combines preoperative and postoperative chemotherapy with surgery, often resection and endoprosthetic replacement or other reconstructions, rather than amputation.[2]

1.2.2. Edwing's sarcoma

In contrast to osteosarcomas, which affect the metaphyseal long bones, Ewing's sarcomas tend to arise in the diaphysis or metaphyseal– diaphyseal portion of long bones, pelvis, ribs and, rarely, in the skull, vertebrae, scapula, and short tubular bones of the hands and feet. Ewing's sarcoma can also occur in the soft tissues without bone involvement.[3]

The presenting features are of pain and swelling. Fever may suggest osteomyelitis, and tissue should be sent both for microbiology and pathology in these circumstances. The tumor arises within the medulla, both diaphysis and metaphysis, then rapidly penetrates the cortex and

periosteum to form a large soft tissue mass. Radiographs show large area of bone destruction and there is often a distinctive multilayered 'onion-skin' periosteal reaction. On microscopy, Ewing's sarcoma is the prototypic malignant round cell tumor of childhood, consisting of sheets of small round cells with uniform nuclei. [2]

The natural history of Ewing's sarcoma is of early metastases both to lung and bone and bone marrow, with a particularly outcome for patients with large tumors notably in the pelvis and with systemic symptoms. Ewing's sarcoma is best treated by a combination of intensive chemotherapy followed by local treatment, often with surgery and radiotherapy.

1.2.3. Chondrosarcoma

Unlike osteosarcoma and Ewing's sarcoma, chondrosarcoma normally affects the middle aged and elderly. It usually arises as a primary tumor, but about 10% of cases arise in relation to a pre-existing benign cartilage tumor. Chondrosarcoma may arise within the medulla as you can see in figure 1.2 or from the bone surface (peripheral). Tumor is seen both in long bones, notably the femur and humerus, and in the axial skeleton, commonly the pelvis, shoulder girdle and ribs; rarely, chondrosarcoma occurs in the distal skeleton, for example in the tubular bones of the hands and feet. Most patients present swelling or pain, the latter is a sinister symptom when associated with a cartilage tumor in an adult.

The typical central chondrosarcoma consists of sheets of cartilage, which often permeate between the cancellous trabeculae and tend to erode the bone cortex. A more aggressive tumor may penetrate the cortex to form a mass in soft tissue. Peripheral chondrosarcomas have a cartilaginous cap, with nodules of proliferating cartilage on the surface thicker than the cap of 1–2 cm seen in a benign exostosis. In both forms, radiographs often show dystrophic calcification with peripheral rings, giving a popcorn pattern. Around 15% of chondrosarcomas metastasize, usually to the lungs. Although most chondrosarcomas grow slowly they tend to recur locally unless excised widely; this is a particular problem with central tumors, for example those of the spine and base of skull, which may cause death in the absence of metastases. As chondrosarcoma responds poorly to chemotherapy or radiotherapy, adequate wide surgical excision at the first operation is the key to cure.

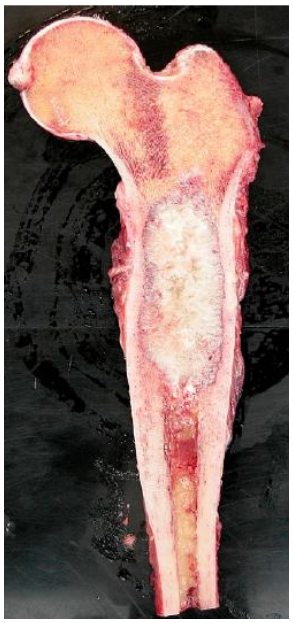

Figure 1.2: Surgical specimen of a chondrosarcoma that has arisen in the medullary cavity and is confined by the cortex.[2]

1.3. Treatment of bone tumor

The most common techniques for the treatment of primary and metastatic bone tumors are:

- Chemoterapy
- Radioterapy
- Surgical approach

The use of chemotherapy in a patient with metastatic disease can help to control the disease, and the obtained results show a partial regression and temporary symptomatic relief.

In most cases treated, tumor site and volume, age of patient are fundamental parameter for the develop of chemio-radio-surgical planification.

In the Edwing's sarcoma the introduction of systemic chemotherapy led to significant improvements in the prognosis in comparison with the prior extremely poor outcome with local therapy only [3]. In early studies, combinations of vincristine, cyclophosphamide, dactinomycin and doxorubicin resulted in survival rates of about 50% [4]. High-dose chemotherapy with busulfan/melphalan may yield benefits for patients suffering from metastasised Ewing's sarcoma compared with conventional chemotherapy.

Radiotherapy is advised only for inoperable lesions. Inoperability is defined by tumors that cannot be resected completely and in tumors of critical sites where complete surgery would result in unacceptable mutilation or is associated with a high risk of serious complications. A dose of 55 Gy

(with a shrinking-field technique after 45 Gy) is described to be a sufficient radiation dose in definitive radiotherapy.[4] However, large tumors may require higher radiation doses.

Surgery is favored if a wide or at least marginal resection is feasible. Intralesional resections should be avoided as they are associated with a higher risk of peripheral and distant relapse.

Surgery, if feasible, is generally preferred because it has resulted in better local control rates than definitive radiotherapy in many trials.[4]

The main objectives of surgical intervention are prevention of fracture, maintenance of limb function, and palliative of pain.

The most common surgical approach was the using of a fixation device in combination with polymethyl methacrylate bone cement. Lesions larger than 3 cm with loss of cortical bone should be considered for supplemental fixation with bone cement. This may be accomplished while inserting an intramedullary device or cementing around a previously placed device. With plates, it is often best to treat the lesion, fill the defect with cement, and place a neutralization plate and screws. Screws placed into a bone-and-cement composite are exceptionally stable. Antibiotic-impregnated cement has not been shown to provide additional benefit compared with regular cement. Cement impregnated with chemotherapeutic agents has been investigated, but thus far it has shown limited efficacy in terms of limiting local disease progression.[5]

The medical needs that has been satisfied concern:

- the inhibition of tumor growth,
- strengthening of bone structure,
- control and delate pain form the patient.

1.4. Bone infection

One possible complication connected to the bone tumor is infection, which can appear after tumor resection. Osteomyelitis indicates an inflammation of bone and marrow canal due to the infectious microorganism[6]. Staphylococcus aureus is among the common bacteria that causes this pathology[7].

In figure 1.3 a osteomyelitis in a young girl, as a consequence of osteosarcoma, is reported. In panel B the radiographs show a bone resorption and loosening of the prosthesisthat created conditions for the proliferation of bacteria and, consequently, the failure of the implant. The

surgeron had to remove the implant and inject antibiotic in the tibia. Due to the fact that the patient didn't response to the therapy, she underwent amputation on the upper knee.

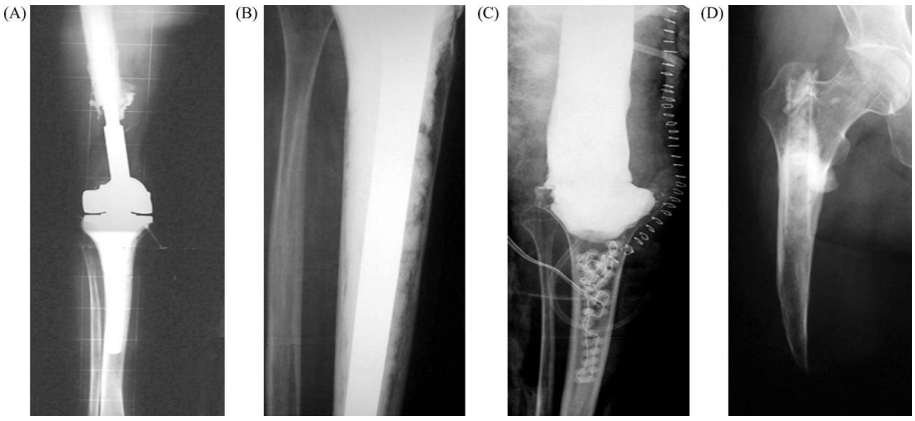

Figure 1.3: Osteomyelitis in a 19-year-old female of the right femur and prosthetic placement. Anteroposterior (A) and lateral (B) radiographs show bone resorption and loosening of the megaprosthesis. Biopsy was positive for osteomyelitis. Because of persistent infection, the megaprosthesis was removed, antibiotic pearls were inserted in the tibia (C). The patient was nonresponsive to antibiotics and subsequently had to undergo an above-the-knee amputation (D).[8]

A problem concerning the use of antibiotics in the treatment of bone infections is the difficulty of obtaining bactericidal levels of antibiotics in the infected tissues without reaching toxic systemic levels. The infected zone is filled by blood and serum which promotes bacteria growth and may lead to implant failure . Antibiotic should have an effect on bacteria without creating any collateral effects to other cells. Moreover, osteomyelitis are a nonspecific diagnosis, so they can present different approaches for the care managing. [8]

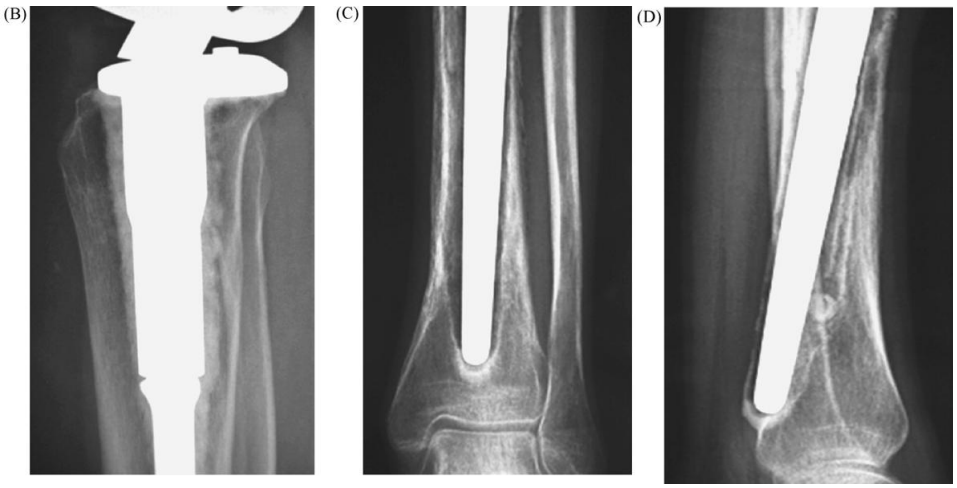

Figure 1.4: Complications of megaprostheses: in an 18-year-old female who received a megaprosthesis after resection of an osteosarcoma of the right femur. One year after resection, anterolateral (B) radiographs of tibia show extensive bone resorption consistent with aseptic loosening.[8]

Figure 1.4 reports another case study where the septic loosening caused the failure of the implant as a main consequence of bone resorption. [8]

1.5. Hyperthermia

The use of Hyperthermia as an adjunct to conventional oncology treatments has increased over the past two decades. It's a non-invasive methods for increase tumor temperature stimulating blood flow, restarting the immune system, increasing oxygenation of the tissues. It's well-tolerated by practically all patients and it's a nontoxic treatment. It works in synergy with radiotherapy increasing tumor control while minimizing damage to healthy tissue and permit the increment of radiation dose and with chemotherapy (cisplatin and related compounds, melphalan, cyclophosphamide, nitrogen mustards, anthracyclines, nitrosoureas, bleomycin, mitomycin C, and hypoxic cell sensitizers) increasing cellular uptake of drug and DNA damage and inhibition of cancer cells repair.[6]

Hyperthermia provides an increasing temperature between 40-43 °C in the tissues in order to kill malignant cells and not health one. Moreover it also sensitize cancer cells to the previous mention treatments (radiotherapy, chemotherapy, gene therapy and immunotherapy).[7]

The duration of heating and high temperature levels achieved during treatment sessions influence a lot the number of death cells. Higher the temperature and longer time that heat is delivered to the tumor site, stronger the lethal effect and less the tumoral cells will be able to develop thermo tolerance phenomena[8]. Moreover not only these parameter are useful for the control of the phenomena but even environmental and vascular conditions are very important. Damage to cancerous cells is promoted by lack of oxygen, decreased pH, absence of nutrients and poor cooling, which are caused by pathological microvasculature within the tumor.[8] In general, the mentioned conditions are not seen in normal tissues which are not seriously affected by thermal treatment. As reported in figure 1.5 the biological hyperthermia principle is based by a vasodilatation of normal blood vessel that are able to increase the blood flow in order to dissipate the overheating. While tumoral cells that composed a solid tumor are unsupplied by this mechanism due to the pathological blood vessel structure which caused the final effect of necrotic or apoptotic death. The vasculature disorder of tumoral cells and reduced blood flow favor hypoxia and acidosis. In this scenario hyperthermia will play in two different way: if the temperature applied is < 42°C the blood flow in the tumor increase in order to favors the action of

the chemotherapy while if the temperature is > 43°C the reduction of blood flow and the increase of hypoxia and acidosis lead the cancer cells in apoptosis.[7]

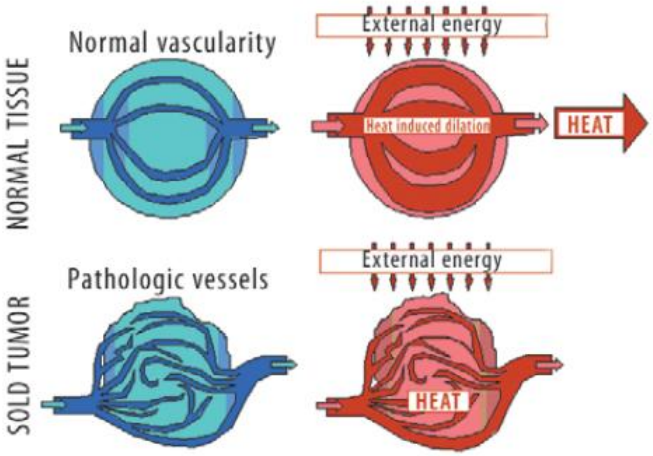

Figure 1.5: Mechanism of tumor overheating with hyperthermia technique. In normal tissue the blood vessels increase our section when physiologically or artificially heated, consequently there is an increase of blood flow through the applied region and a decrease in its temperature. In the tumor site , pathological vessel are not able to dilate in fact most of these collapse because the heat is not dissipate by the tumor vessel. [4]

1.5.1. Hyperthermia methods

Depending on the location, depth and staging of tumor, there are three main clinical methods to generate an increasing temperature in the body: local, regional or whole body hyperthermia, which deliver heat to localized, advanced or deep seated and disseminated malignancy. [5]

Local hyperthermia is applied for superficial tumors and can be achieved by external application of microwaves or radio-waves. **Interstitial hyperthermia** can be applied by inserting an applicator into the target volume and generating localized microwaves, radio waves, or ultrasonic waves.

Endo-cavity hyperthermia is done by inserting an energy-inducing applicator in a natural opening of a hollow organ. These two techniques are a subtype of local hyperthermia.[5]

Regional hyperthermia can be achieved with external heading radiofrequency, isolated limb hyperthermia, or cavity based hyperthermia. Several techniques have been used to raise temperatures in whole body hyperthermia with the aim of increasing tumor response to conventional chemotherapy (mainly in patients with metastatic disease). Temperatures of up to 42°C, maintained for 60–90 min, can be achieved using radiant heaters with long infrared rays.

Energies used to apply heat include microwaves (in the range of wavelengths from 433 MHz to 2,45 GHz), radiofrequency (ranging from 100 KHz to 150 MHz), ultrasound, hot water perfusion

(tubes, blankets), resistive wire implants. Another way to deliver heat in the tumor site concerns the use of magnetic material like ferromagnetic or magnetic nanoparticles. After the in vivo implant they can generate heat due to the stimulation with an alternate magnetic field.

1.5.2. Hyperthermia in bone tumor treatment

Taking into account the common aim of hyperthermia for the treatment of the tumors, it is important to point out that in order to apply the aforementioned techniques two methods are possible: the application of external energy using radiofrequency, microwave or ultrasounds with designed external devices or the application of an implanted magnetic materials that can provide an internal source of treatment. This type of hyper-thermic cancer therapy used magnetic material stimulated with the application of an alternate magnetic field.

Some authors proposed the use of hyperthermia for the treatment of bone tumor with an external application of ultrasounds that has the aim to deliver the optimum energy to destroy the tumor mass. The system uses a spherically arranged applicators, the specific absorption rate ratio has been used to determine the proper heating domain of ultrasound driving frequency and therapeutic tumor diameter. The model has to be tailored respect to tumor size, tumor depth, ultrasound attenuation in the bone tumor tissue, the absorption energy from the bone and the frequency of the transducer. The application of ultrasound energy for hyperthermia is excessively reflected and absorbed by bone, this modality permits for the controlled heating of superficial and deep lesions.

To deliver the ultrasound energy into the tumor site and to avoid the potential damage to the normal tissue, the specific absorption rate (SAR) in the bone tumor site has to be three times higher than that in the surface skin, tumor/marrow, and marrow/bone interfaces. The results will be very useful for the developing of a treatment planning for bone tumor with a design of ultrasound hyper-thermic applicator [8] .

Fan et al. reported treatments of bone tumor with microwave induced hyperthermia on humans instead of a common surgery that create problem of infection, necrosis and local recurrence. The surgical procedure consisted of separating the tumorous segment from surrounding normal tissues with a safe margin, cooling the normal tissues (including the vital neurovascular bundle and the intra-joint structures) with a water circulation system while heating the tumor simultaneously with the microwave antenna array. The device was composed by a microwave generator at 2,4

GHz with a power range 0 – 200 W. Thermocouples were inserted in the tumor site and in the normal tissue for the monitoring of the temperature in real time. The results confirmed the decrease probability of oncological and operative complication and functional saving of limb.[9]

Also microwave induced hyperthermia [8], laser-induced thermotherapy [10-12], and radiofrequency ablation [13] have been recently used especially for spinal and pelvic metastasis, but these therapeutic modalities are unsatisfactory for the lesions located in the long tubular bone of the limb, because pathological fractures cannot be treated without a surgical reinforcement of the bone lesion.

One more effective technique for the care of bone tumors is magnetic hyperthermia. This method uses an external magnetic field that stimulates a per-implanted magnetic material in the generation of controlled heat, normally between 41°C and 43°C, into the body's tissue destroying cancer cells [14-15]. The implanted material is able to magnetizing and produces hysteresis loss that are transformed into a controlled heat. The heating temperature depends on several factors, including materials properties, the magnetic field parameters (intensity, frequency) and bone tissue properties. [16] This technology will be the object of a following chapter.

1.6. References

1. Witting JC, Retrieved from Sarcoma Surgeon & Orthopedic Oncologist.
2. MacDuff E, Reid R, Bone tumour pathology. Surg 2008; 27 (2): 55-62.
3. Chowdhry M, Hayward K, Jeys L , Primary malignant tumours. Surg 2008; 27 (2), 80-85.
4. Chicheł A, Skowronek J, Kubaszewska M, Kanikowski M, Hyperthermia – description of a method and a review of clinical applications. Rep Pract Oncol Radiother 2007; 12(5): 267-275.
5. Bolling T, Hardes J, Dirksen U, Management of Bone Tumours in Paediatric Oncology. Clin Oncol 2013; 25: 19-26.
6. Pignochino Y, Clinical issues and in vivo models in cancer therapy, Sarcoma Unit Medical Oncoloy Division , IRCCS Candiolo Cancer Institute.
7. Quackery,Hyperthermia in cancer: is it coming of age? . Lancet Oncol 2014 ;15.
8. Bing-Yuh Lu, Yang RS , Ling WL, Cheng KS, Wang CY, Kuo TS, Theoretical study of convergent ultrasound hyperthermia for treating bone tumors. Med Eng & Phys 2000; 22: 253-263.
9. Fan Q, Ma B, Qiu X, Li Y, Ye J, Zhou Y, Preliminary Report on Treatment of Bone Tumor with Microwave-Induced Hyperthermia. Bioelectromagnet 1996; 17: 218-222.
10. Vogl TJ, Mack MG, Straub R, Eichler K, Zangos S, MR-guided laser induced thermotherapy of the infratemporal fossa and orbit in malignant chondrosarcoma via a modified technique. Cardiovasc Intervent Radiol 2001 24:432–435.
11. Groenemeyer DH, Schirp S, Gevargez A, Image-guided percutaneous thermal ablation of bone tumors. Acad Radiol 2002; 9:467–77.
12. Uchida A, Wakabayashi H, Okuyama N, Okamura A, Matsumine A, Kusuzachi K, Metastatic bone disease: pathogenesis and new strategies for treatment. J Orthop Sci 2004; 9: 415–420.
13. Groenemeyer DH, Schirp S, Gevargez A, Image-guided percutaneous thermal ablation of bone tumors. Acad Radiol 2002; 9:467–77.
14. Moroz P, Jones SK, Gray BN, Status of hyperthermia in the treatment of advanced liver cancer. J Surg Oncol 2001;77:259–69.
15. Bruno M, Miola M, Bretcanu O, Vitale-Brovarone C, Gerbaldo R, Laviano F, Verné E, Composite bone cements loaded with a bioactive and ferrimagnetic glass-ceramic: morphological, mechanical and calorimetric characterization. J Biomat App 2014;29(2):254-267.

16. Hildebrandt B, Wust P, Ahlers O, Dieing A, Sreenivasa, G, Kerner T, Felix R, Riess, The cellular and molecular basis of hyperthermia.Critical Reviews in Oncology/Hematology 2002; 43: 33-56.

Chapter 2

Poly methyl methacrylate bone cement

2.1. Poly methyl methacrylate

Therapy for vertebral fracture, cemented hip prosthesis and other bone-related disorders, like bone tumor, have made acrylic bone cement based on poly methyl methacrylate (PMMA) integral part of the orthopaedic surgery. The material is named “bone cement” and it is a two component system composed by a powder and a liquid mixed together.

There are two main type of bone cements: polymer-based and calcium phosphate-based. The focus will be on the first category of bone cements, in fact they are most common used in clinical orthopaedic surgery due to higher mechanical properties than the calcium phosphate bone cement in load-bearing application.

The synthesis of bone cements is based on the polymerization of methyl methacrylate (MMA) monomers to poly-methyl methacrylate (PMMA).[1]

2.1.1. Polymer chemistry

Polymers are large molecules composed of individual repeating unit (monomer). Polymerization can occur by two different mechanisms:

- With **condensation reactions** in which a functional group of a monomer reacts with a functional group on the growing chain of the polymer and the chain lengthening occurs with a low molecular weight molecule (es. water) release.
- With **addition reactions** in which the polymer chain grows by reacting directly with the double bond of a monomer and no molecules are released. The chemical mechanism for the polymerization of PMMA is shown in figure 2.1.

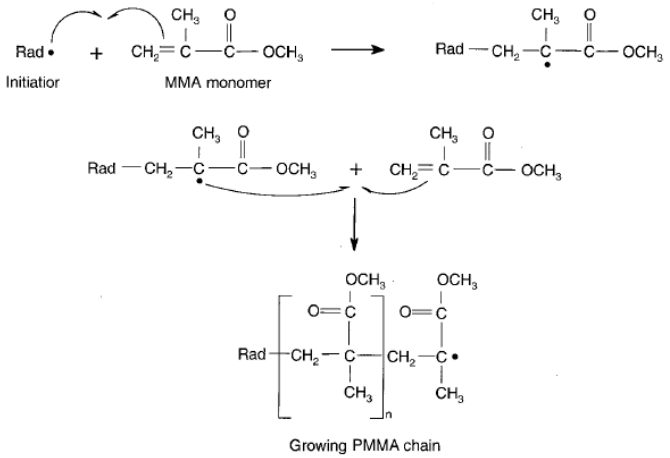

Figure 2.1: Polymerization of PMMA by an addition reaction. MMA monomer reacts with a radical to generate e second radical that can attack the double bond of another MMA monomer. [2]

Polymerization begins by the addition mechanism in which a monomer becomes unstable by reacting with an initiator, a volatile molecule that is mostly commonly a radical (molecules that contain a single unpaired electron). Radical bond with monomers, forming monomer radicals that can attack the double bond of the next monomer by the mechanism shown in figure 2.1 propagating the polymer chain. Since the radicals are unstable, the initiator are often added by as an unreactive peroxide in a much stable chemical form. Radical is formed when heat or light excite the peroxides molecule. For the application in which high temperature are not well tolerable, like bone cement, peroxide is cleaved by adding a chemical activator such as N,N-di-methyl-p-toluidine (DMPT) forming a phenyl radical that attacks the double bond of the MMA monomer. [1]

2.2. Properties of PMMA

PMMA has a linear chain and is a thermoplastic polymer with an un-crystallized structure whose vitreous transition temperature ranges from 110 up to 135°C. At room temperature it is hard, rigid, and brittle with little elongation. It is hygroscopic and, under extreme conditions, the water absorbed will act as a plasticizer and will modify the properties of the material.
It has high mechanical strength, high Young's modulus and low elongation at break. It is one of the hardest thermoplastics and is also highly scratch resistant. It exhibits good dimensional stability.[2]

Physical properties	Value
Density	1,15-1,19 g/cm^3
Water absorption	0,3-2 %
Moisture Absorption at Equilibrium	0,3-0,33 %

Table 2.2: Physical properties of PMMA [2]

2.3. PMMA bone cements

As explained before, bone cements polymerize by radical-initiated addition reactions. The commercially available bone cements have two separate components: a powder containing pre-polymerized beads of PMMA and a liquid containing MMA monomer. The benzoyl peroxide (BPO) initiator is incorporated into the powder and the chemical activator, DMPT, is incorporated into the liquid, so peroxide starts the polymerization mechanism only when the two phases are mixed. To prevent spontaneous polymerization during the storage, the easily oxidized molecule hydroquinone is also added to the liquid. DMPT splits BPO initiator at room temperature. The

growing polymer chains encapsulate the PMMA beads within a solid matrix. Another important component that characterized these material is the radiopaque inorganic phase. The most common are barium sulphate ($BaSO_4$) or zirconium dioxide (ZrO_2). The main reason of their addiction is the easier identification of the material status both during the surgical operation and in follow-up treatment after the implantation. In figure 2.2 a typical composition of a PMMA bone cement is shown. (1)

Table 1
Components of Commercially Available Cement Mixtures (1)

Component	%
Powder	
PMMA beads	88
Benzoyl peroxide	1–2
Radiopacifier	10
Liquid	
MMA monomers	98
Activator (DMPT)	1–2
Hydroquinone	15–75 ppm

Figure 2.2: Components of Commercially cements mixture[1]

2.4. Cement properties

2.4.1. Chemical properties

Cement properties depend very much from the properties of the powder and the liquid component that react together. The effect of each component influences handling and setting time properties, polymerization temperature and mechanical properties.

2.4.2. Liquid-to-Powder Ratio

Liquid/powder ratio (LPR) of a bone cement has an important role in the aforementioned properties. LPR has to be chosen to keep a good trade off among all of them.

Some scientific works show that greater LPR produce higher peak temperatures with an increasing of setting time. One possible explanation is that, at high LPR, an abundance of monomers react exothermically, increasing the peak polymerization temperature. However, the high LPR also decreases the relative concentration of initiator which is included in powder mix, so the monomers are activated slowly, increasing setting time [1].

Pascual et al. report a study on a modified PMMA bone cement with hydroxpropyl methacrylate (HPMA) in which a low LPR is used. The ratio causes a higher temperature peak and a shorter setting time is obtained while residual monomer content increases slightly.[5]

2.4.3. Mixing Methods

One of the most important issue of PMMA bone cements is the presence of different mixing and handling techniques of the components. A first common technique is the manual mixing with spatula and bowl. It is a quite common surgery procedure when a patient undergoes to a cemented hip prosthesis operation. The surgeon, after the generation of a dough, introduces the paste into the hole between implant and bone. After that, in situ hardening appears. Air may become traps in the cement mixture, increasing porosity. Air weakens the cement and provides an interface for the develop of fractures and cracks.

For the decreasing of voids, another way for the preparation of bone cement is the mechanical mixing technique with “vacuum mixing“, where powder and monomer are placed together in a mixing tube and the air is removed under pressure. The tube can placed into an injection gun from which cement can be extruded into the bone cavity. Vacuum mixing devices have been shown to reduce porosity by more than 44% compared with mixing with a bowl and spatula[1]. Another mechanical technique is a centrifugation which is found to remove pores and increase the fracture strength.

All citied techniques produce a mechanical interlock between the bone and the solidified cement that maintains the strength but does not promote any chemical bond between the implant and the bone.[6]

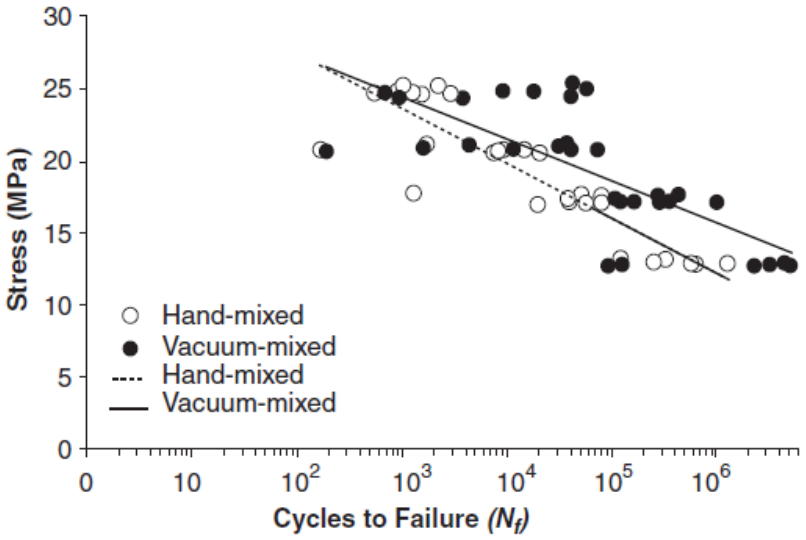

Figure 2.3:A comparison of fatigue strength of hand-mixed and vacuum-mixed bone cement.[6]

As presented in figure 2.3, fatigue strength is evaluated as a function of mixing method. The trends of stresses values for cements produced by vacuum mixing are higher than those produced by hand-mixing.

2.4.4. Handling and setting time properties

During the synthesis of the material it is possible to distinguish three different times:

- **Dough time,** which is the time between starting mixing powder and liquid and the moment when the cement is inserted in the bone cavity
- **Working time,** which permits the workability of the cement in the bone cavity
- **Setting time,** which is the time that elapses for the hardening of the cement. After that time any other modification in shape and quantity is possible. (figure 2.4)

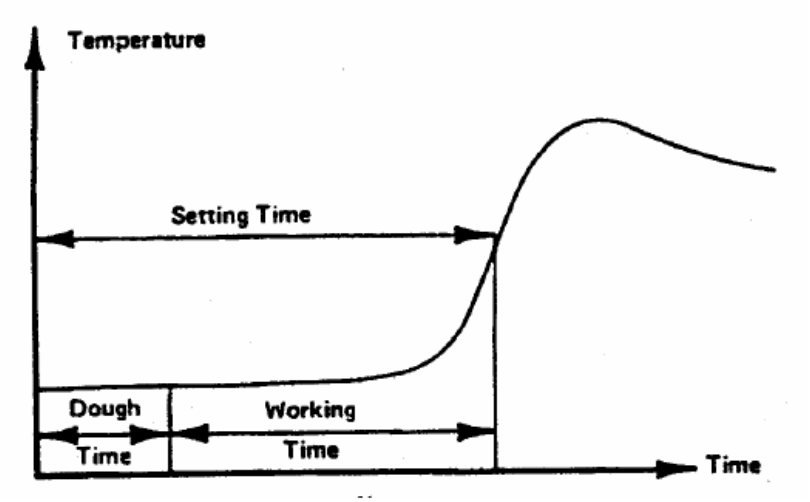

Figure 2.4: Setting time test: evaluation of the hardening time

In figure 2.4 a typical hardening curve of a PMMA bone cement is shown, with the identification of three different times. As evidenced in the curve, the slope of the curve shows the setting time.

The peak of the curve permits the evaluation of the maximum polymerization temperature which has to be the lowest as possible in order to minimise necrosis of surrounding bone .

The workability properties of PMMA bone cements are evaluated with curing parameters and any further modification of the chemical composition of PMMA has to be evaluated as a function of these parameters.

An ISO 5833-2008 has standardized the test in order to provide a methods for comparison different curing parameters of different cements.

For each unit of cement, the setting time is measured from beginning of mixing until the temperature of the polymerizing mass reaches the setting temperature defined as:

$$Tset = \frac{T\max + Tamb}{2} \qquad (2.1.1)$$

$T\max$ = is the highest polymerization temperature measure

$Tamb$ = is the recorded room temperature

The standard provides some restrictions that the bone cement has to respect before the in vivo application (table 2.2).

Mixture	Dough time		Setting time	Maximum temperature	
	Average min	Maximum deviation from average min	Average min	Average °C	Maximum deviation from average °C
Dough state usage	≤ 5	1,5	3 to 15	90	± 5

Table 2.2: Curing parameter requirements [3]

Figure 2.4 evidences that the slope of the setting curve does not change at the beginning but at a certain point it suddenly increases. For this reason the setting time evaluation is crucial because it informs that in a few minutes the cement will be not workability nor injectable into the bone defect and the surgeon has to operate before this time limit.

2.4.5. Radiopaque agents

Radiopaque compounds interrupt the polymerizing matrix and produce discontinuities in the material that can act as fracture initiation sites, diminishing mechanical strength with a not clear effect on polymerization temperature and setting time [1]. To guarantee the structural integrity of radio-opacified cement, it has been noticed that zirconium is structurally superior to barium. Homogeneity of mixed cement is key factor and that a not homogeneous dispersion of barium particles leads to fractures formations. New cross-linking agents and preparation methods that enhance cement strength have been reported. The incorporation of these additives into the cement formulations will minimize any loss of strength or durability due to radio-opacifiers.

Ginebra et al. reports that the radio-opaque agents, both inorganic and organic, have a significant effect on the mechanical properties of the acrylic bone cement. The effect of the inorganic fillers depends on their size and morphology. The addition of zirconium dioxide significantly improves the tensile strength, the fracture toughness and the fatigue crack propagation resistance. In contrast, the addition of barium sulphate produces a decrease of the tensile strength, but does not affect the fracture toughness and improves the crack propagation resistance.[7]

2.4.6. PMMA beads size

The average diameter and size distribution of PMMA beads play an important role in the cure properties of bone cement. This component has a double function: a structural role as a

component of the cement matrix and as a heat sink–dissipating energy released by the exothermic polymerization of MMA monomers. Samples containing PMMA particles with larger mean diameters and widespread distributions of particle size have lower peak polymerization temperatures and longer setting times [1].

Moreover the concentration of activator and the free radical initiator influence the peak temperature, the setting time and the mechanical properties of the cured cement.

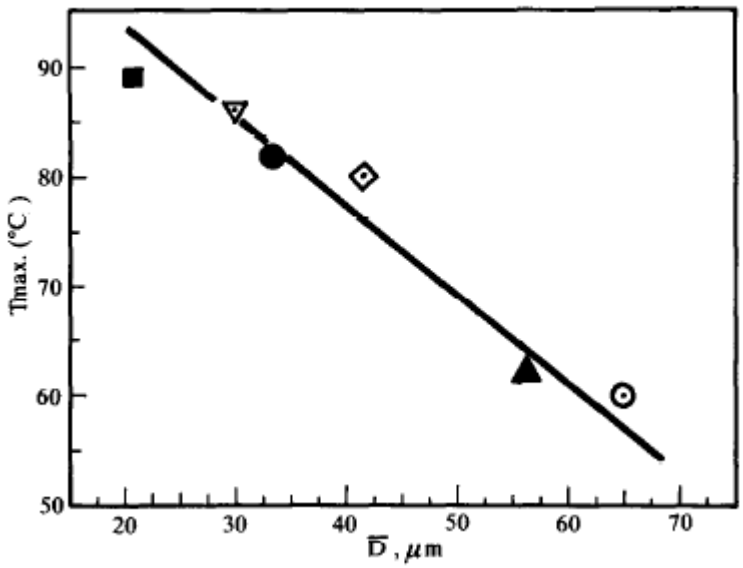

Figure 2.5: Relationship between average size of PMMA and the maximum temperature reached during the polymerization process of acrylic bone cement formulations[2]

In figure 2.5 a linear correlation between the average particle size of PMMA and the maximum polymerization temperature is reported. Increasing the particle size, the maximum temperature statistically decrease . The fact could be explained in a much higher capacity of large beads (50-60 μm) to dissipate the heat in an effective way respect to smaller particles with a size < 20 μm.

If the polymerization temperature reaches or is near to the boiling point of MMA monomer, around 100°C at standard pressure, the vaporization of MMA molecules could give rise to the appearance of voids inside the cured system. This is another interesting reason to lower the polymerization temperature.[2]

2.5. Mechanical properties

In table 2.3 a comparison between the mechanical properties of the cement and the human bone is shown. The compression strength of the PMMA is quite comparable with the same value of the cortical femoral bone.[8]

	Tensile strength [MN/m²]	Compression strength [MN/m²]	Shear strength [MN/m²]	Young Modulus [GN/m²]
Cement	25	77	41	2
Femural cortical bone	123	166	84	17,2
Vertebral cancellous bone	3,9	6,3	2,2	0,34

Table 2.3: Comparison between the mechanical properties of human bone and the PMMA bone cement[8]

Mechanical properties	Value
Hardness, Rockwell M	63-97
Tensile Strength, Ultimate	47-79 MPa
Elongation at Break	1-30%
Tensile Modulus	2,2-3,8 GPa
Flexural Modulus	3-3,5 GPa

Table 2.4: Mechanical properties of PMMA [4]

Compression tests are evaluated referring to ISO 5833 – 2003 specification: the ultimate compressive strength (table 2.4) and Young Modulus should be estimated from the stress strain curve using a 2% offset role and the slope of the initial straight section of the curve. The mechanical results, are influence by two main factors:

1. **Chemical parameters:** quantities of stabilizers, initiators and radiopaocifiers, presence or absence of a copolymer, the powder size and distribution and the rate of change of viscosity with time.
2. **The mixing methods:** this is an important parameter for a given formulations. This factor influences the number and the size of micro- and macropores.[10]

Even flexural and shear mechanical properties depends very much from cement formulation, mixing method, curing and aging conditions.

The method used to mix the liquid monomer and the powder has a significant role in determining the final quality of bone cement. An inadequately mixed cement usually presents a high degree of

porosity . As a consequence, a lot of studies have been conducted on the parameters and variables that affect the quality of bone cement prepared by different mixing methods and devices.

Two important factors have to be taken into account: the depth of penetration of the liquid monomer into the powder (*l*), process that is describable using the Washburn equation, and the associated Reynolds number, *Re*.[11] The study reports in [10] compares variability of the porosity of the cured cement and its bending modulus and bending strength when mixed with a new automated device, compared to the values obtained when the cement is mixed using a commercially-available vacuum cement mixer, that is in current clinical use.

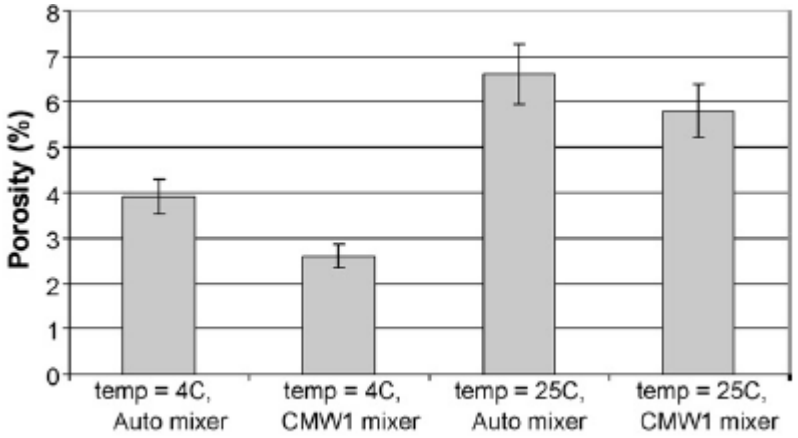

Figure 2.6: Mixing and temperature effect on the porosity of acrylic bone cement

The porosities report in figure 2.6 indicate that there is a statistical difference between cement mixed at 4°C and at 25 °C. The cements cured at 4 °C show an almost 50% decrease in porosity compared to those cured at 25 °C. These reduced porosities depend on the decrease of air entrapped in the cement at the moment of mixing. The material stored at low temperature has a lower viscosity that could influence the decrease of cement porosity.

The comparison of two cement mixing methods has shown a decreasing porosity of 20% using a standard mixer in comparison to an automated mixer. The same trend is observed comparing storing procedures at 4°C and 25°C respectively. Velocity and mixing motion of the cement within the automated mixer caused more air entrapment than conventional paddle stirring.

The mechanical tests have shown a statistical difference between two storage temperatures. At 4°C an increase of bending modulus and strength of 8% and 14% respectively can be observed in respect to higher temperatures. As mentioned before the decrease of air entrapment during the mixing phase and the lower initial storage temperature have improved the mechanical properties. [11]

2.6. Biological properties

PMMA bone cement is classified as an inert material. It is noted that after a certain period from the implant of the cement, there is the formation of a fibrous membrane between the bone and the cement, with a thickness between 50 μm and 3 mm, which allows micro motion occurrence, causing pain into the patient and the space for wear particles accumulation. A possible solution to overcome this problem at the interface is the use of a bioactive bone cement[19].

2.7. Problems

For orthopedic applications, PMMA is used as a filler and it has to guarantee the transfer of the load from the metallic prosthesis to the human bone, avoiding or minimizing stress shielding phenomena. The human bone does not become osteoporotic or subjected to restorable events due to the implant of the material. The material should substitute or fill a bone without modifying its physiology and functionality.

When a new material is implanted into the body an inflammatory response occurs, with the recruitment of macrophages and other repair cells. The worst situation consists in the toxic behavior with the death of surrounding tissue. An inert response create a thin fibrous layer at the interface of 1-3 μm and no bond between the tissues and the implant. On the contrary, bioactive materials are able to stimulate a chemical reaction with living tissues. Hydroxyapatite, bioactive glasses and glass-ceramics are typical examples.

In the previous classification, PMMA bone cement is classified has an inert material. It is well known that when it is implanted in vivo the formation of fibrous collagen capsule occurs., This represents a human response without any osteointegration process. It has been evidenced that a stable bone-implant interface has to be achieved for a long duration of the implant.

Thermal bone necrosis and weakling of the local blood flow are effects generated during in situ curing reactions. Moreover, a chemical necrosis appears with the release of the monomer in the human blood stream, even after several years from the implantation. But the main cause of failure for a PMMA implant is the septic loosening connected with a problem of infections evoked from the cement particles in contact with surroundings tissues.[8]

Loosening is a multi-factorial process and that originates from several causes. Among them, the most important consists in the fatigue failure, that comes from:

- pores in the cement
- stress concentrations at the implant/cement interface
- debonding at the prosthesis/cement interface
- bone resorption, causing stresses in the cement[8]

Huiskes proposes some failure scenario of PMMA bone cement used for fixation of hip prosthesis that can adapt very well to a common cause of failure of this material even when it is used for other applications[9]

The failure scenario includes:

1. **Gradual cracking of bone cement** starting from interface debonding, pores in the cement or increased stress due to peripheral bone losses.
2. **Generation of wear particles** or debris, that develop bone damage with osteolysis at the interface.
3. **High micro motion of the implant** respect to the bone, that can change the bone ingrowth mechanism and, consequently, the strength fixation, which in turn is not high enough to sustain weight-bearing load.
4. **Stress shielding,** which can be another consequence of failure, due to the high stiffness of the implant respect to the bone, that can lead to a degeneration of the fixation. A concentration of the load occurs mainly on the PMMA bone cement if a poor osteointegration is present. The bone is not loaded due to very different Young modulus between bone and PMMA, Being the last higher that the first, and consequently bone resorption occurs.[9]
5. The possible **release of cement particles**, that can directly interact with the surrounding tissues, evoking an inflammatory response and increasing bone destructions. [10]

Looking for an innovative solution to the aforementioned drawbacks, some studies will be presented regarding the synthesis and the characterizations of composite bone cements with high

osteointegration properties. The goal is to design a material with a good compromise among handling properties, bioactivity and adequate mechanical characteristics.

2.8. Bioactive PMMA bone cement

In order to increase the adhesion capability at the interface cement- bone , many research groups have proposed a PMMA composite material where polymer is the matrix and a glass or glass ceramic particles are the disperse phase.[12 -23]

W.F. Musa et al. develop a bioactive PMMA-based bone cements for prosthetic fixation with high bioactivity, high mechanical properties and good handling properties. Commercial PMMA powders different in molecular weights, particle size and shape have been used and loaded with different amount of Apatite/Wollastonite (A/W) bioactive glass-ceramic. The compositions of the investigated formulations are reported in Table 2.5.[20] The authors perform the evaluation of handling properties, mechanical tests and in vivo animal test to verify the bioactive performances of the materials.

Cement	AW-GC	PMMA (M_w)	MMA	BPO	DMPT
B-CMW1	70	15(120,000)	15	—	—
B-Surg Simp	70	12(160,000)	18	—	—
B-270	70	12(270,000)	18	4.0	2.0
B-Palacos 50	50	25(400,000)	25	—	—
B-Palacos 70	70	15(400,000)	15	—	—
B-1200	70	12(1,200,000)	18	4.0	2.0

[a]BPO and DMPT were added in wt% of the monomer.

Table 2.4:Compositions of different PMMA-based bioactive cements [20]

The loading of dry-silanized Apatite Wollastonite-Glass Ceramic filler to the PMMA cement in 70 wt% ratio maintained both bending strength and fracture toughness similar to the control. and the osteoconductivity of the cement increased from 32.1 ±15.8 % to 55.5 ±10.8% for B-CMW1 (commercial Simplex cement matrix). The interaction between the bone and the implant is positively affected, due to the bioactive glass ceramic dispersed into the PMMA matrix, as demonstrated by the in vivo test on six group of rats where the direct contact between the bone and the bioactive cement is evaluated .

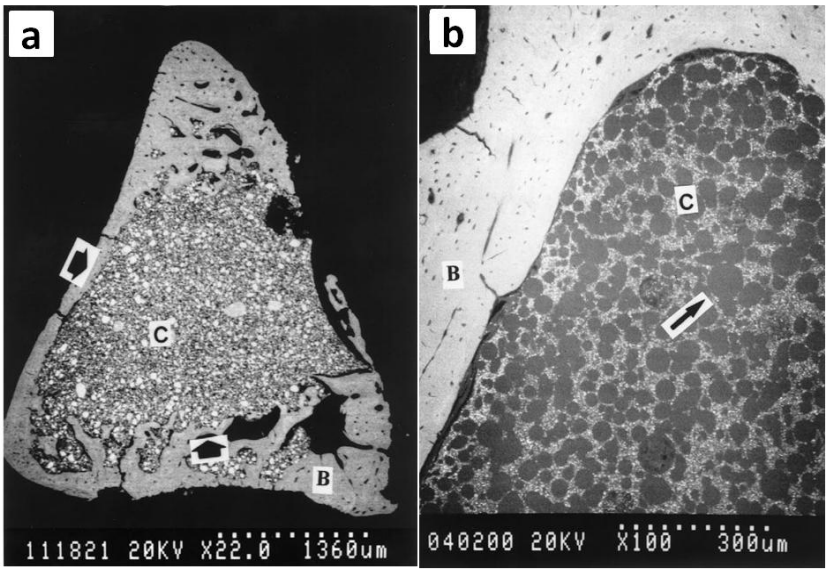

Figure 2.7: SEM microphotographs showing axial sections of rat tibiae 8 weeks after the implantation.(a) bioactive bone cement and(b) control cement with no bioactive phase;

Figure 2.7 reports a SEM microphotograph showing a section of a rat tibiae with the injection of a bioactive bone cement (a) and with a control material (b) after 8 weeks from the implantation. A very high level of osteointegration is noticed in figure 2.7a respect to the poor property of the PMMA

Another example of bioactive bone cement was present by Yamamuro et al. [21] where an apatite wollastonite glass ceramic was added to a cement based on the bisphenol-a-gycidic methacrylate (Bis-GMA) resin. The main advantage in using a different matrix was explained in a decreasing of the curing temperature in respect to PMMA.

The glass ceramic with the composition CaO 44.7, SiO_2 34.0, P_2O_5 16.2, MgO 4.6 and CaF_2 0.5 (weight ratio) was melted in a SiC furnace at 1500°C. The melt was quenched in water then pulverized with an alumina ball mill. The average diameter of the glass-ceramic powder particle was 5 μm. The powder was added to the resin and maximum polymerization temperature and mechanical properties were evaluated together with animal experiments.[2121]

Histological examinations reveal the formation of fibrous tissue between PMMA cement (used as a control) and the bone, while the bioactive cement bonds to bone at 3 and 6 months after surgery through a CaP-rich layer. This CaP-rich layer, about 30 μm thick, is crystallographically confirmed to be an apatite layer.[21]

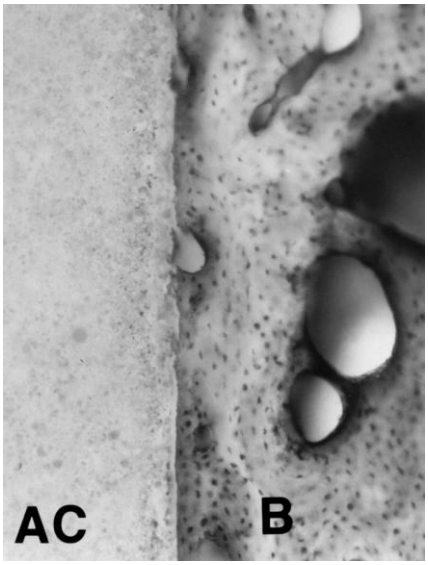

Figure2.8: HAp precipitation at the bone implant interface. The effect is due to the presence of a bioactive phase into the polymer. AC is a bioactive bone cement while B is a bone [21]

After three months new regenerated bone is observed at the bioactive cement surface, and the bone between the cement and the femoral endosteum become dense. (figure 2.8)

Hamizanh et al. [22] reports the realization of a PMMA bone cement modified with the addition of a bioactive glass-ceramic phase. The glass-ceramic has been produced by melting techniques and controlled crystallization. The synthesized glass-ceramic composition is 55 SiO_2, 10 Na_2O, and 35 CaO (wt %) 3 wt % of P_2O_5 .[22] A comparison between bioactive PMMA bone cement and hydroxyapatite bone cement composites is performed.

The sample with 16 wt % of filler loading broke at a higher strain compare with that at 4 wt %.

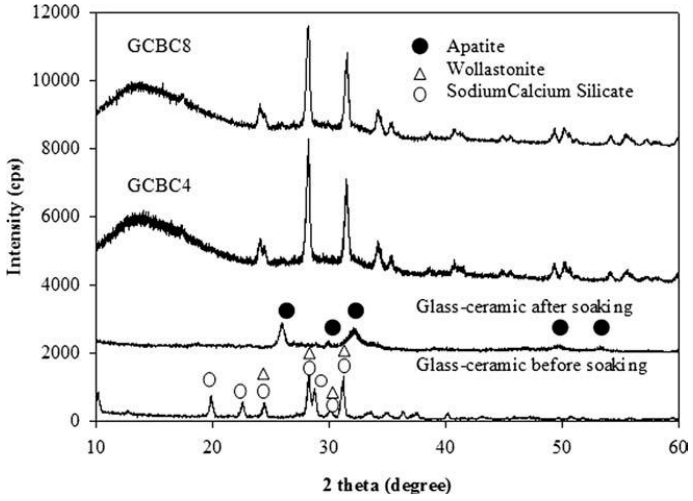

Figure 2.9: XRD patterns of bioactive glass-ceramic before and after soaking in SBF for 7 days while, GCBC4 is a composite bone cement with 4% of glass ceramic, and GCBC8 is bone cement with 8% of glass ceramic after soaking in SBF for 7 days.[22]

Figure 2.9 evidences the X-Ray Diffraction pattern of the glass ceramic before and after bioactivity process . A low peaks of apatite is noticed only on glass ceramic after soaking for 7 days in SBF. While on the composites GCBC4 and GCBC8 no apatite is detected , but only a wide halo at 2Θ= 10°-23° which indicate the presence of an amorphous phase.

The authors affirm that the glass ceramic phase disperse in the polymer is not sufficient to produce the precipitation of apatite on the surface of the composite.

Shinzato et al. [23] propose a bioactive PMMA bone cement containing a glass of different particles size in order to study how they influences the mechanical properties and the osteoconductivity of the composite. Four different formulations of cement have been prepared, containing glass particles with a diameter of 4, 5, 9, 13 μm respectively. The glass belongs to the system MgO-CaO-SiO_2-P_2O_5-CaF_2 and it is mixed in a proportion of 70% with the PMMA. The cement is inserted into the medullary canals of rat tibiae and the bone-cement interface is examined by scanning electron microscopy (SEM). Affinity index is used to measure the osteoconductivity of the material. The index is calculated as the length of bone in direct contact with the cement surface without any intervening soft tissue divided by the total length of the cement surface, and this value was multiplied by 100 [23]

Mechanical Properties	GBCs4	GBCs5	GBCs9	GBCs13	PMMA (CMW-1)
Bending strength (MPa)	138 ± 4	137 ± 4	134 ± 5	133 ± 2	93 ± 1[a]
Young's modulus (GPa)	7.7 ± 0.3	7.7 ± 0.7	7.9 ± 0.4	7.7 ± 0.6	2.7 ± 0.1[a]

Table 2.6: Mechanical Properties of Composite bone cements after 1 day soaking in SBF at 37°C [10]

The mechanical results shown in table 2.6 evidences a decreasing trend in bending strength with the increase of particle size, even if the values of four tested formulation remain significantly higher than that of the control (PMMA). The Young Modulus does not follow the same trend of the bending strength, in fact no variation has been evaluated with the increasing of particle size.

SEM evaluation for all four types of cement shows a very good interaction with bone at 4 and 8 weeks. The affinity index decrease at 4 and 8 weeks with the increase of the glass particles.

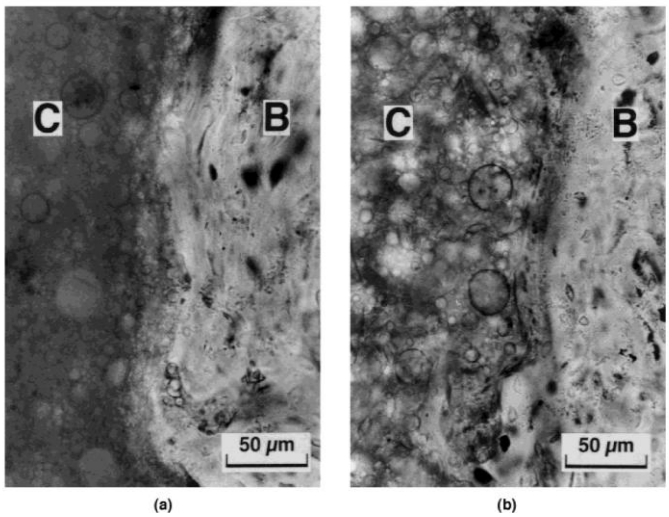

Figure 2.10: (a) bioactive cement with 4 μm disperse glass particles and (b) bioactive cement with 13 μm disperse glass particles in rat tibiae at 4 weeks after implantation. Direct bone formation was observed on two different bioactive glass cement formulations without intervening soft tissue layer. C, cement; B, bone. Original magnification at 400x.[23]

In figure 2.10 a better result is presented, using a bioactive particle phase in the polymer matrix. C is the cement and B is the bone; the cement is very well osteointegrated with a continuity solution. A very good interconnectivity between the bone and the composite and direct bone formatioare evidenced.[23]

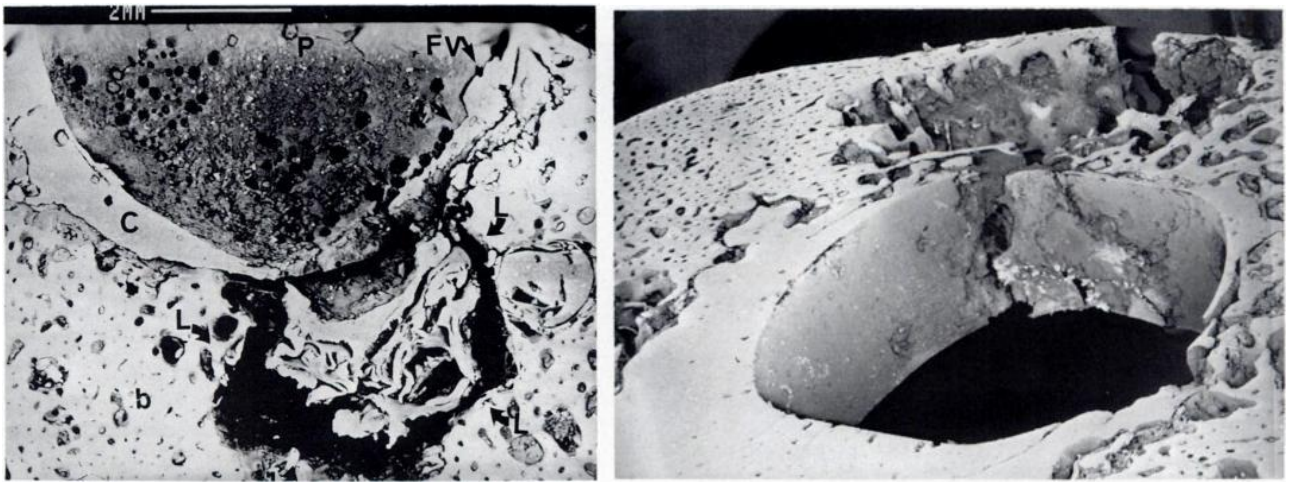

Figure 2.11: Scanning electron micrograph of a post-mortem specimen. The image on the left shows multiple cement fractures and adjacent fragmentation to the osteolysis area. P is a cement plug at the tip of the prosthesis; FV is a fracture through voids in the cement; C is bone cement; b is bone; L is focal lysis in the cortical bone. On the right a detail where it is possible to distinguish the fracture of the PMMA cement and behind it the fracture and resorption of cortical bone.[24]

In figure 2.11 a scanning electron micrograph of a post-mortem specimen of a failed cemented hip prosthesis is reported. Many fracture of the PMMA bone cement combined with a large zone of osteolysis and bone resorption are very clear. This is an example of non-bonding effect between

the implant and the tissue[24]. This local cement failure had generated particulate debris and endosteal bone lysis adjacent to the local cement fragmentation.

In conclusion , the addition of a glass ceramic phase to a bone cement has to be take into account for improving the performance of the material in the interaction with bone.

2.9. References

1. Nussbaum DA, Gailloud P, Murphy K, The Chemistry of Acrylic Bone Cements and Implications for Clinical Use in Image-guided Therapy. J Vasc Interv Radiol 2005; 15: 121-126.
2. Pascual B, Vazquez M, Gurruchaga I, Goni I, Ginebra MP, Gil FJ, Planell JA, Levenfeld B, San Roman J, New apects of the effect of size and size distribution on the setting parameters and mechanical properties of acrylic bone cements. Biomater 1996; 17: 509-516.
3. International Standard ISO 5833, Implant for surgery -acrylic resin cement 2008.
4. Kolevam M, Poly(methyl methacrylate) (PMMA). Technical University of Gabrovo.
5. Pascual B, Gurruchaga M, Ginebra MP, Gil FJ, Planell JA, Goñi I, Infuence of the modifcation of P/L ratio on a new formulation of acrylic bone cement. Biomater 1999:20: 465-474.
6. Prendergast PJ, Orthopedics Prosthesis Fixation for. Encyclopedia of Medical Devices and Instrumentation, Second Edition, edited by John G. Webster 2006 John Wiley & Sons, Inc.
7. Ginebra MP, Albuixech L, Fernàndez-Barragàna E, Aparicioa C, Gila FJ, San Roman J, Vàzquez B, Planell JA, Mechanical performance of acrylic bone cements containing different radiopacifying agents. Biomater 2002; 23: 1873–1882.
8. Cicagna P, Master Thesis on PMMA Bone cement.
9. Huiskes R, Failed innovation in total hip replacement. Diagnosis and proposals for a cure. Acta Orthop Scand 1993;64:699–715.
10. Lewis G, Properties of Acrylic Bone Cement: State of the Art Review. J Biomed Mater Res A, 1997;38: 155-182.
11. Walker GM, Daly C, Dunne NJ, Orr JF, Liquid monomer-powder particle interaction in acrylic bone cement. J Chem Eng 2008;139: 489-494.
12. Shinzato S, Nakamura T, Ando K, Kokubo T, Kitamura Y, Mechanical properties and osteoconductivity of new bioactive composites consisting of partially crystallized glass beads and poly(methyl methacrylate). J of Biom Mater Res A 2002;60(4): 556–563.
13. Senaha Y, Nakamura T, Tamura J, Kawanabe K, Iida H, Yamamuro T, Intercalary replacement of canine femora using a new bioactive bone cement. J Bone Surg [Br] 1996;78-B:26-31.

14. Lopes PP, Garcia MP, Fernandes MH, Fernandes MHV, Acrylic formulation containing bioactive and biodegradable fillersto be used as bone cements:Propertiesand biocompatibility assessment. Mater Sci Eng C 2013;33:1289–1299.
15. Okada Y, Kawanabe K,Fujita H, Nishio K, Nakamura T, Repair of segmental bone defects using bioactive bone cement: Comparison with PMMA bone cement. J Biom Mat Res A 1999;47:353-359.
16. Shinzato S, Nakamura T,Kokubo T,Kitamura K, PMMA-based bioactive cement: Effect of glass bead filler content and histological change with time. J Biom Mat Res A 2001; 59(2):225-232.
17. Shinzato S, Nakamura T,Kokubo T,Kitamura K , In Vivo Aging Test for a Bioactive Bone Cement Consisting of Glass Bead Filler and PMMA Matrix. J Biom Mat Res B: Applied Biomaterials 2003;68B: 132-139.
18. Tamura J,Kawanabe K, Kobayashi M, Nakamura T, Kokubo T, Yoshihara S, Shibuya T, Mechanical and biological properties of two types of bioactive bone cements containing: MgO-CaO-SiO,-P,O,-CaF, glass &d glass-ceramic powder. J Bio Mat Res A 1998;30(1):85-94.
19. Harper EJ, Bioactive bone cements. J Eng in Med 1998; 212: 113.
20. Mousa WF, Kobayashi M, Shinzato S, Kamimura M, Neo M, Yoshihara S, Nakamura T, Biological and mechanical properties of PMMA-based bioactive bone cements. Biomater 2000; 21: 2137-2146.
21. Yamamuro T, Nakamura T, Iida H, Kawanabe K, Matsuda Y, Ido K, Tamura J, Senaha Y, Development of bioactive bone cement and its clinical applications. Biomater 1998; 19: 1479-1482.
22. Hamizah AS, Mariatti M, Othman R, Kawashita M, Noor Hayati AR, Mechanical and Thermal Properties of Polymethylmethacrylate Bone Cement Composites Incorporated with Hydroxyapatite and Glass-Ceramic Fillers. J of Appl Poly Sci 2012; 125: E661–E669.
23. Shinzato S, Nakamura T, Kokubo T, Kitamura Y, Bioactive bone cement: Effect of filler size on mechanical properties and osteoconductivity. J Biom Mat Res 2001; 56(3):452–458
24. Maloney WJ, Jasty M, Rosenberg A, Harris HW, Bone lysis in well-fixed cemented femoral components J Bone Joint Surg [Br] 1990; 72-B :966-970.

Chapter 3

Bioactive ferrimagnetic and antibacterial glass ceramics

3.1. Glasses

A glass is an amorphous material obtained by a progressive stiffening of a liquid that does not crystallise during a fast cooling (figure 3.1).

Figure 3.1: Cast of a glass into a mould[1]

In a crystalline solid material a transition between a liquid to a solid state become in a discontinuity way at a precise temperature called solidification temperature.

In an amorphous material the passage from a liquid to a solid becomes with a progressive and continuous increase in viscosity during cooling up to completely stiffness.

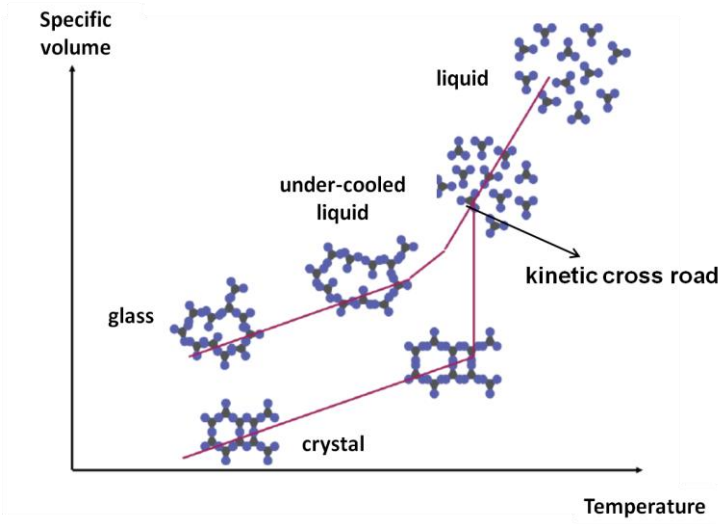

Figure 3.2: Mechanism of glass formation Specific volume vs temperature diagram . [2]

During the cooling of a liquid the elementary structures (atoms and molecules) are able to move and get close one to another. At a certain temperature value of the diagram evidenced in figure 3.2 , named kinetic cross road, two scenarios are possible: an abrupt decreasing of specific volume at a constant temperature, T melting for a solid, where the unit structures join themselves in order

to form a crystalline solid. The process is completed only when the crystals have reached a maximum possible order.(figure 3.2)

The second solution regards the formation of a glass, in which there is a transition from an under cooled liquid where the atoms and molecules rearrange up to glass state. The movements are blocked and the structure of a liquid becomes fixed and is no longer temperature-dependent. The passage from a state to another occurred with a progressive increase of viscosity.

The glass is characterized by a Transition Temperature (T_g) which is an useful indicator of the appropriate temperature at which the under-cooled liquid converts to a solid during cooling.

On the contrary, T_g, indicates when the solid begins to behave as a viscoelastic material during heating. As we can see from the diagram in figure 3.2, the structure of a glass is more open than the structure of a crystalline solid. An amorphous material is characterized by a continuous reduction of volume, occurring during the temperature decrease, and by a change of curve slope at a glass transition temperature.

During the cooling, the glass is characterized by a spatial organization with a short range order and an high degree of long range disorder, similar to the liquid from which it originated.

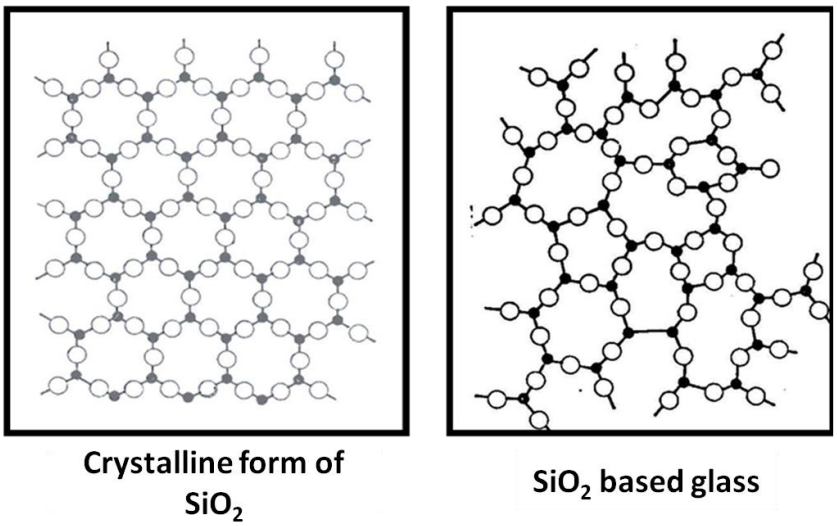

Figure 3.3:Difference between crystalline and amorphous SiO2 [1]

Figure 3.3 evidences the structure of the amorphous silica respect to the crystalline silica. In the first panel the silica tetrahedrons are disposed regularly in a three dimensional lattice network; this structure presents a long range order and periodic atomic arrangement, which is typical of a crystalline solids; while in the second panel the silica glass is characterized by a long range disorder. However a glass can be defined as a material with a short range order composed by silica tetrahedron .

Zachariasen proposed a glass formation theory according to silica crystals, which form glass instead of recrystallizing after melting and cooling, have a network and not a close-packed structures. This network is composed by tetrahedral which are connected at all four corners, Network is not periodic and symmetrical as in crystals. It extends without a preferential direction and in fact glass is considered an isotropic material. Its properties do not depend from a preferential direction

The theory of Zachariasen proposes four rules for the formation of glass. These rules affirm:

1. Each oxygen atoms is linked to no more than two cations
2. The oxygen coordination number of the network cations is three or four
3. Oxygen polyhedral shares only corners and not edge or face
4. At least 3 corners of each oxygen polyhedron must be shared in order to form a 3-dimensional network.

Sufficient network cations must be present to allow a continue open structure to form a glass.[3]

Another theory was proposed by Stanworth, he classified the oxides that compose a glass into three groups: glass formers, intermediate and modifiers on the basis of the electro-negativity of the cations. The only anion is the oxygen and the theory approach is based on the evaluation of a cation-anion bond. Cation that form covalent bond with oxygen should act as former and produced good glasses. Cations with lower electronegativity form more ionic bonds with oxygen so they cannot form glasses by themselves, but they can partially replace cations from the previous group. Since the behavior of these ions is transitional between the cations that form a glass and other which never form glasses, they are defined as intermediate. Cations, which have very low electronegativity and therefore they form highly ionic bond with oxygen, never act as a network formers. Since these ions can only modify the network structure created by network forming oxides, they are termed modifiers. As it will discuss later, they are very important in the bioactive and antibacterial properties of the glass. In table 3.1 there are some example of inorganic oxide divided in these three categories.[3]

Glass formers	modifiers	intermediates
SiO_2	Na_2O	Al_2O_3
GeO_2	K_2O	PbO
P_2O_5	Li_2O	CdO
B_2O_3	MgO	TiO_2
As_2O_3	CaO	
As_2O_5	BaO	
V_2O_5	ZnO	

Table 3.1: Classification of inorganic oxides in the structure glass theory[5]

Bond strength is another criterion for predicting the glass formation. Sun [3] states that strong bond prevents reorganization of the melt structure into the crystalline structure during cooling and thus promotes glass formation. The bond strength is defined as the energy required to dissociate an oxide into its atomic component. The best glass former are characterized by a high bond strength. Using this criterion the division into glass former, intermediate and modifiers is also applicable.

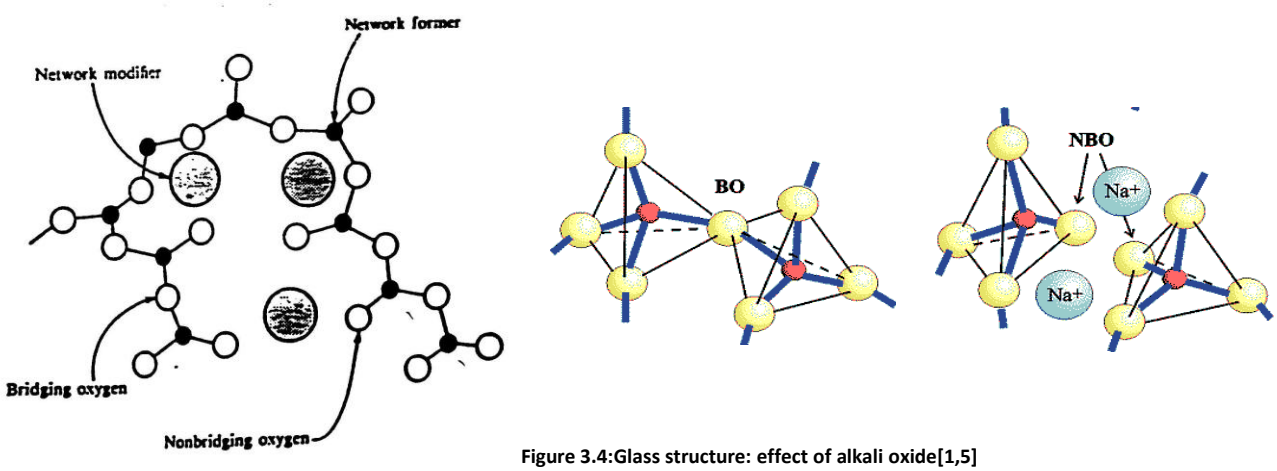

Figure 3.4:Glass structure: effect of alkali oxide[1,5]

In figure 3.4 a typical structure of silica glass is shown, it can distinguish the silica tetrahedron with bridging oxygen (BO), which connect one tetrahedral to another and a non-bridging oxygen (NBO) which interrupts the silica network. The NBO usually are surrounded by some ions like Na^+ or Ca^{++} which modified the network. Sodium and calcium ions do not form glass alone and cause a breakdown of the glass network, they can easily diffuse inside the material, their incorporation aims at reducing melting and working temperatures. In fact Na_2O decrease the melting temperature of the glass and CaO increase the chemical durability. [3]

3.2. Glass ceramic materials

When a liquid became solid by a vitrification process the cooling rate is higher than the crystallization rate.

A de-vitrification process is expressed by nucleation and growth of a crystalline species. It can happen if the glass remains for a long time at a certain temperature in which the speed of crystallization rate is high.

The crystallization process requires the presence of a nucleus, on which the crystals will subsequently grow to a detectable size.

The passage from the liquid state to a crystalline phase will not became instantaneously in all the mass because should be a cooperative movement of all atoms of the material but for progressive growth of nucleus composed by clusters of few hundreds of atoms.

Both the nucleation crystal and growth processes are thermally activated, in fact they require the overcoming of energy barriers by thermal energy.

A glass-ceramic can be obtained from a base glass by controlled crystallization (figure 3.5): the glass, after its synthesis, is subjected to a heat treatment at a temperature T_1, at which it is maintained for a certain period of time in order to promote the formation of nuclei, which act as centres of crystallization. In a next step, these nuclei increase by a heat treatment at a temperature T_2 (growth) greater than T1.

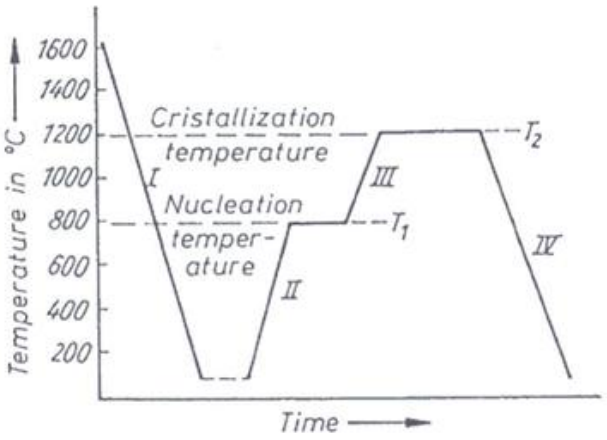

Figure 3.5: Nucleation and crystallization thermal treatments[1]

The new crystals produced in this way grow directly in the glass phase and at the same time slowly change the composition of the remaining glass.

3.3. Bioactive glasses

Bioactive glasses are a particular category of glass characterized by:

- A typical composition of SiO_2, CaO, Na_2O, P_2O_5
- A SiO_2 content inferior than 60% mol
- High presence of Na_2O and CaO
- High ratio CaO/P_2O_5

The Na_2O-CaO-SiO_2 diagram in Figure 3.6 is used for the design of a bioactive glass . This ternary diagram is divided in different zones and each zone has different chemical characteristics.

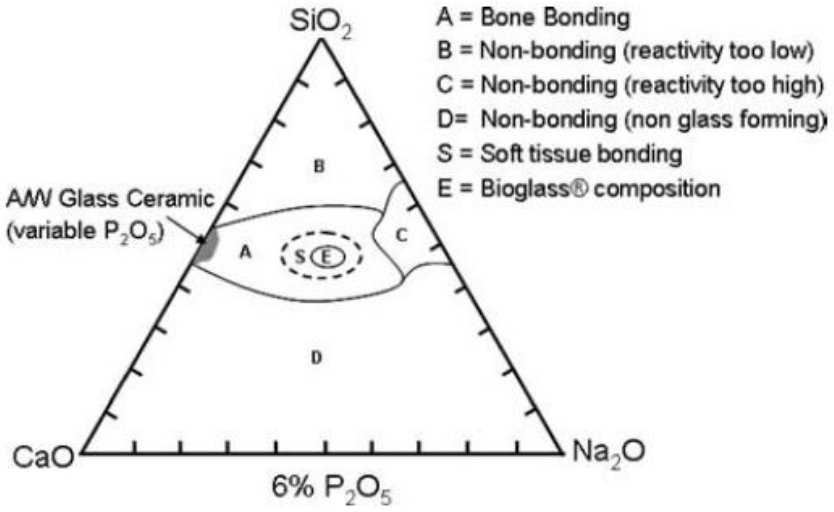

Figure 3.6: The graph shows compositional dependence (in weight percent, %wt) of the ternary compounds for the identification of the best bioglass formulation P_2O_5 is constant at 6 %wt.[4]

The chemical glass compositions in the middle of the diagram, in region A, can create a chemical bond with bone. In fact region A defines the bioactive bone-bonding boundary. Silicate glasses inside region B, such as glasses used for window or bottle behave as inert materials and highlight formation of a fibrous capsule at the implant–tissue interface, in fact the reactivity of these materials is very low due to the presence of a high SiO_2 content. Glasses within region C are resorbable and disappear within 10–30 days of implantation, because the presence of calcium oxide is too low and the durability of the glass is not guarantee. Glasses within region D are not technically practical and, therefore, they have not been tested as implants due to the lack of network former compound. In the middle of the diagram in zone E there is the composition of Bioglass® that Hench discovers in 1970. The composition of Bioglass® is 45% SiO_2, 24.5 % CaO, 24.5

Na_2O, 6% P_2O_5 (% in wt). The discovery of this material permitted the explanation of the bioactivity process that takes place when the glass is put in contact with biological fluids.[4]

The most important application of these materials is the orthopaedic surgery where there is an elevated request of material which can induce a fast osteointegration between the bone and the implant.

3.3.1. The bioactivity process

As mentioned before, glasses for biomedical use can be classified into three categories: resorbable, **bioactive** and inert materials. A bioactive material is defined as a material that present a specific biological response at the interface with tissue.

A bioactive glass undergoes to a surface dissolution in a physiological environment, which cause the formation of a hydroxycarbonate apatite (HCA) layer on its surface. An elevated solubility of a bioactive glass causes an increase of bone tissue growth.[4]

The bioactivity process is a time dependent surface modification. This can happen *in vitro* in presence of a simulated body fluid (SBF) or *in vivo* with biological fluids contact.

The expected result is the completely osteointegration of the material with soft or hard tissues.[6]

For the glass-ceramics, generally, the process of bioactivity depends only on the amorphous phase.

The glass dissolution causes both the chemical composition and pH solution variations. The formation of HCA on bioactive glasses and the release of soluble silica and calcium ions to the surrounding tissue are key factors in the rapid bonding of these glasses to tissue.

The bioactive process can be divided into 11 stages: stages 1–5 are chemical and can occur *in vitro,* stages 6–11 are biological and occur only *in vivo*:

1. The modifiers ions, Na^+ and Ca^{++}, produced an ion exchange between them and the hydrogen ions present in the solution.

$$\text{Si-O-Na}^+ + \text{H}^+ + \text{OH}^- \rightarrow \text{Si-OH}^+ + \text{Na}^+_{(aq)} + \text{OH}^-$$

In this step the pH of the solution increases (> 7,4) as a result of the decreasing of H^+ ions in the solution, since they are substituted by cations. Figure 3.7a

2. Due to the ion exchange of the previous step there is the formation of the silanols at the material surface. The hydrogen ions combine with the non bridging oxygen due to rupture of Si-O bond.

$$Si\text{-}O\text{-}Si + H_2O \rightarrow Si\text{-}OH + OH\text{-}Si$$

For the same reason the release of soluble silica in a $Si(OH)_4$ form happen.

3. The silanols polycondesate of and create a silica gel: the re-polymerized silanols provide Si-O-Si with high water content. Figure 3.7c

$$\equiv SiOH + \equiv SiOH \rightarrow \equiv Si\text{-}O\text{-}Si\equiv + H_2O$$

This silica layer acts as a preferential nucleation site for the CaP layer [11]

4. Precipitation of an amorphous phase enriches of Ca^{++}, PO_4^{3-}, CO_3^{2-} on the SiO_2-rich layer.Figure 3.7d
5. Crystallisation of the amorphous $CaO\text{-}P_2O_5$ film by incorporation of OH- and CO_3^{2-} anions from solution to form a mixed hydroxyl carbonate apatite (HCA) layer. Figure 3.7e

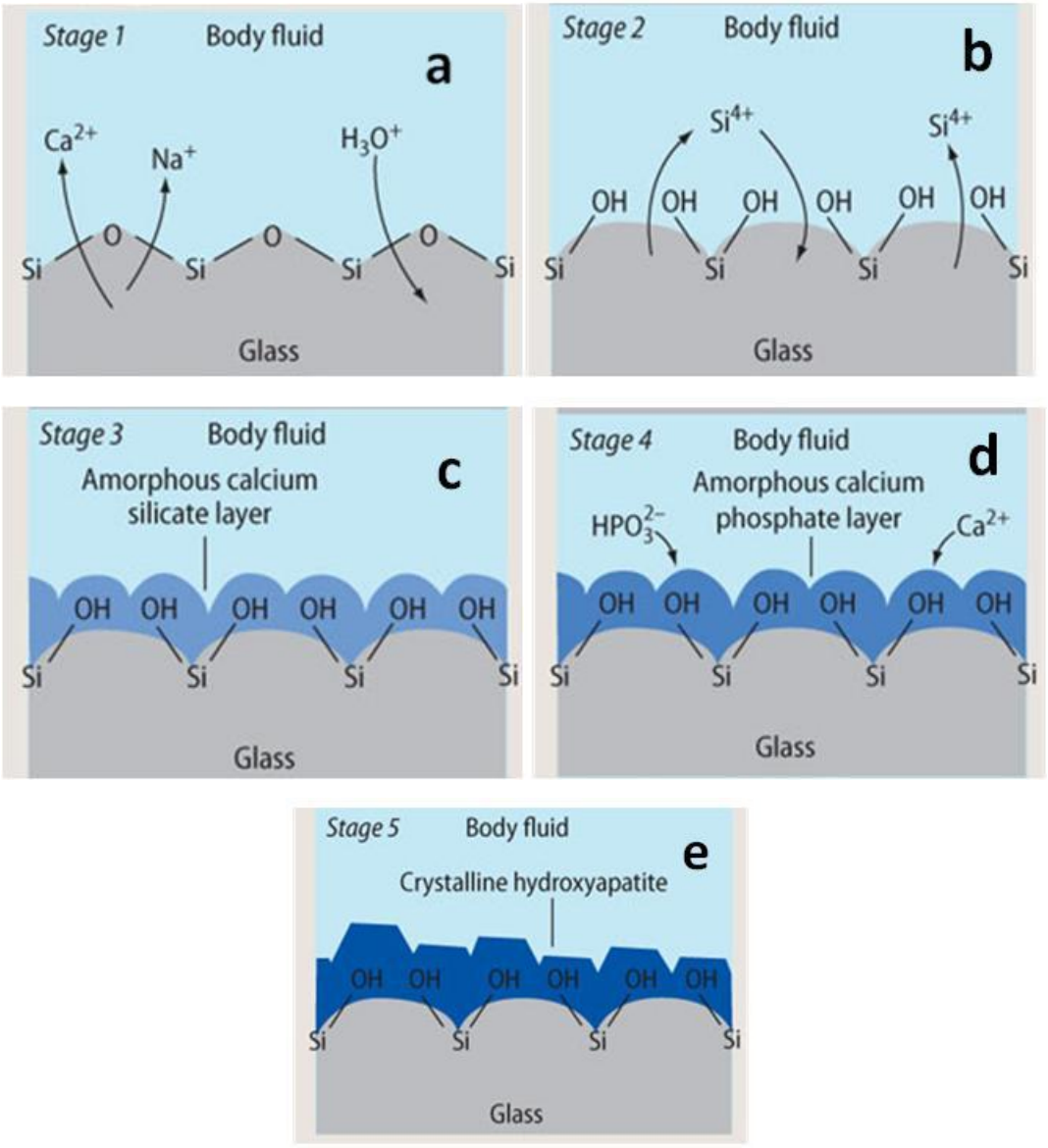

Figure 3.7: Chemical bioactivity steps[1]

6. Adsorption and desorption of biological growth factors, in the HCA layer (continues throughout the process), to activate differentiation of stem cells.
7. Action of macrophages: they intervene always when a foreign body invades the body.
8. Attachment of stem cells on the bioactive surface.
9. Differentiation of stem cells to form bone growing cells, osteoblasts.
10. Generation of extracellular matrix by the osteoblasts to form bone.
11. Crystallisation of inorganic calcium phosphate matrix to enclose bone cells in a living composite structure.[1-4]

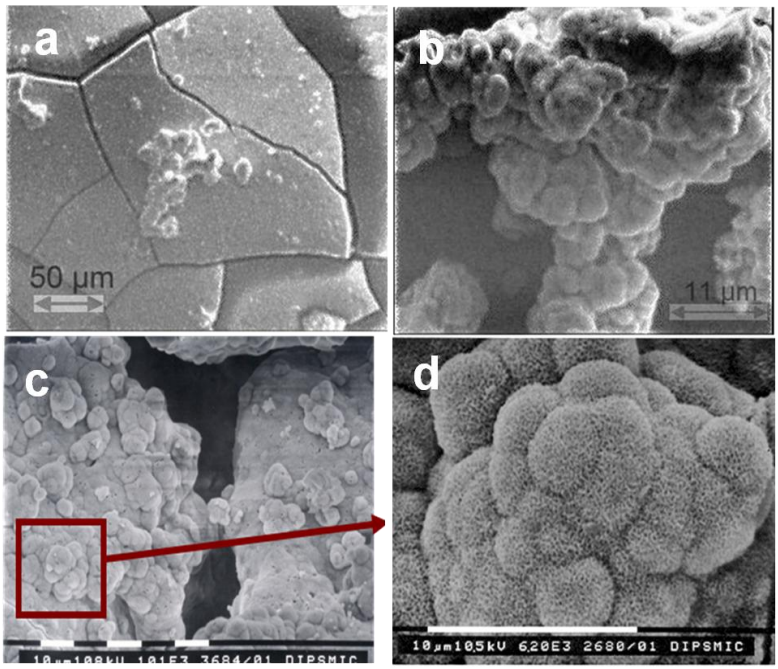

Figure 3.8: Scanning electron microscopy of different step of bioactivity process[1]

Figure 3.8 shows three steps (a, b and c) and one magnification (d) of the bioactivity process: in figure 3.8a the formation of a silica gel on the surface of a glass, with some isolated precipitates, is represented. Here an early stage of bioactivity is reported. In figure 3.8b and 8c the amount of precipitations increases and covers the whole surface of the glass. A calcium phosphate laver is forming. Figure 3.8d shows a magnification, in which it is possible to see the typical morphology of hydroxyapatite formed at the end of 5 steps of bioactivity. This behaviour provides an useful proof of material osteointegration capacity .

The bioactivity depends a lot from the chemical composition of the glass and from the kinetics of exchange with surround fluids.

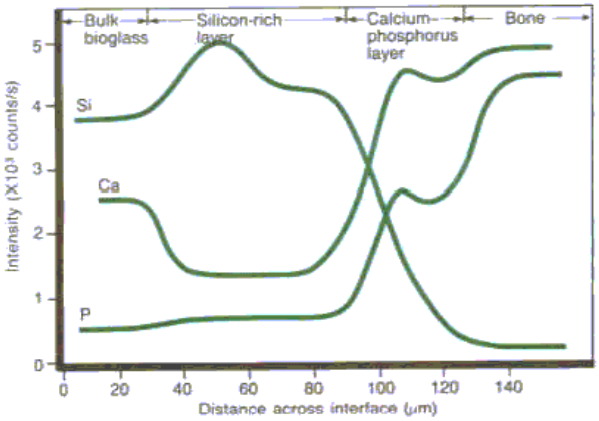

Figure 3.9: Bioactivity profile from bulk bio glass to bone[1]

Figure 3.9 shows a theoretical reaction layer between an implant and the bone. The bulk glass contains silica, calcium and phosphorus, when the glass is put in contact with biological fluids there is the formation of silicon rich layer, which acts as substrate for the precipitation of Ca-P rich layer. This last layer, very similar in morphology and composition to the natural HAp, integrates itself with bone. With the increasing of the distance from the bioactive substrate the silicon rich layer decrease respect to an increase of calcium and phosphorus intensity .

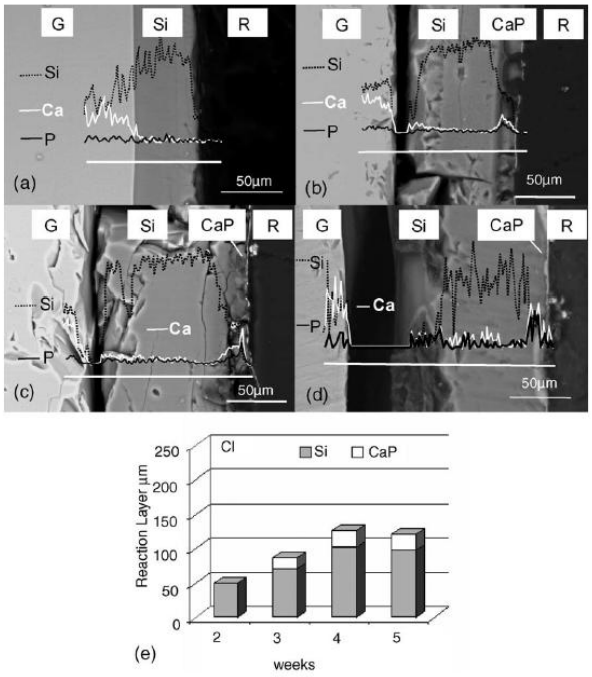

Figure 3.10: shows the SEM images of a cross-section of glass, soaked in simulated body fluid for: (a) 2, (b) 3, (c) 4, and (d) 5 weeks with its line scan profiles, the reaction layer is characterized by the different gray tones: G-glass, Si-Silicon-rich layer, CaP-calcium and phosphorous-rich layer. (e) Shows the reaction layer Si and CaP development with time in this type of glass.[11]

De Arenas et al. showed a cross section of a bioactive glass at different times where it possible to distinguish the bioactivity steps and the trend of the ions, the silica gel and the HAp formation. Reaction layers of silica and CaP depend on time soaking of the glass; in fact the trend of the calcium and phosphorus increase with increasing of soaking time in SBF(figure 3.10). [11]

3.3.2. Osteoinductive behaviour of bioactive glasses

Another important property of bioactive glasses regards their capability to slowly degrade and dissolve when they are implanted. Release products stimulate progenitor cells to differentiate into a bone cell (osteoblast). The pathway of stimulating genes is associated with osteoblast differentiation. This phenomenon is called osteoinduction. The use of bioactive glasses encourages the formation of new bone in two different way by osteoconduction, and by osteoinduction. In the first the glass establish a chemical bond with the existing bone. The stimulation of new bone on and along its surface is confirmed by the bioactivity process . In the second the material is able to activate genetic pathways for the production of new bone cells.[7]

In a research work[8] Hench clarified the genetic activation mechanism in the differentiation of bone cells induced by Bioglass®specific ion release .

In the developing of genetic theory of bone regeneration, he stated that not only the glass but also the ionic dissolution products released from 45S5 influence and control the cell cycle of osteogenic precursor cells. Cells that were not be able to achieving a fully differentiated phenotype characteristic of mature osteocytes died by programmed cell death.

The transformation of undifferentiated cell population towards mature osteoblasts became fast, in few hours, and led to a formation of new mineralized bone in culture, without the addition of organic bone growth factors, such as bone morphogenetic proteins (BMP). This a very important advantage connect to the material. This work evidences the effective ionic dissolution products (Si^{4+} and Ca^{++} ions) released at slow rates from 45S5 glass. The ions produced osteostimulation when they are present at a particular ratio and at a particular concentration range: of 15–30 ppm for Si^{4+} and 60–90 ppm Ca^{2+}.[8]

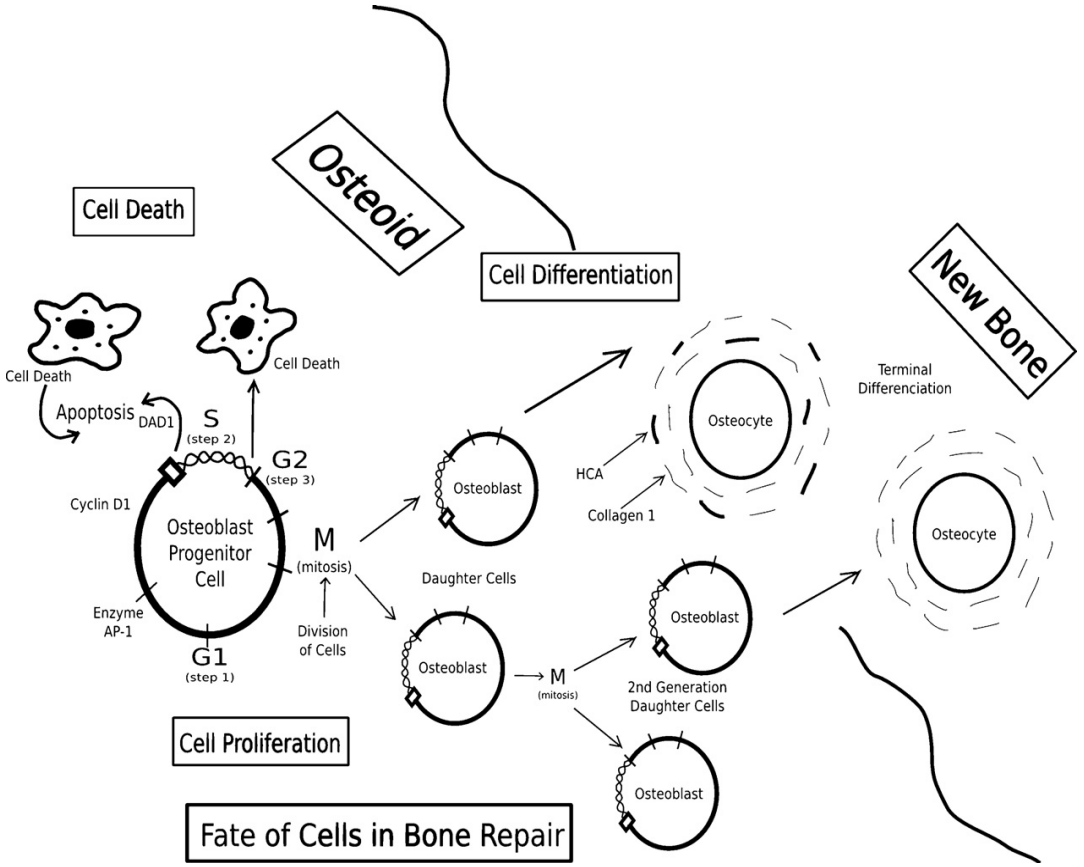

Figure3.11: Schematic of osteogenic progenitor cell cycle leading to (1) programmed cell death (apoptosis); (2) mitosis and cell proliferation; or (3) terminal differentiation and formation of a mineralized osteocyte (mature bone).[8]

Figure3.11 shows biological and genetic steps in the process of cell differentiation in presence of ionic dissolution products.

3.4. Mechanical properties of bioactive glasses

The most important advantage of bioactive glasses is a fast rate of surface reaction, which leads to rapid tissue bonding. Their main disadvantage is the weakness and low fracture toughness due to amorphous glass network. Bending strength of most of the composition studied is in the range of 40-60 MPa which make them unsuitable for load-bearing applications. Therefore this material can be applied as an osteointergation device as a coating, where interfacial strength between metal and the coating is the limiting factor, or in low loaded or compressive loaded device or in powders form as a bioactive phase in a composite. [9]

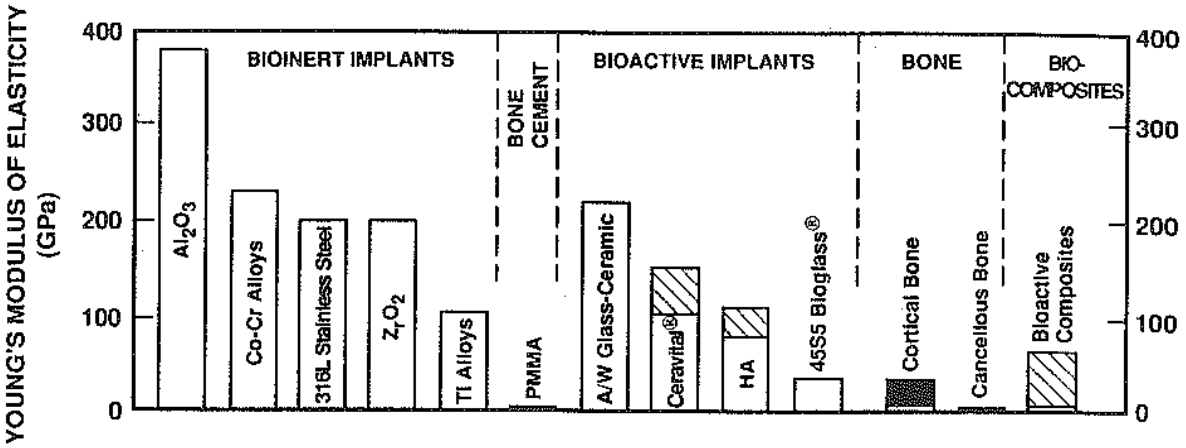

Figure 3.12: Modulus of elasticity (GPa) for prosthetic materials compared with bone[9]

In Figure 3.12 is reported the Young modulus of different categories of biomaterial compared with bone. It can be seen that the bioinert implants have the highest elastic modulus, which is very different from the bone one. The bioactive implants show more comparable values. The best choice is represented by Bioglass® and bio-composite; the last one consists in a matrix based on a polymer and bioactive glass particles dispersed in the matrix. These two solutions permit the best trade-off between the material and the young modulus similar to the bone [9].

3.5. Bioactive and ferrimagnetic glass ceramic

If a ferro- or ferrimagnetic material is subjected to an alternating magnetic field, a certain amount of heat is generated. The heat generated per cycle depends on the hysteresis losses, which varies depending on the nature of ferromagnetic material and magnetic field conditions. Magnetic particles of glass embedded in a tumour site and placed within an oscillating magnetic field will heat up to a temperature dependent on the magnetic properties of the material, the strength and the frequency of the magnetic field, and the cooling capacity of the blood flow in the tumour site. Among these materials a large category of them produced heat with magnetite nucleated in the glass ceramic matrix. [12-18]. The mechanism of heat production depends on the size and the state of magnetic material.

Bioactive and ferrimagnetic glass-ceramics are expected to be useful as thermoseeds for hyperthermia treatment of cancer, especially deep-seated cancers such as bone tumours. When they are implanted after the tumor removal, they promote the formation of bone like apatite on

them, and destroy cancer cells if they are located near bones. After heating, they can also reinforce weakened tumours bone by bonding to bone.

Bioactive and ferrimagnetic glass are obtained by a crystallization process of iron oxide present in the glass composition containing Fe^{2+} and Fe^{3+} ions. Moreover they possess a good biocompatiblity Bretcanu et al. report the preparation and characterization of a bioactive and ferrimagnetic glass-ceramic belong to the system SiO_2–Na_2O–CaO–P_2O_5–FeO–Fe_2O_3 . It is prepared by melting of coprecipitation-derived raw materials. The unique ceramic phase is magnetite included in an amorphous matrix. Magnetite crystals precipitate during cooling from melting temperature. This glass-ceramic would no longer require any nucleation and growth thermal treatment, since the maximal quantity of magnetite crystals is produced during cooling.[12]

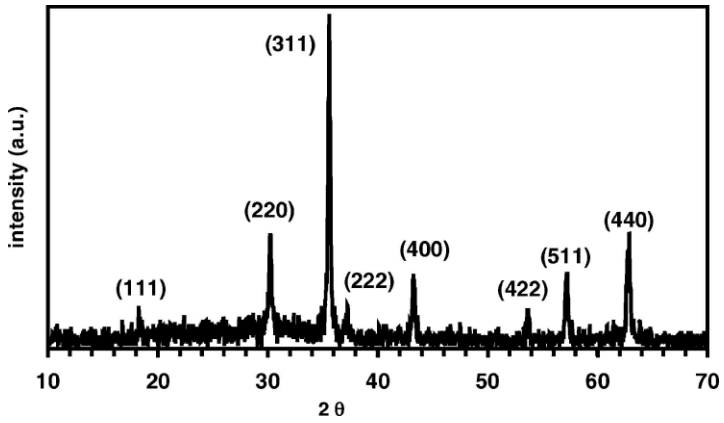

Figure 3.13: X-ray diffraction pattern (XRD) of glass ceramic[12]

The XRD in Figure 3.13 shows the presence of a typical magnetite peaks nucleated in the amorphous matrix. Any other crystalline phase is reported.

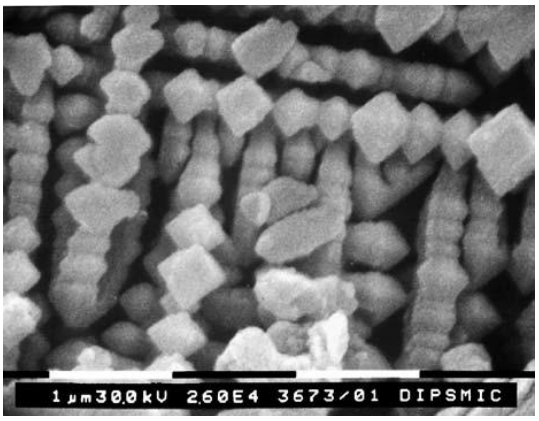

Figure 3.14: Scanning electron microscopy of magnetite crystals after etching[12]

Figure 3.14 reports a SEM image of the morphology and disposition of magnetite crystals after an etching of the amorphous matrix. The crystals have a columnar disposition and an octahedral shape.

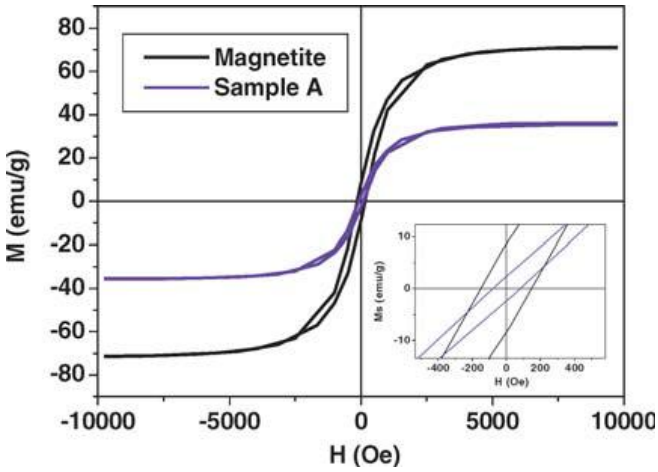

Figure 3.15: Hysteresis loops of the glass in comparison to the pure magnetite[12]

In Figure 3.15 authors evaluate also the hysteresis loops of the glass ceramic compare with a pure magnetite. It can see the value of saturation magnetization is higher for magnetite The amount of ferrite is higher in pure magnetite respect to the glass ceramic[12].

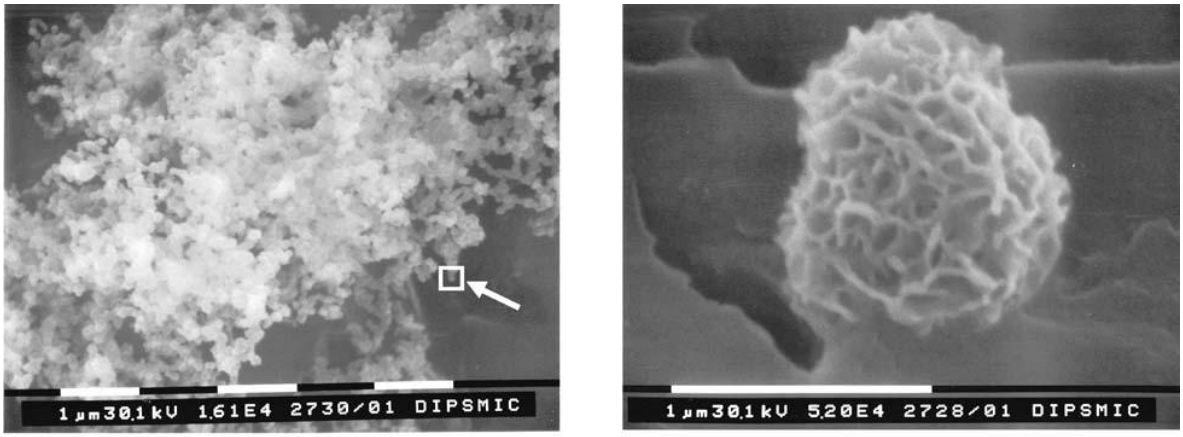

Figure 3.16: Results of Bioactivity test on the glass surface[12]

Figure 3.16 reports the results of bioactivity characterization of the magnetic glass. In the figure 3.16a several CaP precipitates are observed, figure 3.16b shows the typical morphology of HA.

Ebisawa et al. propose a bioactive and ferrimagnetic material as a thermoseed for the treatment of cancer with hyperthermia. Different glass ceramics are prepared by heat treatment of base glasses compositions 40(FeO,Fe_2O_3)-6OCaO-SiO_2 (wt%) with various additives at 100:3 weight

ratio. After that, they evaluate *in vitro* bone-like apatite formation in a simulated body fluid and the magnetic properties. .[13]

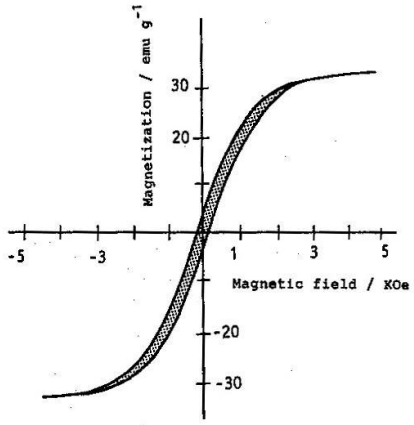

Figure 3.17: hysteresis loop of CSFe+B_2O_3+P_2O_5 (CSFe+BP) glass heat treat at 1050 °C [13]

Figure 3.17 reports the hysteresis loop of CaO-SiO_2-Fe_2O_3-P_20_5-B_2O_3 glass-ceramic (CSFe+ BP) heat treated at 1050 °C. The saturation magnetization is 32 emu/g and the coercive force is 120 Oe. This saturation magnetization is equal to that of the CSFe glass-ceramics heat treated at 950 °C, whereas the coercitive force is lower (500 Oe for CSFe).The lower coercive force is attributed to the larger size of the magnetite crystallites.

The results of bioactivity evidences that an addition of Na_2O alone or in combination with B_2O_3 and P_2O_5 to the basic composition produces apatite formation on the surface of the heat treated glass in the simulated body fluid within 10-30 days (Figure3.18).

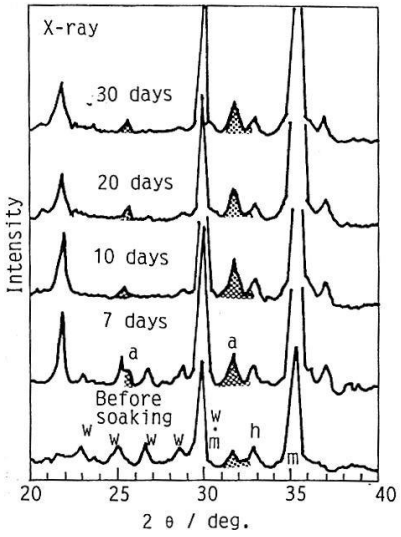

Figure3.18: Thin-film X-ray diffraction patterns of glass-ceramic CSFe + B soaked in simulated body fluid for various periods: m, magnetite; W, P-wollastonite; g, glassy phase.[13]

In another work Bretcanu et al. analyse the generation of magnetite at different melting temperature of glass ceramic belong to the system SiO_2–Na_2O–CaO–P_2O_5–FeO–Fe_2O_3. The material is produced using commercial reagents, melting and quenching process in the temperature range of 1400-1550 °C is performed.

The magnetic properties result to be strongly influenced by glass-ceramic microstructure, which depends on the melting temperature. As results the increasing of melting temperature up to 1550 °C allows the formation of the highest amount of magnetite, while the amount of hematite decreases (Figure 3.19). At 1500°C temperature the only crystalline phase is magnetite in an amorphous phase. No hematite is present at this temperature. Hematite is an unwanted phase because it does not possess magnetic properties since it is an antiferromagnetic material. [14]

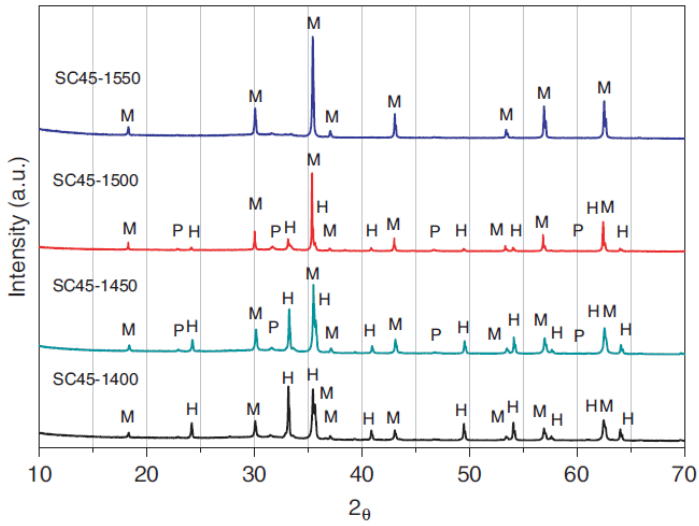

Figure 3.19: XRD patterns of ferrimagnetic glass-ceramic samples (M = magnetite, H = hematite, P = sodium calcium silicate).[14]

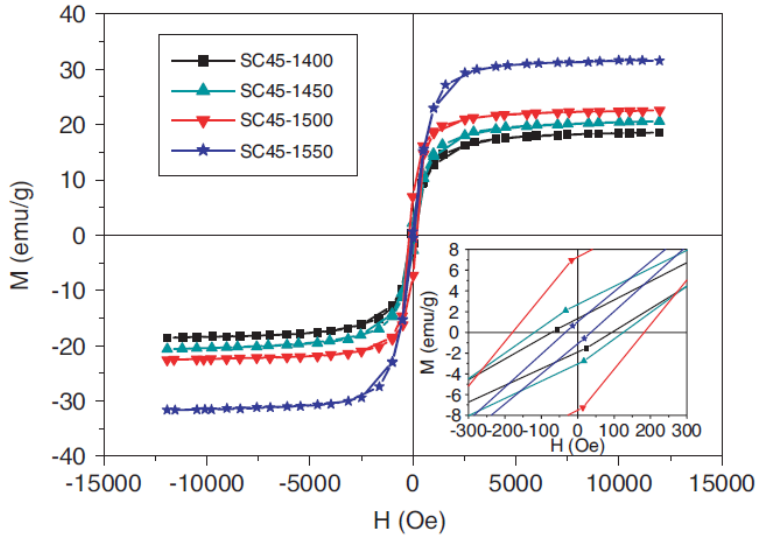

Figure3.20: Room temperature hysteresis cycles up to 12 kOe of glass-ceramic samples.[14]

The saturation magnetisation of different tested glass ceramic varies from 18.6 to 31.5 emu/g, while the coercive field varies from 35 to 180 Oe.(figure 3.20) SC45-1550 is the sample with the high saturation magnetization value.

Samples	Power loss (W/g)	ΔT (°C/g)
SC45-1400	28	40
SC45-1450	29	41
SC45-1500	61	87
SC45-1550	19	27
M 1400	27	39
M 1450	28	40
M 1500	25	36
M 1550	29	41

Table 3.2:calorimetric data of glass ceramic samples[14]

The highest power loss is obtained for sample SC45- 1500, which presents the highest hysteresis area, while the lower value is obtained for sample SC45-1550.(table 3.2)[14]

A ferrimagnetic glass ceramic is proposed by Saqlain et al. belong to a system $xZnO\text{-}25Fe_2O_3$ $(40x)SiO_2\text{-}25CaO\text{-}7P_2O_5\text{-}3Na_2O$, (x=4, 6, 8, 10). It is prepared by melt-quench method.

Magnetic induction measures is developed at 500 Oe and at 440 KHz , 1 g of sample is put in the center of coil with 20 ml of water in plastic container. The alternate magnetic field is switch on for 2 minutes.

The results indicate an increase of the power loss for X8 and X10 which is in agreement with the increase of hysteresis area and magnetic material for the same samples.(figure 3.21)

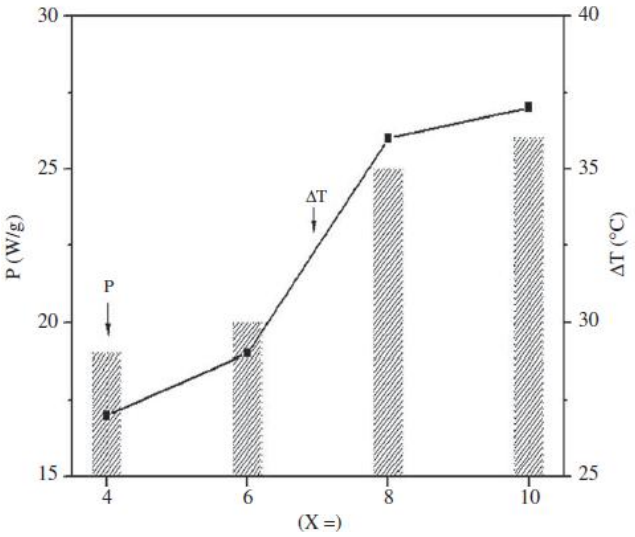

Figure3.21: variation of specific power loss and temperature as a function of iron oxide content.[17]

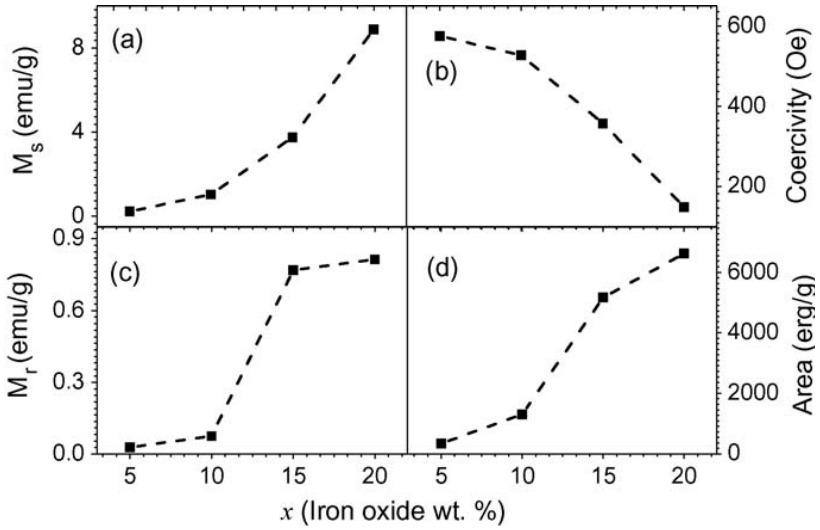

Figure3.22: Variation of room temperature (a) saturation magnetization, (b) coercive field, (c) remanent magnetization, and (d) area under the M–H loop of glassceramics as a function of iron oxide content.[17]

Figure3.22 collects the magnetic parameters obtained from the M–H cycles of samples with different iron oxide content. The increase in M_r, M_s and hysteresis area, and the decrease in H_C with an increase in iron oxide content can be attributed to increase in the amount and size of magnetite crystallites in the glass-ceramic samples. The area under the hysteresis loop increases with an increase in iron oxide content (figure. 3.22d). The area under the loop is proportional to the energy loss and hence the heat generated by a sample subjected to an alternating field. The results obtained indicate that samples with higher iron oxide concentration are capable of generating more heat for the same applied magnetic field.

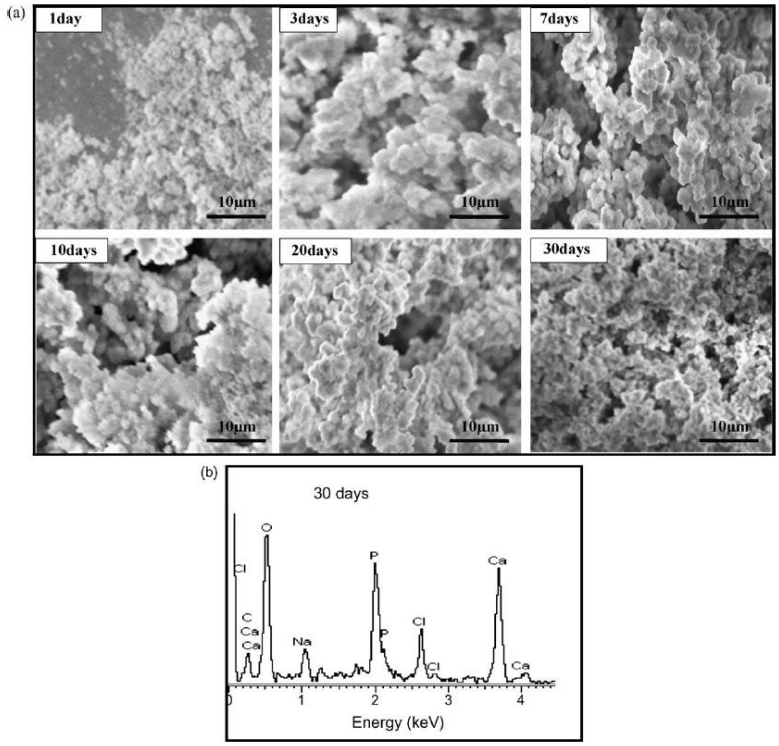

Figure3.23: (a) SEM micrographs of the surfaces of glass-ceramic sample with x = 15 wt.% soaked in SBF for various days (magnification: 1000×) and (b) EDS spectra of x = 15 wt.% soaked in SBF for 30 days.[17]

Figure3.23 reports the SEM micrographs of glass ceramic with x = 15% of iron oxide after soaking in SBF for 1 to 30 days. The images clarify the increasing of calcium and phosphorus precipitation on the glass surfaces by increasing immersion days in SBF. EDS analysis evidences the gradual formation of HA since at 30 days the Ca/P ratio is quite near to 1.67 which is closed to the value of HA. [17]

Leventouri et al. published a paper on a magnetic properties of a ferrimagnetic glass ceramic belong to the system $0,45(CaO,P_2O_5)$ $(0,52-x)SiO_2$ xFe_2O_3 $0.03Na_2O$ with different heat treatments. Four different types of glass are prepared as a function of iron oxide content.

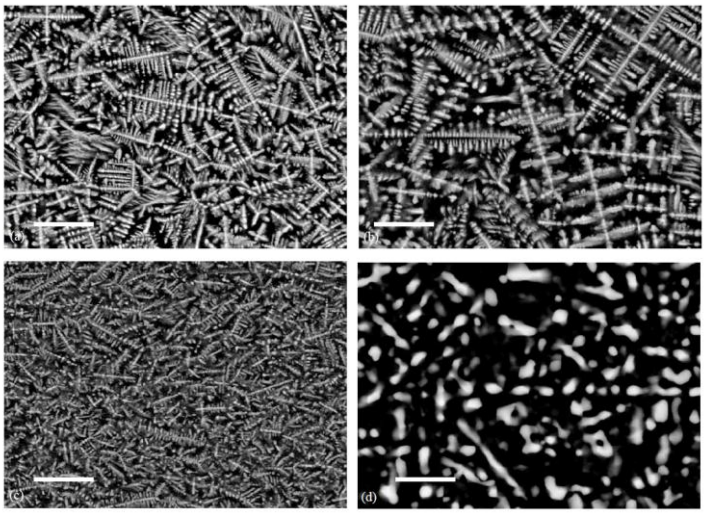

Figure 3.24: SEM images from samples of the series 20G presenting the effect of heat-treatment temperature on the microstructure of FBC: (a) as prepared,(b) heat-treated at 600 1C, (c) at 800 1C and (d) at 1100 1C. Bar is 2 mm.[18]

SEM analysis evidences a strong variation in the microstructure of glass in function of the composition and the heat treatment. The dendritic structure of magnetite crystals is well defined up to 800 °C and starts to break up at 1100 °C where only a trace of dendritic phase separation is seen. (figure 3.24)[18]

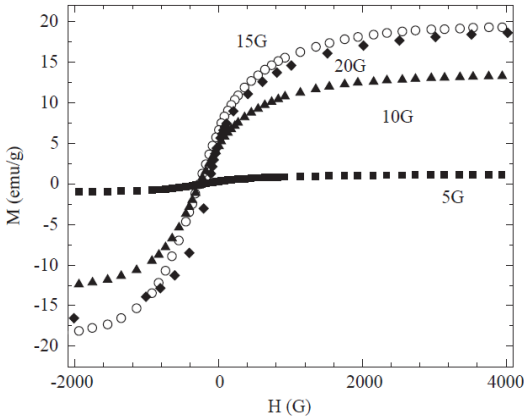

Figure 3.25: M–H plots of the samples with 5%, 10%, 15% and 20% molar fraction of Fe2O3 in the reacting oxides. The response in applied magnetic field H up to 4 kG is shown.[18]

The magnetization curved are reported in Figure 3.25 as a function of iron oxide content: by increasing the magnetic phase the value of saturation magnetization increases.

3.6. Structure of magnetite

Magnetite (Fe_3O_4) is a combination of two iron oxides FeO and Fe_2O_3 in 1:1 molar fraction. Magnetite is a representative ferrimagnetic material. The atoms of oxygen are packed in a face

centered cubic lattice, in which the iron atoms, smaller than oxygen, fill the interstices. (figure 3.26)

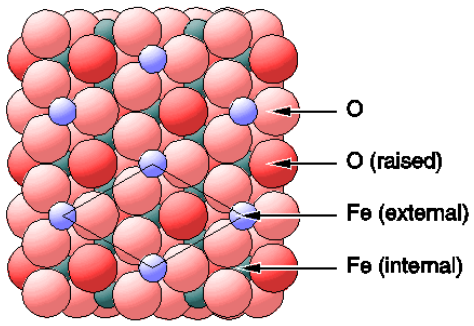

Figure 3.26:Crystalline structure of magnetite: The iron in tetrahedral position are in light gray while in octahedral position are in dark gray, the other atoms are oxygen [10]

In such way the oxygen around the metal ions occupying the corners of a tetrahedron or of an octahedron. The metal ions surrounded by an oxygen tetrahedron are in an A site and the metal ions surrounded by an octahedron are in a B site as it can be observed in figure 3.27.

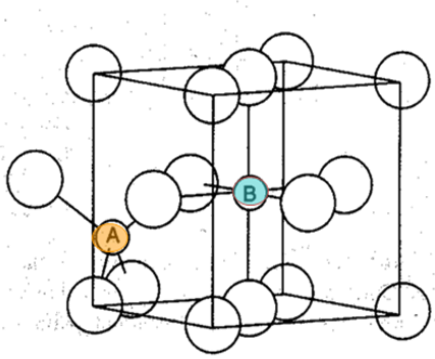

Figure3.27:Tetrahedral and octahedral cation sites in the crystal structure of magnetite (Fe_3O_4). In a tetrahedral site A the iron ion is surrounded by 4 atoms of oxygens while in octahedral site the iron ion is surrounded by six oxygen atoms.[10]

Magnetite has an inverse spinel structure, in which the tetrahedral sites are occupied by trivalent iron ions Fe^{3+} and the octahedral sites are shared by a 50:50 number of divalent Fe^{2+} and trivalent iron ions Fe^{3+}. To maintain charge balance to the four oxygens (O^{2-}), there are two $Fe^{3+}$and one Fe^{2+}. So all the divalent iron ions reside in the octahedral lattice sites, whereas the trivalent iron ions are split evenly between octahedral and tetrahedral sites. As it can be seen in figure 3.28, in the octahedral coordination, $Fe^{3+}$and Fe^{2+}ions are coupled ferromagnetically. The electron, whose spin is directed in the opposite direction of the others and coloured red, can be exchanged between two octahedral coordination. On the other hand, the Fe^{3+} ions in tetrahedral and

octahedral sites are coupled antiferromagnetically implying that the Fe^{3+} spins cancel out each other and thus only unpaired spins of Fe^{2+}in octahedral coordination contribute to the magnetization. This magnetic moment configuration explains the ferrimagnetism seen in magnetite.(figure 3.28)

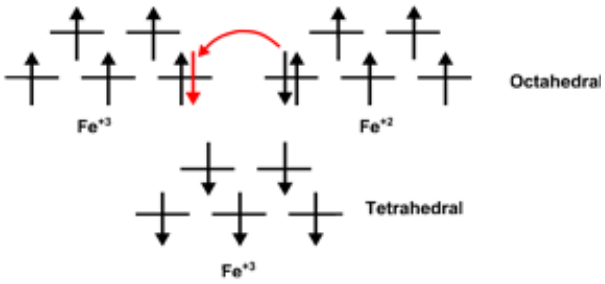

Figure 3.28: Schematic depiction of the splitting of the 5d orbitals in octahedral and tetrahedral coordination[10]

Magnetite is the unique crystalline phase which has magnetic properties among those presented in the glass-ceramics previously reported.

3.7. Doping of glasses with antibacterial effect

One of the main complication connected with bone diseases regards the problem of infection. The problem is quite diffused both when a hip prosthesis is implanted and a tumor is removed. After a surgical operation the area around the implant has a lower immune resistance to pathogens agents and for this reason it is sufficient a minimal bacterial concentration to give rise to an extended infection. If the problem is not considered the bacteria colonization bring to failure of the implant.

Escherichia Coli and *Staphylococcus aureus* are two examples of bacteria stains that have a high adhesion capacity on a biomaterial surface, the adhesion is favoured by the presence of porosity and roughness that facilitate the formation of a stable bond between bacteria and the surface. The most common bacteria encounter in infections belong to the family of staphylococci, in particular they are *Staphylococcus aureus* (Figure 3.29) and *Staphylococcus epidermidis* (Figure 3.30), the second is considered harmless lying naturally in the bacterial micro flora epidermal, however, in contact with biomaterials become particularly aggressive. The first can be found primarily on the surfaces of metal implants, while the second is typical of polymeric implant. A possible solution to avoid surface contamination consists in the treatment of the implanted material with antibiotics, but some disadvantage are connected with this prophylaxis as allergic

reaction, microbial flora decay and bacterial resistance. The last is the most important disadvantage because bacteria can develop a capacity to resist drug and so an antibiotic therapy can be completely ineffective as antibacterial treatment.

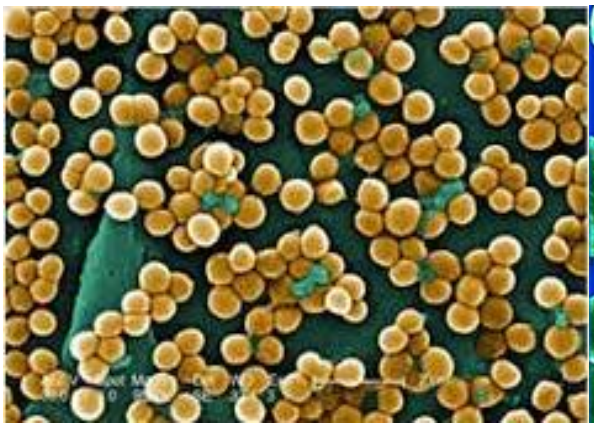

Figure 3.29: S*taphylococcus aureus*

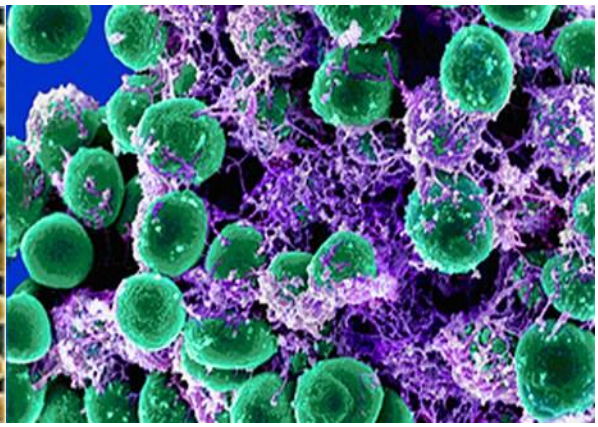

Figure 3.30: S*taphylococcus epidermidis*

Many researchers tried to solve this problem studying and developing biomaterials enriched with some ions, which posses antibacterial properties, like silver(Ag), copper(Cu) and zinc (Zn), and a multiple mechanism of action. One of the most important factor is the correct regulation of antibacterial ionic concentration in the body in order to avoid toxic reactions for healthy cells. One of the most common antibacterial agent is silver, since it has a broad spectrum antibacterial activity and exhibits few toxicological side effect.

3.8. Effect of silver on bacteria

As it is explained in Figure 3.31, silver ions interact with bacteria in different ways: the ions can penetrate cellular membrane, interact with the DNA and stop proliferation and division of bacterial cells.

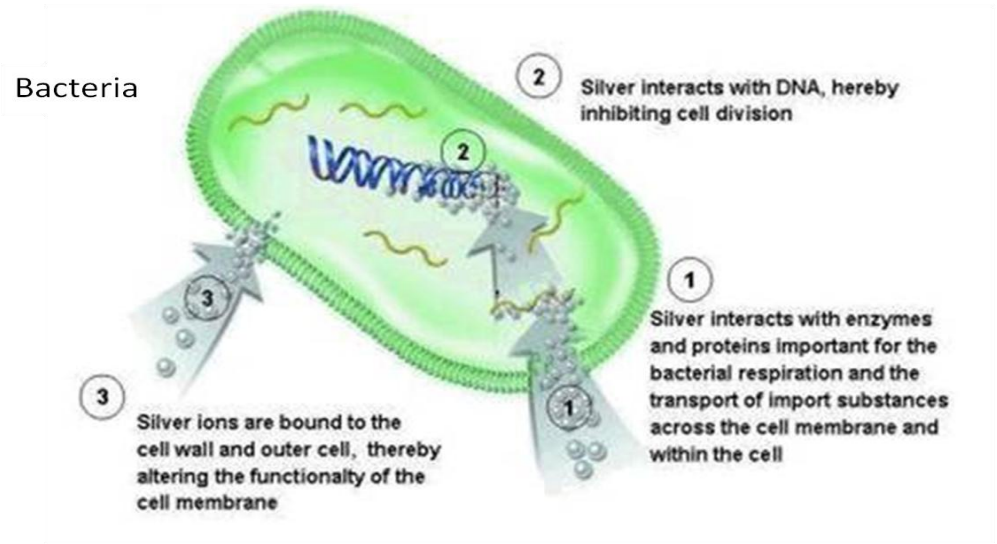

Figure 3.31:Effect of Ag ions with interact with bacteria: Mechanism of action of silver ions on bacteria. (1) The silver interacts with enzymes and proteins, cross the cell membrane and get into the cell. (2) interacts with DNA by inhibiting cell division. (3) is linked to the cell wall and inhibit the functionality of the membrane.

3.9. Effect of copper on bacteria

The antibacterial mechanism of copper has been attributed to the fact that copper ions are absorbed by the bacteria. First, the bacterial surface absorbs ions, which causes damage to the cell membrane and protein structure or by altering the enzymatic function; later the bacterial cells are immobilized due to the presence of ions and this leads to inhibition of the replication process and the subsequent cell death.(figure 3.32)[28]

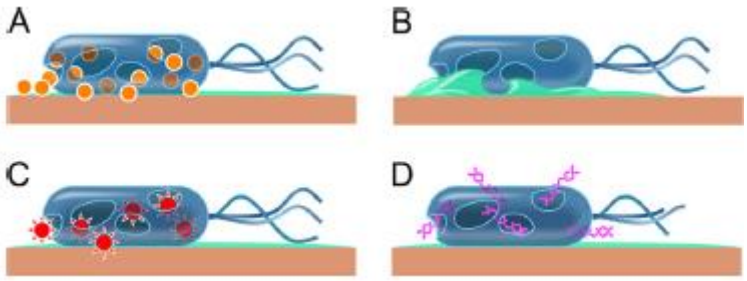

Figure3.32: Interaction between copper and bacteria: A. The copper diffuses from the surface towards the bacteria and cause cellular damage B. The breakage of the cell membrane due to the copper lead to a loss of cytoplasmic contents C. The copper ions lead to the generation of reactive species that cause further damage D. The bacterial DNA is degraded and the cells die. [27]

3.10. Silver ion doping techniques

Different techniques exist to dope glasses and glass-ceramics, among them the ion-exchange technique and the introduction of silver during the melting and quenching process are the most used processes. The ion-exchange process occurs when a glass/glass-ceramic has one mobile ions

A species that is exposed to a source (usually molten salts bath or aqueous solution) of a second diffusion mobile ion B species[3,19-26] (figure 3.33).

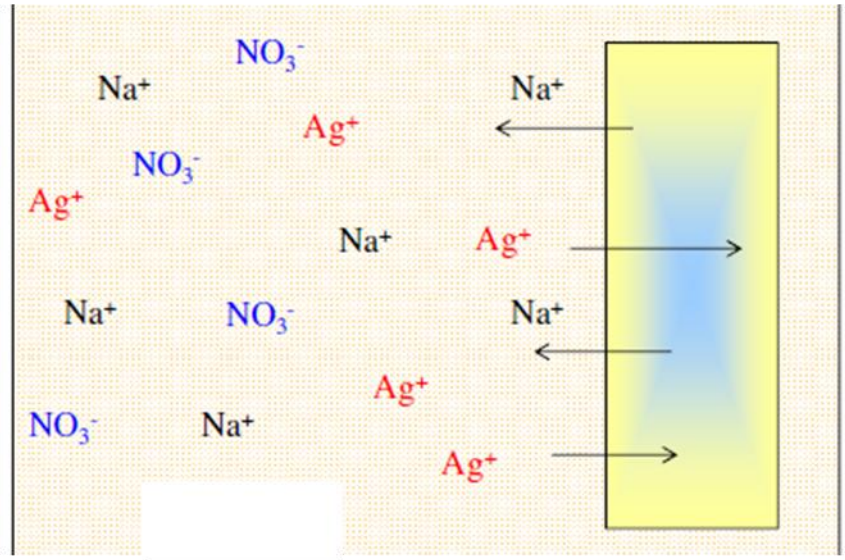

Figure 3.33:Ion exchange mechanism

The most important parameters that govern the ion exchange process are the molar concentration of the molten salts, the duration of the treatment and the temperature of the solution. The Houndle-Walter research group reported that the interdiffusion of cations in the soda lime glass strongly dependent on the concentration of the non bridging oxygen (NBO). Therefore, to improve the ion exchange process and to control precisely the silver distribution in the glass, it is necessary to understand the diffusion mechanism of silver and how it is influenced by the defects in the ion-exchange glass under heating and cooling.

At temperatures of < 100°C the growth rate of total silver (oxidized and metallic forms) is low, then it grows rapidly until 350 °C and finally slow down. The concentration of oxidized silver increases a little before 300 °C and then decrease until 450°C whereas the metallic silver increases steadily from room temperature to 450°C. [20]

It exists an inverse proportionality between the silver concentration in the molten salt and the time treatment. In fact an high silver concentration guarantees a low exposure time of the material while a low bath concentration implies a long ion-exchanging times. [21]

The silver surface content is both dependent on the ion-exchanging time and on the bath concentration.

The melting and quenching technique expects the use of a silver oxide that can be added in the glass composition. After that all the oxides that composed glass ceramic are melted and quenched

and silver has modified the chemical structure of the material conferring an antibacterial properties. Glass/glass ceramic can be potential carriers of antibacterial ions like silver because these material can accommodate these ions in their structure. Moreover they can induce nucleation in the glass matrix and affect the local arrangement of the particles. [36].

3.11. Copper ion doping techniques

Even for doping a glass/glass-ceramic with copper ions different techniques can be followed . Among them, ion exchange in molten salts and melting and quenching techniques are the most common ones. Ion exchange occurs when a monovalent alkali ions is typically replaced from ions present in a molten salt bath or an aqueous solution. It can be done by bringing glasses in contact with molten salt at a temperature below the glass transition temperature In this case univalent alkali ions in glass are ion-exchanged by copper ions, even if the oxidation state of copper is different respect to silver and it depends from the substrate composition. In fact, copper exchange process involves different copper states, Cu^{+} and Cu^{+2} or the possible formation of either Cu or Cu_2O clusters critically depending on both glass and bath composition as well as on the process parameters [30].

The diffusion profile of copper inside the glass does not follow the common ordinary diffusion equation because of the presence of different copper oxidation states that have different mobility.[28] Generally, higher-valent cations are difficult to diffuse in and out though glasses compared to monovalent cations such as alkali [31].

When a monovalent copper salt is employed as an ion exchange medium the Cu^{+}/R^{+} prevails and Cu^{2+} ions which are found in glasses ion-exchange in air are formed by the oxidation of Cu^{+} ions depending on glass basicity. [28-35].

The melting and quenching technique, even for doping with copper, expects the use of a copper oxide (CuO or Cu_2O) that can be added in the glass or glass ceramic composition. After that, all the oxides are melted and quenched and copper has modified the chemical structure of the material.[37]

3.12. Antibacterial and ferrimagnetic glass-ceramics

Some researchers developed a glass ceramic with antibacterial properties, by different chemical process, in order to permit the release of silver or copper ions and inhibit bacterial growth and proliferation.

Sharma et al. propose a silica glass containing magnetite as mayor crystalline phase with the addition of silver by melt quenching tecnique, they propose a structural and magnetic investigations. Moreover the authors study the antimicrobial effect of the ferrimagnetic glass ceramic. The glass belong to the system $25SiO_2$–$(50\text{-}x)CaO$–$15P_2O_5$–$8Fe_2O_3$–$2ZnO$–x Ag (where x = 0, 2 and 4 mol%). Two different heat treatment are performed: one with annealing treatment that produce a magnetic annealed glass ceramic (MAGC) and the other without annealing that produced a magnetic glass ceramic (MGC) For each heat treatment three samples are synthesized respect to Ag %mol. The XRD analyses (figure 3.34) evidences the presence of magnetite, hematite, calcium silicate and calcium phosphate as crystalline phases but not silver or silver compound in every glass formulations are detected.

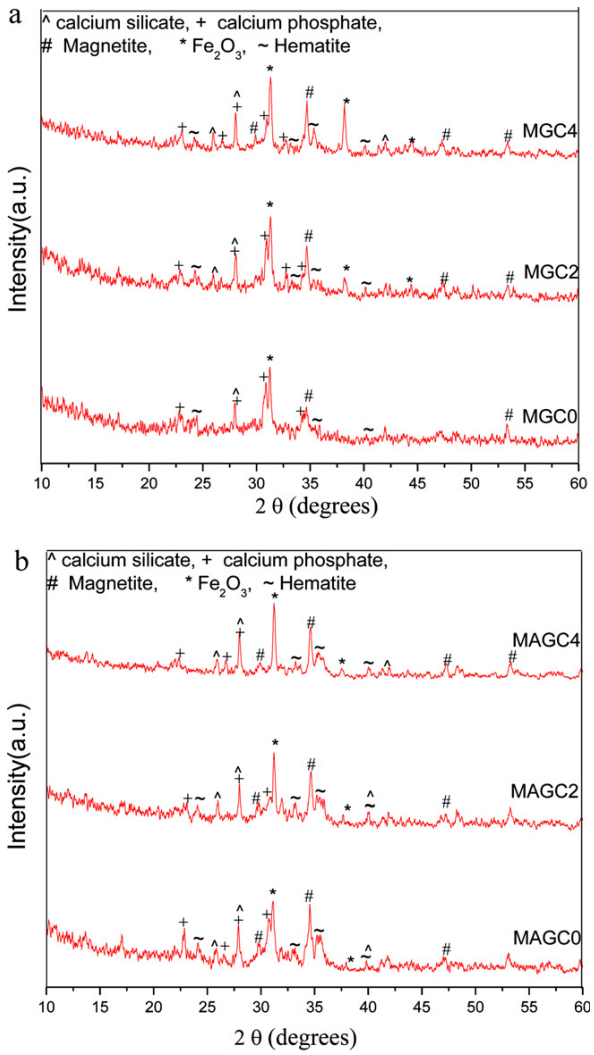

Figure 3.34: XRD patterns of glass-ceramics with different Ag ion concentration (a) MGC, (b) MAGC [36]

Glass-ceramics	Coercive field (Oe)	Remanence magnetization (emu g^{-1})	Saturation magnetization (emu g^{-1})
MGC0	102	0.08	0.75
MGC2	100	0.09	0.78
MGC4	166	0.95	4.34
MAGC0	8	0.056	3.3
MAGC2	14	1.28	3.1
MAGC4	35	1.2	4.4

Table 3.3: Magnetic parameter estimated by M-H loops of glass-ceramics samples.[36]

The magnetic characterization are shown in Table 3.3. Silver behaves as a nucleating agent and promotes nucleation and crystallization of magnetite crystals in the amorphous glass matrix. The fact is confirmed by increasing of saturation magnetization both on samples without annealing (MGC4) and with annealing treatments (MAGC0, MAGC2, MAGC4).

Concentration (%, w/v) of glass in LB broth	Colony forming unit (cfu ml^{-1}) in presence of MGC2	Colony forming unit (cfu ml^{-1}) in presence of MGC4
1	7.4×10^8	3.7×10^8
5	2.1×10^6	1.6×10^5
10	4.5×10^3	Nil
15	2.3×10^2	Nil
20	Nil	Nil

Table 3.4 Antibacterial test of glass ceramic (MGC) samples against E. Coli[36]

Ag ions released from the glass matrix may attach to the negatively charged bacterial cell wall and damage it, leading to cell death. It has also been hypothesized that oxygen associates with silver reacts with the sulfhydryl (S-H) groups on cell wall to form R-S-S-R bonds, subsequently blocking cellular respiration and causing cell death.

The antibacterial activity of Ag containing glass-ceramics is evaluated using *E. coli* , and the observations are shown in Table 3.4 . The glass-ceramic containing 4% Ag shows complete inhibition of bacterial growth at a concentration of 10% (w/v). However also the glass-ceramic containing 2% Ag shows the similar effect at 20% (w/v).[36]

Another group of researchers present a study regard the influence of copper oxide (CuO) on a magnetic properties of glass ceramic belongs to a system of $Fe_2O_3 \cdot CaO \cdot ZnO \cdot SiO_2$.syntetized with melt and quenching technique. They evaluated phase separation, microstructure, amount and crystalline size of magnetite after controlled crystallization by gradual addition of CuO to the glass composition and with different heat treatments. No antibacterial tests were performed.

The XRD performed after a melting temperature between 1450°C and 1455°C as a function of copper oxide reviled the presence of magnetite as the unique crystalline phase up to 5 mg of CuO present in the sample. Increasing the amount of CuO at 10g, 20g and 30g in the glass ceramic compared cuprite (Cu_2O) and delaffosite ($CuFeO_2$) as further crystalline phases . From reference pattern the magnetite peaks in these spectra resulted a little bit shifted.

Other samples underwent an heat treatment at 800 °C for 2 hours or 8 hours and a new M2 magnetite phase was detected. Heat treatments favours the crystallization of cuprite (Cu2O) and delaffosite (CuFe2O) with the increasing of CuO, reducing the formation of magnetite.

Analysing the crystallography parameters, the replacement of Fe by Cu results in a decrease of the cubic parameter. The a-axis shrinks due to the smaller ionic radius of Cu^{2+} (0.57 Å) cations, which substitute Fe^{3+} (0.65 Å).

The increase of Cu amount , heat treatment applied and substitution of Fe ions by Cu ions imply an increase in crystallized magnetite but not in crystalline size .

Sample no.	Heat treatment parameters °C/h	Coercivity (Hci) G	Magnetization (Ms) emu/g	Retentivity (Mr) emu/g
0.5 Cu	800/8	41.78	4.84	0.183
5 Cu	800/8	34.26	15.88	0.785
30 Cu	800/8	27.69	9.35	0.393
30 Cu	800/2 in air	32.72	10.78	0.583
30 Cu	800/2 under reducing atm.	22.98	10.65	0.422
5 Cu	800/2	19.96	12.79	0.353
30 Cu	Without heat-treatment	21.88	19.63	0.765

Table 3.5: Magnetic parameter of some selective samples[37]

The magnetic characterization are reported in table 3.5. The samples without heat treatment show maximum saturation magnetization.[37] Adding CuO > 10 g/100 batch there is a separation of large amount of delaffosite ($CuFeO_2$) phase causes decreasing in the amount of Fe ions present for magnetite crystallization, so, M_s is decreased in 30 Cu than in 5 Cu (800 °C/8 h) sample. The formation of delaffosite reduces the magnetic signal because the iron ions are not in a spinel structure.

3.13. Reference

1. Vernè E, Biomaterial Lessons.
2. Slavo VM ,Proprietà dei vetri, Università degli Studi di Trento.
3. Shelby JE, Introduction to Glass Science and Technology 2nd Edition , RCS Advancing the chemical sciences, 2005.
4. Hench LL, Jones JR, Sepulveda P, Bioactive materials for tissue Engineering Scaffolds. In: Pollak JM, Hench LL, Kemp P, editors.Future strategies for Tissue and Organ Replacement. Singapore :Word Scientific Pub.Co Inc;2002:3-24.
5. Smeacetto F, Ph.D course Vetri innovativi e componenti a base di vetri innovativi, 2013-2014.
6. Hench LL, Bioceramics, J. Am. Ceram. Soc., 1998; 81(7): 1705–1728.
7. Jones JR, Clare AG, Bio-Glasses An Introduction Wiley, A John Wiley & Sons, Ltd, Publication, 2012.
8. Hench LL, Genetic design of bioactive glass , J Eur Ceram Soc 2009; 29: 1257–1265.
9. Hench LL, Wilson J, An Introduction to Bioceramics 2nd ed. London: Word Scientific;1999:285-344.
10. Fiorillo F, Introduzione ai materiali magnetici, Istituto Elettrotecnico Nazionale Galileo Ferraris, Torino, 2002.
11. De Arenas IB, Schattner C, Vàsquez M, Bioactivity and mechanical properties of Na_2O-CaO-SiO_2-P_2O_5 modified glasses, Ceram Interl, 2006; 32: 515–520.
12. Bretcanu O, Spriano S, Brovarone Vitale C, Verne' E, Synthesis and characterization of coprecipitation-derived ferrimagnetic glass-ceramic, J Mat Sci 2006; 41: 1029–1037.
13. Ebisawa Y, Miyaii F, Kokubo T, Ohura K, Nakamura T, Bioactivity of ferrimagnetic glass-ceramics in the system FeO-Fe_20_3-CaO-$Si0_2$ Biomat 1997: 18; 1277-1284.
14. Bretcanu O, Verne´ E, Coisson M, Tiberto P, Allia P, Magnetic properties of the ferrimagnetic glass-ceramics for hyperthermia. J Magn and Magn Mat, 2006; 305: 529–533.
15. Yano T, Azegami K, Shibata S, Yamane M, Chemical state of oxygen in Ag^+/Na^+ ions-exchanged sodium silicate glass. J of Non Crystal Sol 1997; 222:94-101.

16. Saqlain AS, Hashmi MU, Alam S, Shamim A, Magnetic and bioactivity evaluation of ferrimagnetic $ZnFe_2O_4$ containing glass ceramics for the hyperthermia treatment of cancer, Journal of Magn and Magne Mat 2010; 322: 375–381.
17. Singh RK, Srinivasan A, Bioactivity of ferrimagnetic $MgO–CaO–SiO_2–P_2O_5–Fe_2O_3$ glass-ceramics, Ceram Intern 2010; 36: 283–290.
18. Leventouri Th,, Kisb AC, Thompson JR, Andersond IM, Structure, microstructure, and magnetism in ferrimagnetic bioceramics, Biomater, 2005; 26: 4924–4931.
19. Yano T, Azegami K, Shibata S, Yamane M, Chemical state of oxygen in Ag^+/Na^+ ion exchange sodium silicate glass. Journal of Non-Crystalline Solids , 1997;22:94-101.
20. Wang PW, Zhang C, Thermal Behaviour of Silver in Ion-Exchange Soda-Lime Glasses , J Amer Soc , 1997; 80(9): 2285-93.
21. Di Nunzio S, Vitale Brovarone C, Spriano S, Milanese D, Vernè E, Bergo V, Maina G, Spinelli P, Silver containing bioactive glasses prepared by molten salt ion-exchange, J of the Eur Ceram Soc 2004;24:2935-2942.
22. Vernè E, Di Nunzio S, Bosetti M, Appendino P, Vitale Brovarone C, Maina G, Cannas M, Surface characterization of silver-doped bioactive glass, Biomater 2005;26: 5111-5119.
23. Catan F, De Sousa Meneses D, Blondeau JP, Allam L, Structural changes of Ag+-Na+ ion exchange soda-lime glasses investigated by scanning electron microscopy and infrared reflectivity, J of Non-Cryst Sol 2008;354:1026-1031.
24. Araujo RJ, Likitvanichkul S, THibault Y, Allan , Ion exchange equilibria between glass and molten salts , J of Non-Cryst Sol 2003;318:262-267.
25. Yamane M, Shibata S, Yasumori A, Yano T, Takada H, Structural evolution during Ag^+/Na^+ ion exchange in a sodium silicate glass, J of Non-Cryst Sol 1996;203:268-273.
26. Newby PJ, Gendy REI, Kirkham J, Yang XB, Thompson ID, Boccaccini AR, Ag-doped 45S5 Bioglass-based bone scaffolds by molten salt ion exchange: processing and characterization, J of Mat Sci : Mat in Med 2011; doi 10.1007/s10856-011-4240-8.
27. Grass G, Rensing C, Solioz M, Metallic Copper as an Antimicrobial Surface ,Appl Environ Microbiol 2011; 77(5):1541- 1547.
28. Gonnella F, Caccavale F, Bogomolova MD, D'Acapito F, Quaranta A, Experimental study of copper-alkali ion exchange in glass, J App Phys, 1998; 83 (3):1200-1206.

29. Gonnella F, Quaranta A, Padovano S, Sada C., D'Acapito F, Maurizio C, Battaglin G, Cattaruzza E, Copper diffusion in ion-exchange soda-lime glass, App Phys 2005; 81: 1065-1071.
30. Gonnella F, Quaranta A, Cattaruzza E , Padovani S, Sada C, D'Acapito F, Maurizio C, Cu-alkali ion Exchange in glass: a model for the copper diffusion based on XAFS experiments, Comput Mat Sci 2005;33:31-36.
31. Yoko T, Nishiwaki T, Kamiya K, Sakka S, Copper Alkali ion Exchange of Alkali Aluminosilicate glasses in Copper-Containig Molten Salt: I Monovalent Copper Salt CuCl, J.Amer. Cer. Soc 1991; 75: 1104-11.
32. Yoko T, Nishiwaki T, Kamiya K, Sakka S, Copper Alkali ion Exchange of Alkali Aluminosilicate glasses in Copper-Containig Molten Salt: II Divalent Copper Salts CuCl2 and CuSO4, J.Amer Cer. Soc,1991; 75 :1112-15
33. Sakka S, Kamira K, Kato K, Incorporation of copper into glass by the Cu-Na ion exchange, J of Non Cryst Sol 1982 ;52 :77-90.
34. Yoko Y,Kamichi K,Ishino Y, Copper Alkali ion Exchange of Alkali Aluminosilicate glasses in Molten CuCl An ion exchange controlled by the Cu^{+}=Cu^{++} oxidation reaction in glass, Communications of the American ceramic society,1894.
35. Borsella E,Del Vecchio A,. Garcia MA, Sada C, Gonella F, Polloni R, Quaranta A, Van Wilderen LJGW, Copper doping of silicate glasses by the ion-echange tecniques: A photoluminescence spectroscopy study, J of Appl Phys, 2002;91:90-98.
36. Sharma K, Meena SS, Saxena S, Yusuf SM, Srinivasan A, Kothiyal GP, Structural and magnetic properties of glass-ceramics containing silver and iron oxide, Mat Chem and Phys 2012; 133:144– 150.
37. Abdel-Hameed SAM, Marzouk MA, Abdel-Ghany AE, Magnetic properties of nanoparticles glass–ceramic rich with copper ions. J of Non-Cryst Sol 2011; 357: 3888–3896.

Chapter 4

Composite ferrimagnetic bone cements

4.1. Composite bone cements

In this chapter it is presented the state of the art of the ferrimagnetic bone cement for the care of bone tumor using magnetic hyperthermia. In these composites cements a magnetic phase is embedded in a polymeric matrix in order to develop a cement that can be used as bone filler or for the fixation of prosthetic devices.[1-8]

4.1.1. Magnetic bone cements

A poly-methyl-methacrylate bone cement loaded with Fe_3O_4 particles is proposed by Kawashita et al. and the evaluation of the composite properties is performed[1]. Magnetite particles have an average particle size of 5 µm, while spherical PMMA powder has an average molecular weight of 270 kDa. PMMA powder/MMA liquid weight ratio is 2/3. Three different cement formulations are synthesized with 40 %wt (M-40c),50%wt (M50c),60 %wt (M60c) of magnetite micro particles added to a polymer matrix.

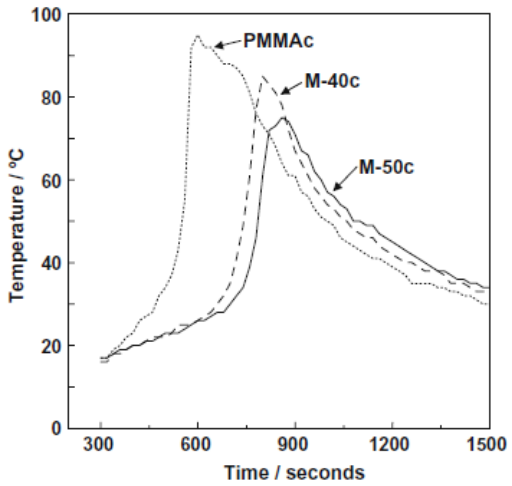

Figure 4.1: Changes in the temperature of the cement samples during the setting reaction.[1]

The reduction of maximum polymerization temperature occurred with an increased of magnetic microparticles (figure 4.1).

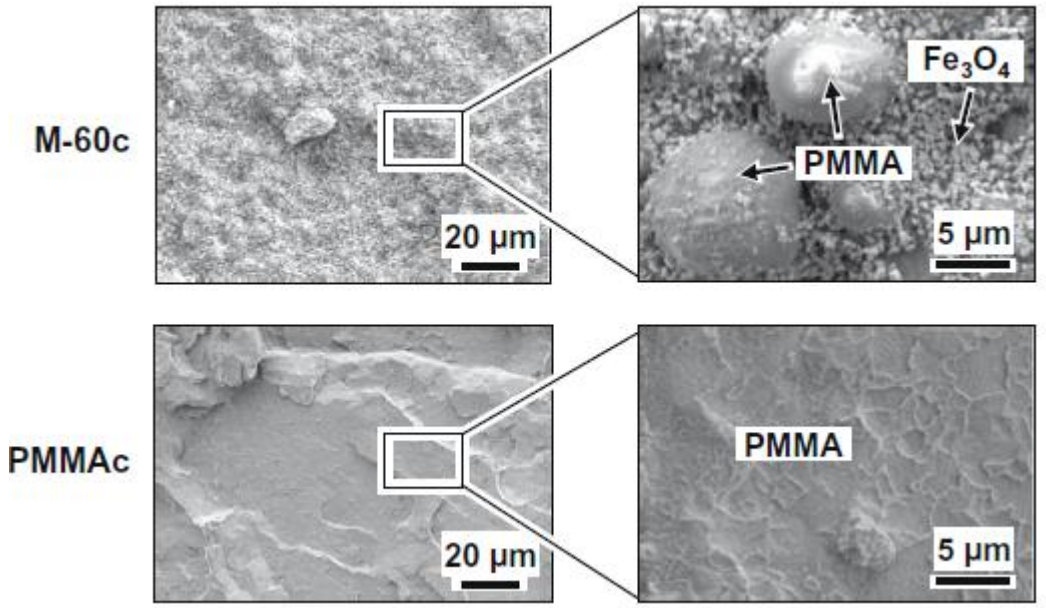

Figure4.2:SEM analysis of cross- sectional areas of the cement samples.[1]

The SEM analysis evidences no chemical interaction between PMMA and magnetic microparticles that are dispersed uniformly in the polymer .(figure 4.2)

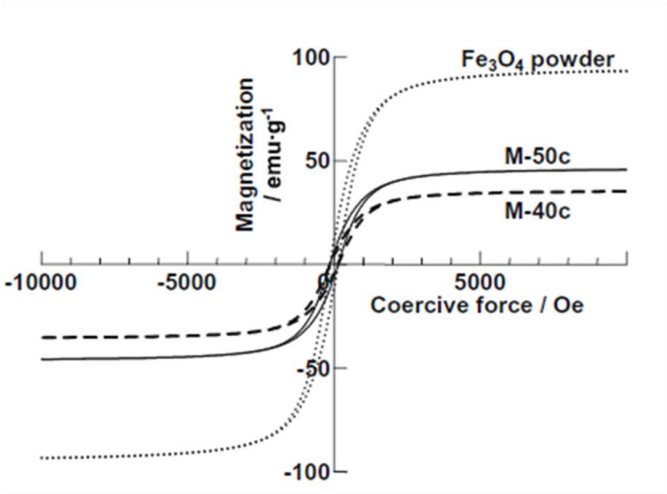

Figure 4.3: Magnetization curves of Fe_3O_4 powder and sample M-50c and M-40c under magnetic fields of 10 kOe

Figure 4.3 reports saturation magnetization curves of Fe_3O_4 powder and samples M-40c and M-50c in magnetic fields of 10 kOe, It can be seen in figure 4.3 that the Fe_3O_4 powder is ferromagnetic, with a saturation magnetization value of M_s = 83 emu g^{-1} and a coercive force of Hc = 141 Oe. This value of M_s is close to that of bulk magnetite M_s = 89– 95 emu g^{-1}. Figure 4.3 also shows that sample M-40c have an M_s of 35 emu g^{-1} and an H_c of 139 Oe, while sample M-50c has an M_s of 46 emu g^{-1} and an H_c of 143 Oe

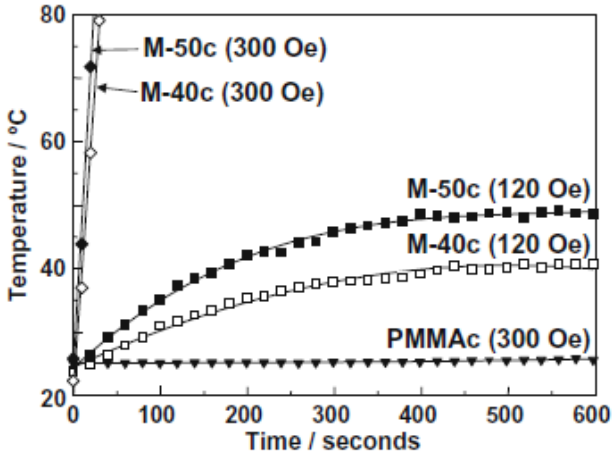

Figure4.4: Calorimetric curve of different samples at different alternating magnetic field of 120 and 300 Oe at 100 kHz[1]

The surface temperature of the control sample (PMMAc) remains constant in a magnetic field of 300 Oe, whereas the surface temperature of samples M-40c and M-50c increases over 70 °C within a very fast time with the same magnetic field. While using a magnetic field of 120 Oe, the surface temperature of samples M-40c and M-50c reached around 40 and 48 °C within a period of about 8 min (figure 4.4). These last temperatures are in agreement with the hyperthermic treatment .

Li et al. propose [2] a PMMA bone cement loaded with different size of Fe_3O_4 nanoparticles (300, 35, 11 nm). They assess mechanical strength, biocompatibility and heating capability. The heat generation strongly depends on the dimension of the magnetic nanoparticles and from applied magnetic field and frequency.

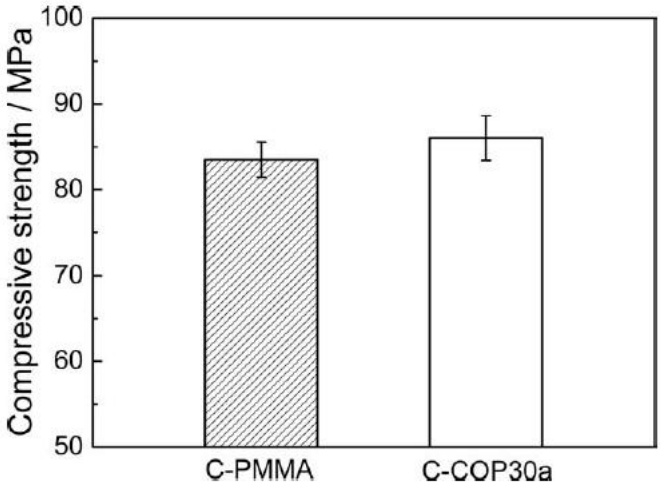

Figure4.5: Compression strength without and with magnetite nanoparticles.[2]

The inclusions of magnetic nanoparticles into the PMMA matrix by 30% wt do not decrease compression strength (figure 4.5).

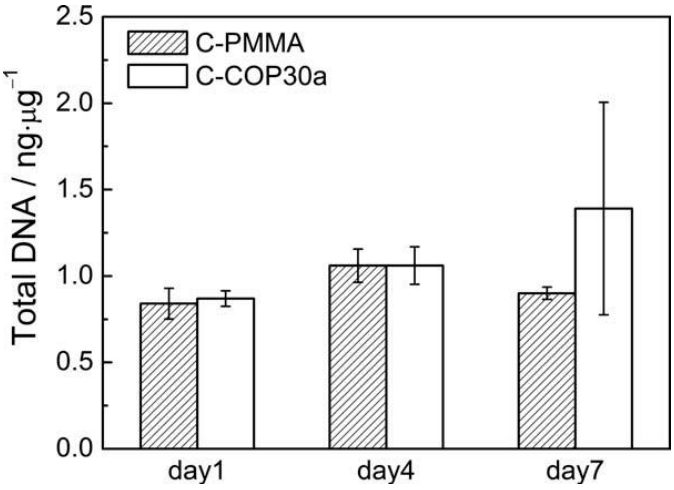

Figure4.6: The total DNA concentration of Rat-1 fibroblast cells adhered on cement discs. Data are shown as the mean 6 SD (n ¼ 5). p > 0.05 indicates no significant increases in the DNA concentration measured until day 7 of the culture for both types of cement discs.[2]

From a biological point of view, the DNA analysis evidences no inhibition effect on cell proliferation connected with magnetite nanoparticles.(figure 4.6)[2]

Tang et al report the synthesis of Fe_3O_4 nanoparticles by chemical co-precipitation method. After that the nanoparticles are embedded into PMMA matrix and four type of cement are prepared (table 4.1) [3].

Cement	Powders(g)		Liquid(ml)
	Fe_3O_4	PMMA	MMA
PMMAc	0	20	10
PF-10	2	18	10
PF-20	4	16	10
PF-30	6	14	10

Table 4.1: Composition of PMMA based cements containg Fe_3O_4 powders

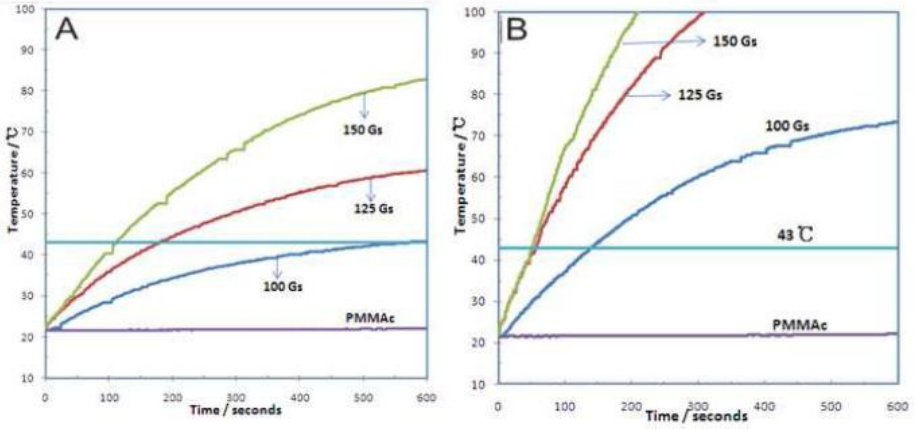

Figure 4.7: Surface temperature change of PMMAc, PF-10 (A), PF-20 (B) in the AMF of 100 Gs, 125 Gs,150 Gs at a frequency of 500 kHz[3]

The *in vitro* heat generation is shown in figure 4.7. In the first graph is reported the sample with the lowest amount of magnetite nanoparticles at three different applied magnetic field. The best result is obtained at 100 Gs after 600 s where the sample reaches the necessary superficial temperature for cells apoptosis (43°C-45°C) In figure 4.7b is reported the heating capability of PF-20 sample. It can be noticed how the temperatures reached at three applied magnetic field are too high respect to the hyperthemic treatment.[3]

A clinical study on a treatment of bone metastasis is developed and reported by Matsumine et al.[4] They divide the patients in three groups: patients who undergo to hyperthermia treatment with a magnetic material (HT group). Two control group: one who undergo to palliative operation (OP group) without postoperative radiotherapy and another who undergo an operation in combination with postoperative radiotherapy (OP+RT group).

The HT group is divided into two sub-categories: eight patients with a very critical tumor situation, are treated with an intramedullary nail reinforcement without any stripping of metastatic lesion. Eight patients, who are expected to have a better clinical situation, after lesion removing, followed a prosthetic substitution or reinforcement with a metal intramedullary nail or plate (n = 7). Calcium phosphate cement (CPC) containing Fe_3O_4 powders is implanted into the cavity.[4]

An alternating electromagnetic field generator is developed with 1.5 MHz in fixed frequency. The intensity of the magnetic field is modulated in order to obtain a temperature of around 43°C at the interface bone-implant. Hyperthermic treatment is performed postoperatively on days 8,10,12,15,17, 19,22,24,26,and 29. The exposure time is 15 min per day.

	HT (%)	Op (%)	Op + RT (%)
Excellent	8/16 (50)	0	7/22 (32)
Good	6/16 (37)	3/8 (38)	13/22 (59)
Poor	2/16 (13)	5/8 (62)	2/22 (9)

HT a group treated with hyperthermia, *Op* a group treated with palliative operation, *Op + RT* a group treated with operation in combination with postoperative radiotherapy

Table4.2: Radiographic outcomes[4]

About 50% of patient treated with hyperthermia improved their quality of life.(table 4.2)

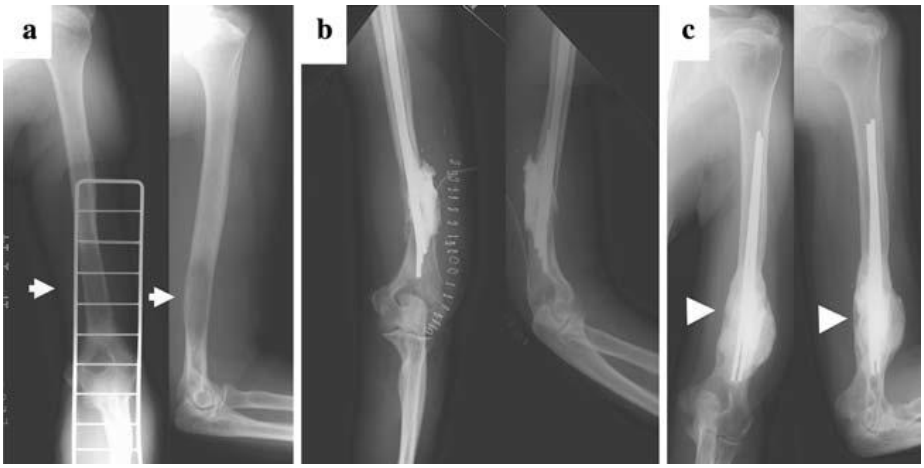

Figure4.8: 63-year-old patient with metastatic lung cancer to the humerus (arrow). (b) After curettage of the lesion followed by reinforcement with intramedullary wire, CPC containing Fe3O4 was implanted into the cavity. (c) At 6 months after undergoing hyperthermia, massive new bone formation has become visible (triangle) [8]

Figure 4.8 reports a solution in the treatment of bone metastasis: the patient presented cancer formation in the homerus (see fig 4.8a). The surgical operation provides the implant of a metallic reinforcement with the addition of CPC with magnetite (see fig 4.8b). The heat is monitored at surface of a cortical bone using a thermometer.[4] After 6 mouth of hyperthermia treatment a new massive bone formation is seen in the radiograph(figure 4.8c).

4.1.2. Magnetic and bioactive bone cements

Takegami et al. propose a bone cement containing silica particles and magnetite powder embedded in a bis-GMA based resin composed of bis-a-glycidylmethacrylate and triethylene-glycol dimeth-acrylate.(figure 4.9). The average particle size of the magnetic powders is 13 μm and for silica glass powder is 3 μm[5]

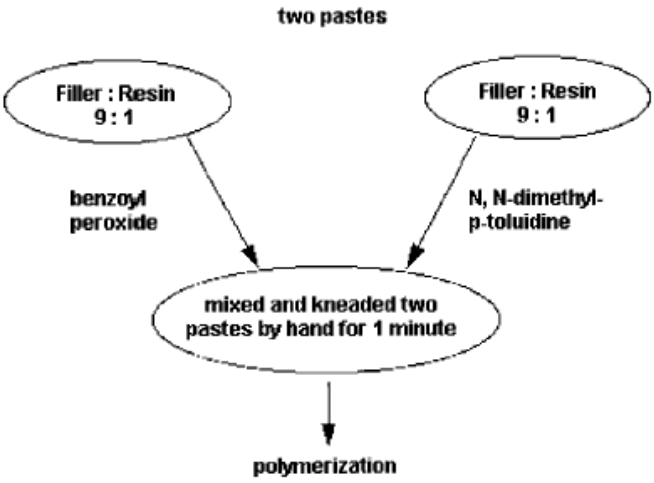

Figure 4.9: Ferromagnetic bone cement. Filler: magnetite powder and silica glass powder. Resin: bis-a-glycidymethacrylate and triethylene glycol dimethacrylate[5]

As previously mentioned, one of the most important properties of this type of magnetic material is the ability to generate heat under stimulating of an alternate magnetic field. The energy generated from hysteresis cycle is transformed into heat with a consequently increasing of temperature of the surrounding tissues.[5]

The heat generation of ferrimagnetic bone cement is evaluated as a function of the amount of magnetite, volume of the cement and intensity of magnetic field.

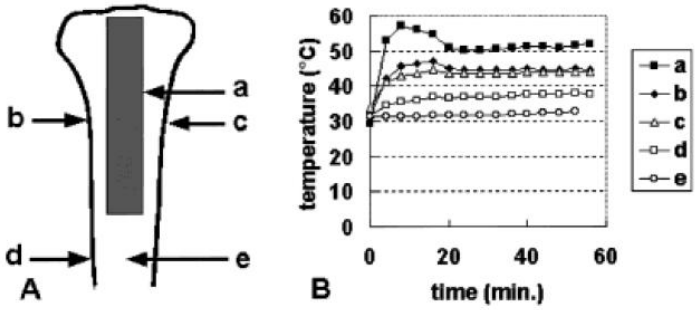

Figure 4.10: (A) The position of sensors in the rabbit tibiae. (B) Time/temperature curve. a, the surface on the cement; b–d, the interface between bone and muscle; e, medullary canal[5]

Figure 4.10 shows the results of distribution of heat into the bone. The cement is injected in a rabbit tibiae and five temperature probes are located in different areas of the bone. The sensors are at the surface of the cement (a), at the interface between bone and muscles (b-d) and in the medullary canal (e). The results evidence a correlation between the position of the sensor an the

temperatures measures. For e sensor which is the farthest from the heat source the temperature profile remain flat at 37°C.[5]

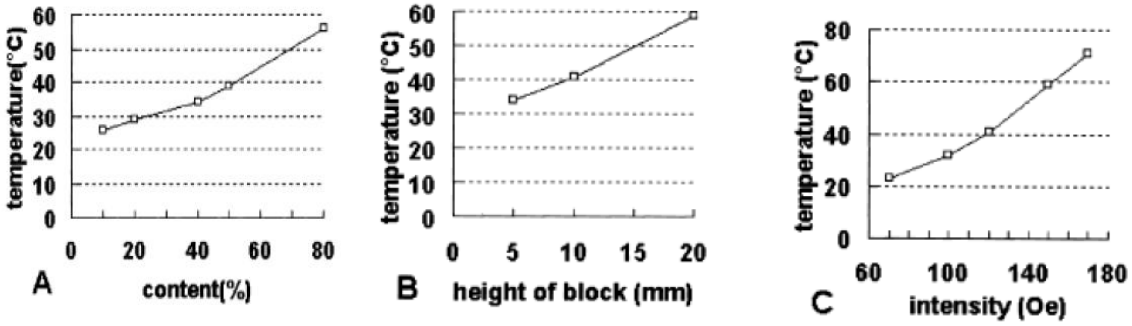

Figure 4.11: (A) Relationship between temperature and content of magnetite with a magnetic field of 80 Oe) . (B) Relationship between temperature and volume. Volume is shown as the height of the block (base of block, 20x20 mm; content of magnetite, 40%; magnetic field, 100 Oe) . (C) Relationship between temperature and intensity of magnetic field (block, 20x 20 x 5 mm; content of magnetite, 40%) .[5]

Figure 4.11 shows the temperature increase as a function of content of magnetite, volume of the cement and intensity of the magnetic field.

For the control of the hyperthermia treatment exists an inverse correlation with time and temperature, if high temperature, about 50°C, are obtained the heating will maintained for few minutes .If temperature reaches 43°C it can heat even for 1 hour in order to avoid local recurrence. [5]

Other authors realize an electromagnetic field generator at a fixed frequency of 1,5 MHz[6]. They synthesize a bone cement loaded with a glass ceramic that is partially substituted by magnetite Fe_3O_4 powder.

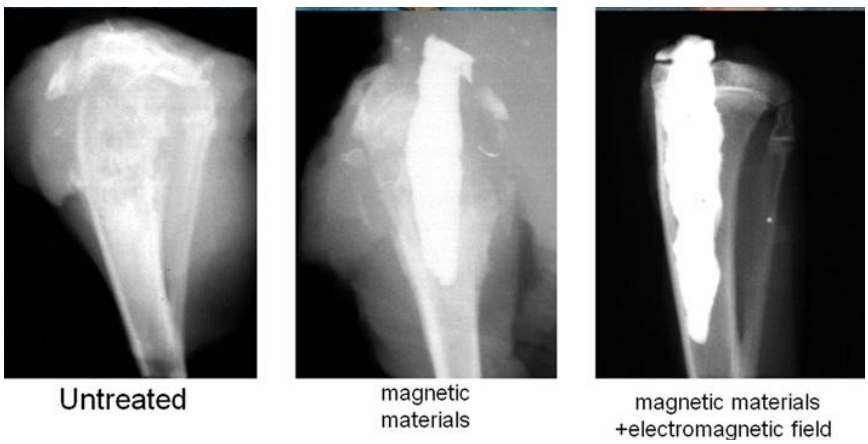

Figure 4.12: Three different behaviour of a bone tumor: left panel show a bone tumor untreated, in the middle a bone tumor with an injection of magnetic material an on the right panel a double effect of a magnetic material with the stimulation of an electromagnetic field.[6]

They introduce tumor cells into a tibia of rabbits and evaluate the status of bone by X-ray radiographies in three different situations: without cement implant, with magnetic cement and with cement + hyperthermia treatment. In the first situation the tumor proliferates and massive bone destruction is observed. Instead when magnetic material and an electromagnetic field are applied for 50 minutes the bone tumor is sensibly reduced as it can be observed in figure 4.12. The cement is composed by 60% wt. of magnetite.[6]

Portela et al. proposed a ferrimagnetic silicate cement (FC) with high amount of iron oxide, with the following oxides chemical composition (%wt) : 10 SiO_2, 2 Al_2O_3, 52 Fe_2O_3, 0.6 MgO, 33 CaO, (SO_3+K_2O) R. The maximum powder/water combination ratio (3:2) is used. Paste flows and the product is able to be injected.[7]

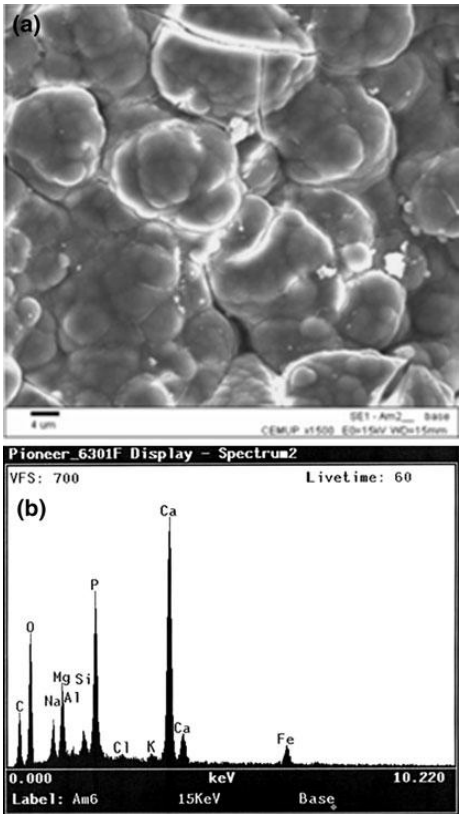

Figure 4.13:Ferrimagnetic cement immersed in normal SBF. A Precipitates covering the initial surface . b The precipitation of Ca and Mg phospjate compound is detected. All the initial cement peaks of Si and Fe decreased and a high peak of P can be observed[7]

Figure 4.13 reports the results of bioactivity test, as it can be noticed a large layer of apatite precipitates on cement surface after the immersion in SBF for 4 days. In the EDS spectrum the Ca and P peaks are higher than silica and iron, demonstrating the precipitation of precipitates rich in Ca and P.[7]

They test the injectability of the cement evaluated as the ratio between volume of paste ejected from a syringe respect to a total volume of paste before ejection. After a determination of a suitable powder liquid ratio an injectability value is found during 5 min after mixing.[7]

Kusaka et al. propose a cement composed by a a resin (bis-*a*-glycidymethacrylate) and magnetite and silica powders as filler phase. They introduce a tumoral mass into a hole create into a tibia of a rabbit. After seven days they open the wound, tumor is removed and the defect is filled with cement. Nine rabbits are exposed to a magnetic field for 50 min with an hyperthermic treatment (HT group) and 9 animals are not exposed to the magnetic field (non-HT group). After the animals sacrifice the maximum circumference of the skinned leg is measured to record tumor growth.[8]

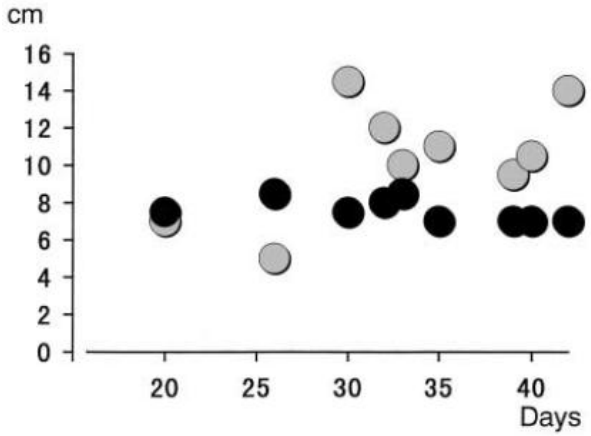

Figure 4.14: Maximum circumference of the skinned leg as a function of time after inoculation of VX2 tumor in hyperthermic therapy (HT) group (*black circles*) and non-HT group (*gray circles*). A significant difference is shown between groups ($P < 0.05$)[8]

In figure 4.14 back dots are values of leg diameter subject to an hyperthermic treatment while the gray dots represented the non HT group as a function of time.[8] Size of leg do not change with time for treated rabbit and remain between 6-8 cm while measure of non-treated legs increase over 8 cm. The maximum diameter is 16 cm. [8] The hyperthermic treatment stabilized the tumor and do not induce its proliferation

The object of the present research activity regards an experimental study on a new magnetic and bioactive bone cement .

4.2. Reference

1. Kawashita M, Kawamura K, Li Z, PMMA-based bone cements containing magnetite particles for the hyperthermia of cancer, Acta Biomat 2010; 6: 3187–3192.
2. Li Z, Kawamura K, Kawashita M, Kudo T, Kanetaka H, Hiraoka M, In vitro assessment of poly(methylmethacrylate)-based bone cement containing magnetite nanoparticles for hyperthermia treatment of bone tumor, J Biomed Mater Res Part A 2012:00A:000–000.
3. Tang Z, Wang X, Pan L, Hu Y, Wu Y, Zhang J, Cui S, Kang J, Tang J, Preparation and Characterization of PMMA-based Cements Containing Magnetic Nanoparticles for the Magnetic Hyperthermia, Adv Mater Res 2013;647: 155-159.
4. Matsumine A, Kusuzaki K, Matsubara T, Shintani K, Satonaka H, Wakabayashi T, Miyazaki S, Morita K, Takegami K, Uchida A, Novel hyperthermia for metastatic bone tumors with magnetic materials by generating an alternating electromagnetic field , Clin Exp Metastasis 2007; 24:191–200.
5. Takegami K, Sano T, Wakabayashi H, Sonoda J, Yamazaki T, Morita S, Shibuya T, Uchida A, New ferromagnetic bone cement for local hyperthermia, J of Biom Mater Res, 1998; 210-214.
6. Matsumine A, Takegami K, Asanuma K, Matsubara T, Nakamura T, Uchida A, Sudo A, A novel hyperthermia treatment for bone metastases using magnetic materials, Int J Clin Oncol 2011; 16: 101–108.
7. Portela A, Vasconcelos M, Branco R, Gartner F, Faria M, Cavalheiro J, An in vitro and in vivo investigation of the biological behavior of a ferrimagnetic cement for highly focalized thermotherapy, J Mater Sci: Mater Med 2010; 21:2413–2423.
8. Kusaka M, Takegami K, Sudo A, Yamazaki T, Kawamura J, Uchida A, Effect of hyperthermia by magnetite cement on tumor-induced bone destruction, J Orthop Sci 2002; 7: 354–357.

Aim of the work

The European Society for Hyperthermic Oncology (ESHO) officially recognizes the hyperthermia treatment in oncology as "the therapy which uses the generation of a higher temperature at a tumor-involved region of the body". This approach uses a variety of temperature ranges (from 39 – 40 °C up to 80 – 90 °C) and, accordingly, a great number of techniques to induce those temperatures under well-controlled conditions.

During the past, physicians have tried to utilize artificial temperature elevations for the treatment of various diseases, included tumor diseases, but due to the complexity of interactions, the attempts were often too unspecific to be really successful.

Today it is widely recognized that a large number of intracellular processes exist with a specific temperature-dependent behaviour.

For example, there is evidence of:

- Enhancement of anti-tumor effects of various drugs and radiation (typically in the range 40-43°C)
- Induction of immunological processes (39 – 41 °C, fever range)
- Induction of gene expression and protein synthesis (40 – 42 °C)
- Influencing the tumor microenvironment in a way that makes the tumor better accessible for some therapies.

The most beneficial contribution of hyperthermia for oncological treatments is based on the enhancement of the effectiveness of other treatments (radiotherapy, chemotherapy, radio chemotherapy, gene therapy, immune therapy etc) without additional toxicity.

Taking into account the state of the art regarding the problem of bone tumours, the materials developed for their care and the techniques for their application, in the following chapters the new approach developed during my PhD research activity will be presented.

The research is intended to study and develop an innovative multifunctional composite material useful for the treatment of the primary and secondary bone tumours, by means of non-invasive hyperthermia, and for the prevention of the associated complications, such as osteoporosis, osteomyelitis and inflammation.

The principal aim of the research was to develop a composite bone cement which possess at the same time biocompatibility, bioactivity, ferromagnetic properties and suitable mechanical properties. A further aim, developed in the last part of the experimental work, was the modification of one constituent of the bone cement with antibacterial ions.

The developed material is a composite PMMA-based bone cement. The polymeric matrix is a commercial cement produced and distributed by Haeraus Medical (Germany). The added phase is a glass ceramic powder developed and realized in the laboratory of the Department of Applied Science and technology (DISAT) at Politecnico di Torino. The glass ceramic belongs to a system $Na_2O–CaO–SiO_2–P_2O_5–FeO–Fe_2O_3$.

The proposed material possess several innovative characteristics compared to previously developed formulations, both in academia and industry, and have strong potential for the treatment of the primary and secondary bone tumours. It can be used as fillers for bone cavities, even of complex shaped, promises faster restoration of functionality, reduces the frequency of infection and provides an opportunity to apply hyper-thermal therapy, without additional surgical operation, in order to kill the tumor cells, which were not surgically removed or those formed during an eventual relapse

The innovation concerns the development of the glass ceramic to be added to the polymeric matrix, which can contribute to the resolution of three important problems connected with bone tumor: poor mechanical and biological interaction between bone and implant, poor efficiency of radio- and chemotherapy as well as other hyperthermia treatments of bone tumor (ultrasound or microwave) and bacteria colonisations. The osteointegration of the implant is imparted by the glass-ceramic composition. Ferrimagnetic properties confer the ability of generate heat under an alternate magnetic field in order to kill tumor cells that can appear after implantation. Antibacterial properties conferred by the chemical modification of the glass-ceramic with silver and copper ions are aimed to avoid or reduce osteomyelitis, which are often associated to bone tumours surgery. The peculiarity and the surplus value of the proposed material, respect to the actual commercial and experimental formulations, is to simultaneously perform several functions by the addition of a single dispersed phase to the polymeric matrix.

Chapter 5
Materials and methods

5.1. Design of the Research

The research was designed to be developed in sequential steps in order to obtain progressive confirmation of the feasibility of the main aim.

First step

In the first step synthesis and characterization of the bioactive and ferromagnetic glass ceramic (identified in the following with the abbreviation SC45) were performed:

- Optimization of melting parameter in order to obtain a high degree of crystallized magnetite into the glass-ceramic
- Morphological and compositional analysis with Scanning Electron Microscopy (SEM) and energy dispersion spectroscopy (EDS)
- Study of the crystalline phase with X-ray diffraction pattern (XRD)
- Estimation of % wt. of formed magnetite with different methods based on :
    - Calorimetric measurements
    - XRD analysis with an internal standard calibration curve
    - Quasi static electro-magnetic tests with hysteresis loops
- Elemental mapping of chemical atomic compound

Second step

In the second step the synthesis and characterization of the composite bone cements was performed, by adding different %wt (10%,15%, 20%) of bioactive and ferrimagnetic glass-ceramic to a commercial PMMA matrix (identified in the following with the abbreviation P10-P15-P20) by:

- Morphological and Compositional evaluations with SEM and EDS
- Mechanical tests:
    - Uniaxial Compression test according ISO 5822-2002 standard
    - Four point bending test according ISO 5822-2002 standard
- Analysis of surface fractures after bending tests
- Setting time evaluation according ISO 5822-2002 standard
- Calorimetric measurement for the quantification of heat generation
- Analysis of the glass-ceramic and porosity distribution with Micro Computed Tomography (MicroCT)

- Hysteresis cycles on both the SC45 and the composites with high and low external magnetic field
- Impedance measurements for the evaluation of dielectric and magnetic permittivity

Third step

In the third step an *in vitro* characterization of the composites was performed by:

- Bioactivity tests after soaking in SBF for one month
- Iron leaching tests
- Cytocompatibility tests

Fourth step

In the fourth step the effect of heating on both health and tumoral cells up to 40- 43 °C by an external alternating magnetic field was evaluated.

Fifth step

In order to add antibacterial properties to the material, the SC45 glass-ceramic was doped with silver and copper ions with two different methods:

- **Melting and Quenching**:
    - 3% wt of Ag_2O was added in the glass composition, identified as SC45 3Ag
    - 5% wt of CuO was added in the glass composition, identified as SC45 5Cu

With the follow characterizations:

- XRD analysis
- SEM and EDS analysis
- Calorimetric measures
- Hysteresis cycles at low and high external magnetic field
- Antibacterial tests with inhibition halo

- **Molten salts ion exchange**

The synthesis considered three different molar concentrations of silver and copper used for doping SC45:

- Na/Ag = 2000 [mol/mol], identified as SC45 Ag2000
- Na/Ag = 200 [mol/mol], identified as SC45 Ag200
- Na/Ag = 20 [mol/mol], identified as SC45 Ag20
- Na/Cu= 2000 [mol/mol], identified as SC45 Cu2000

- Na/Cu= 200 [mol/mol], identified as SC45 Cu200
- Na/Cu= 20 [mol/mol], identified as SC45 Cu20

With the follows characterizations:

- XRD analysis
- SEM and EDS analysis
- Calorimetric measures
- Antibacterial tests with inhibition halo

5.1.1. Production of the glass-ceramic (SC 45)

The chemical composition of SC 45 is reported in table 5.1. It contains SiO_2, CaO, Na_2O and P_2O_5 in the same ratio as the bioactive glass 45S5 (Bioglass®) [1], with the addition of two different types of iron oxides. The amounts of two iron oxides were chosen to obtain the formation of a high amount of magnetite (ideally the theoretical value of 45 wt%). This value was optimized by previous studies as a good trade-off between heat capacity generation and bioactivity of the material [2-4]. Magnetite is a ceramic phase that confers a ferrimagnetic behaviour to a glass. The chemical composition of the glass ceramic is reported in table 5.1.

Fe_2O_3	FeO	SiO_2	CaO	Na_2O	P_2O_5
31	14	24,7	13,5	13,5	3,3

Table 5.1: Glass ceramic composition (%wt)

For the synthesis of the glass-ceramic high purity raw materials were used: Na_2CO_3 (Sigma-Aldrich) with a purity ≥99,5%, $CaCO_3$ (Sigma-Aldrich) with a purity ≥99, SiO_2 (Sigma-Aldrich) with a purity ≥99%, $Ca_3(PO_4)_2$ (Fluka) with a purity ≥96%, $FeSO_4*7H_2O$ (Sigma-Aldrich) with a purity ≥99% and Fe_2O_3 (Sigma-Aldrich) with a purity ≥99%. Each component was weighted and, before melting, the powder reagents were mixed in a flask on a mixing roller for 15 minutes.

As reported in Bretcanu et al.,[2] the reactants were melted in a platinum crucible at 1550°C inside a high temperature furnace (Nabertherm - Carbolite 1800) for 25 min, using a heating rate of 10°C/min. The melt was cooled at room temperature in air and poured into a brass mold, obtaining partially crystallized (glass-ceramic) bulk samples. As reported in [2], the value of melting point permitted a high conversion of iron oxide in magnetite. The obtained bulk samples were polished with SiC abrasive paper P320 and P600 in order to remove the thin oxide layer that often formed on their surface.

The bulk was milled and sieved to reach a grain size below 20 μm. The milling process was performed with a Planetary Ball Mill (Vibratory Micro Mill PULVERISETTE 0 Fritsch) in a Zirconia jar and the milling conditions were optimized in order to minimize the production of particles of grain size < 5 μm (checked by SEM analysis). Specific Particle size was chosen because previous studies demonstrated that a particle size <5 μm is characterized by high agglomeration phenomena and,

on the contrary, too many larger particles can cause a decrease in the mechanical properties of the final sample.

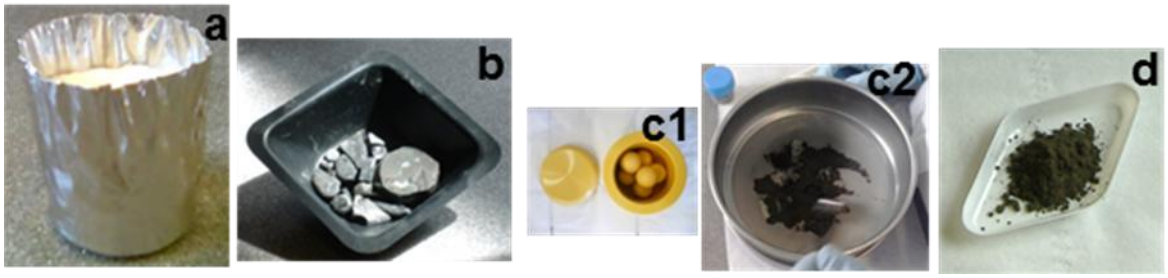

Figure 5.1: Synthesis steps for the glass ceramic production with melting and quenching technique : Reagents in a platinum crucible(a), pouring on plate (b), milling (c1) and sieving up with 20 micron mesh sieve (c2), ferrimagnetic glass ceramic powder < 20 µm (d).

Figure 5.1 shows a summary of all the SC45 glass ceramic production steps.

5.1.2. Production of the composite (P10, P15, P20)

The composite cements were synthesized using a commercial Poly methyl methacrylate (PMMA)-based cement with medium viscosity (Palamed®, produced by Heraeus Kulzer S.r.l.) containing zirconium dioxide (ZrO_2) as radio-opaque phase. The Palamed® cement is commercialized in a kit with one packet of a solid phase containing poly-(methylacrylate, methylmethacrylate), ZrO_2, benzoylperoxide, colorant E141 and one ampoule of liquid containing methyl methacrylate, N,N-dimethyl-p-toluidine, hydroquinone, colorant E141.

The commercial cement was prepared by manually mixing the polymer powder component with the liquid monomer component. A ductile dough was formed, which cured within a few minutes. The ratio of PMMA powder/ MMA liquid used was 2 g/ml as specified in the product technical data sheet.

Composite bone cements were produced adding different wt% of glass-ceramic (10, 15, 20 wt%) using a solid phase (PMMA+ SC 45)/liquid phase (MMA) ratio of 2 g/ml and these were identified as P10, P15 and P20, while the commercial formulation was named control.

The mixed powders were put in an orbital shaker for at least one hour, in order to obtain a good level of homogenization. Subsequently, they were mixed with the liquid monomer for 30 s to start

the polymerization reaction. The dough was put into a polished aluminum mold (100x100x5mm with 25 holes of 10mm in diameter) and after hardening the samples were extruded.

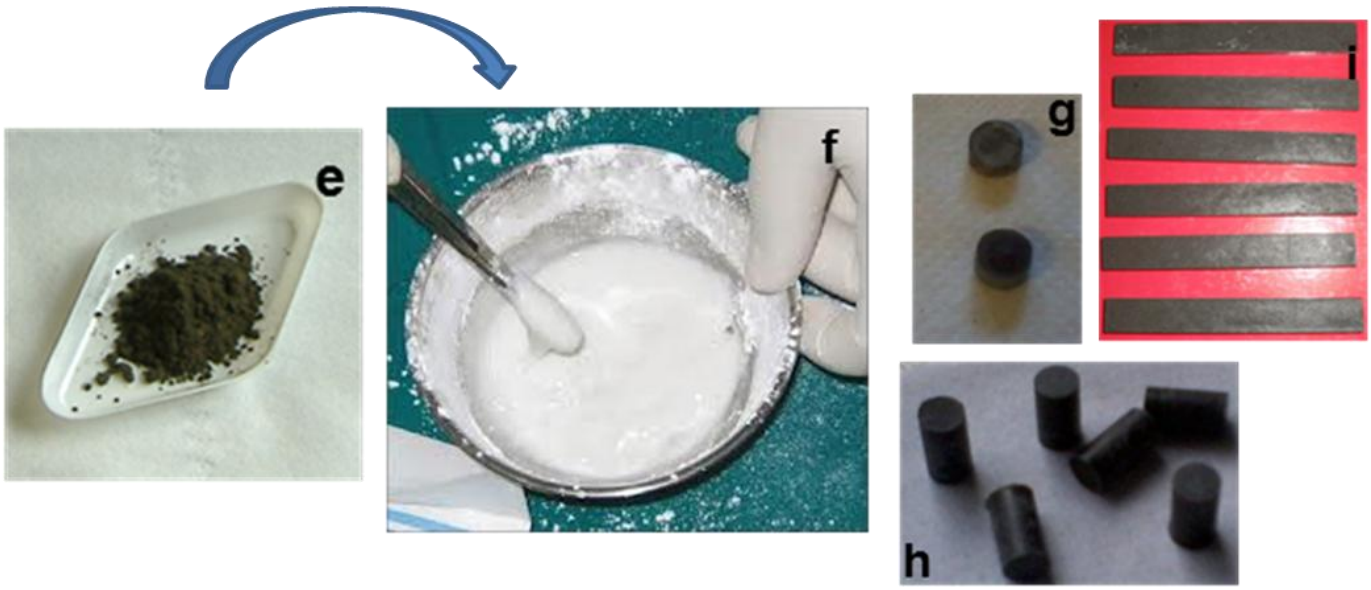

Figure 5.2: Synthesis steps of magnetic bone cement production: manual mixing with PMMA/MMA + SC45 < 20 µm in different % wt proportion (10-15-20) (e-f). After setting and extrusion from mould , different samples are prepared for different test: compression test (h), bioactivity and calorimetric tests (g), four point bending test (i).

As for the glass ceramic, figure 5.2 shows the composite bone cement synthesis process and all different size and dimension of the prepared samples.

It was chosen to start with three different synthesis of composite bone cement in order to evaluate which formulation could be the best trade-off among all the next characterizations.

5.1.3. Glass ceramic characterizations

The complete structural, morphological-compositional and in vitro characterization of the glass-ceramic was performed in previous works.[2,6] Here the attention was focused on the identification of the real magnetite percentage in the glass-ceramic, as already done on similar materials obtained by co-precipitation derived precursors.[7]

In order to identify the real wt% of magnetite inside the residual amorphous glass matrix three different methods were used: X-ray diffraction (XRD), calorimetric tests and saturation magnetization of the hysteresis cycle.

5.1.4. X-ray diffraction

The first method consists in the realization of a calibration curve calculated as an interpolation of the single points using fluorite (CaF_2) as an internal standard. The single points were obtained by performing the XRD analyses of samples containing 0%, 25%, 50%, 75%, 100% of pure magnetite with 20% wt of CaF_2, mixed in an amorphous phase (powders) of Bioglass® 45S5, simulating the composition of the magnetic glass-ceramic synthetized in this work (the values are the mean of three measurements). The obtained diffraction data patterns of the mixtures were fitted and the intensity ratio between the (311) magnetite diffraction line and (111) fluorite line was determined and plotted against the weight fraction of magnetite. The ratio increases with the increasing % wt of pure magnetite powder with respect to a constant % wt of CaF_2. The same amount of CaF_2 was added to the SC 45 sample and XRD analysis was performed. The value is a mean of three measurements.

The crystalline phase in the glass-ceramic was analysed by Philips X'Pert diffractometer with CuKa radiation, using a step of 0,02 (2θ) with a scan step time of 1 s. The diffraction lines were identified using the ''X'Pert High Score'' program, with the PCPDFWIN database (2002 JCPDS- International Centre for Diffraction Data). The profile fitting of the diffraction pattern was performed by using the same software in order to determine the crystalline phase.

5.1.5. Calorimetric test

The second method was based on a calibration curve obtained by calorimetric measurements.

The single points were obtained performing heating cycle of samples containing 0%, 25%, 50%, 75%, 100% of pure magnetite mixed in an amorphous phase (powders) of bioactive glass 45S5, simulating the magnetic glass-ceramic composite. The cycle was performed with an induction furnace, Egma 6, product by FELMI S.r.l at 48mT (1 kW) for a constant time of 3 min and registering the initial and final temperature before and after the heating with a digital thermocouple (Datalogger Tersid). All the measurements were performed in 10 ml of distilled water.

5.1.6. Saturation magnetization

The third method was based on the evaluation of the hysteresis loops of the glass ceramic and the pure magnetite. Then the %wt of magnetite crystalized into the amorphous glass network was calculated as the ratio between the saturation magnetization value of SC45 with respect to a values of pure magnetite with the following formula:

$$\%Magnetite = \frac{MsSC45}{MsFe_3O_4} * 100 \quad (5.1.1)$$

Where

Ms SC45 = Saturation magnetization at 800 kA/m of the SC45

Ms Fe_3O_4 = Saturation magnetization at 800 kA/m of the pure magnetite

The particles of magnetite (Sigma-Aldrich) have a dimension < 5 μm.

Hysteresis cycles were measured up to 800 kA/m by means of a DC magnetometer/ AC susceptometer (Lakeshore 7225) equipped with a Cryogen-Free Magnet at room temperature in quasi static condition. At 800 kA/m the hysteresis cycles both of SC45 and of the pure magnetite were already closed and so it was possible to determine the saturation magnetization values.

5.1.7. Composite bone cement characterizations

5.1.8. Morphological and compositional characterization

A morphological and compositional analysis was developed on composite bone cements (P10, P15 and P20) by SEM-EDS techniques in order to investigate the glass ceramic dispersion in the PMMA matrix. The analyses were performed both on the surface and on the section of the samples.

5.1.9. Calorimetric tests

In order to estimate the heating ability of the composite bone cements, they were subjected to calorimetric measurements using an alternate magnetic field and detecting the increase in temperature of a volume of water containing the samples. The test was developed using a magnetic induction furnace Egma 6 (Felmi S.r.l) generating a magnetic field intensity in the range 0– 118 mT at fixed working frequency of 220 kHz. For each cement formulation (P10, P15, P20) two composite samples were put inside a glass test tube with a diameter of 10 mm and a height of 160 mm.

The samples were immersed in 10 ml of distilled water and the initial temperature T_{in} was measured with a thermocouple. Then, the tube containing the samples was positioned in the middle of the coils of the inductor. A magnetic induction of 48mT was applied and the final temperature T_{fin} was measured after 2, 4, 6, 8, 10 and 12 min. After each measurement the samples were cooled in air at room temperature (figure 5.3).

The same test was repeated three times for each cement formulation to minimize the data scattering.

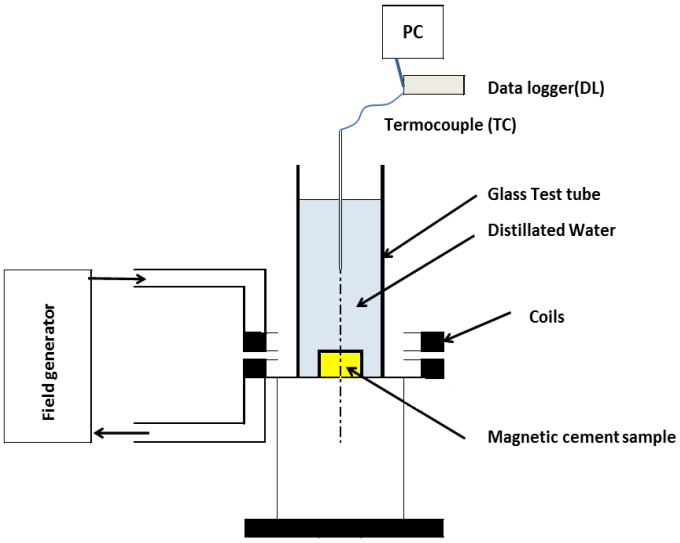

Figure 5.3: Calorimetric set-up for heating measures

The measured temperature as a function of the field application is used to calculate the specific power generated by magnetic hysteresis loss by applying the heat diffusion equation[8]:

$$MCp\,\frac{dT}{dt} - W + KS\,(T - T_{amb}) = 0 \qquad (5.1.2)$$

where

- The first term of the equation concerns the heating term of overall system.
- The second term is the power generated by the sample due to magnetic hysteresis
- The third term is the thermal dissipation toward the external environment.

The solution of this equation, assuming an isothermal behaviour of the system (the same temperature of the components subject to heating) and the temperature of beginning transitional (T_{in}) equal to the room temperature (T_r), is:

$$T = \frac{W}{KS} * \left(1 - e^{-\frac{KS}{MC}t}\right) + T_r \quad (5.1.3)$$

that solved as a function of W becomes:

$$W = \frac{(\Delta T * KS)}{(1 - e^{-\frac{KS}{MC}t})} \quad (5.1.4)$$

where:

W= thermal generated power [Watt], the specific power [W/ g] is obtained by dividing W by the weight of the sample under examination.

$\Delta T = T - T_r$: increase of water temperature in the period of field supply [°C]

t = exposure time to magnetic field supply [s]

M = mass of all physical component of the system [kg]

C_p = specific heat [J/(kg °C)]

$M*C_p$ = MC = thermal capability of the system, intended as the sum of the thermal capacity of the components subject to heat [J/°C] calculated as:

$$MC = m_{water} * c_{p\ water} + m_{sample} * c_{p\ sample} + m_{glass\ tube\ test} * c_{p\ glass\ tube\ test} \quad (5.1.5)$$

where

m_i is the mass of the i-component

c_{pi} is the specific heat of related material, for the composite cement was assumed the specific heat of PMMA.

KS = global transmittance calculated as:

K = transmittance surface towards the ambient [W/(m^2 °C)]

S = exchange surface of the heat towards the ambient [m^2]

The data ΔT and t are subjected to experimental survey, MC and S are calculated on the basis of the physical properties of the materials and the geometry of the system. K was estimated on the basis of data available in the literature [8] and considered not dependent on the surface temperature because of its reduced range variation.

S = the outer surface of the tube (limited to the free surface of the water) = 0,005 [m^2]

K = transmittance of a vertical tube in still air at a mean temperature of 40 ° C = 13 [W/m^2 ° C]

Having defined the constant terms, MC and KS, it is possible to construct a temperature versus time curve whose comparison with experimental measurements allows the evaluation of the better fitting function that represents the thermal phenomenon.

5.1.9.1. Experimental model with thermal insulator

In order to better quantify the temperature increase of a precise volume of water and specific power losses, a similar set up was optimized by the addition of a dark thermal insulator around the test tube in order to reduce the heat dispersion toward the environment and for a better quantification of all heat generated from three different sample formulations (P10, P15, P20) .

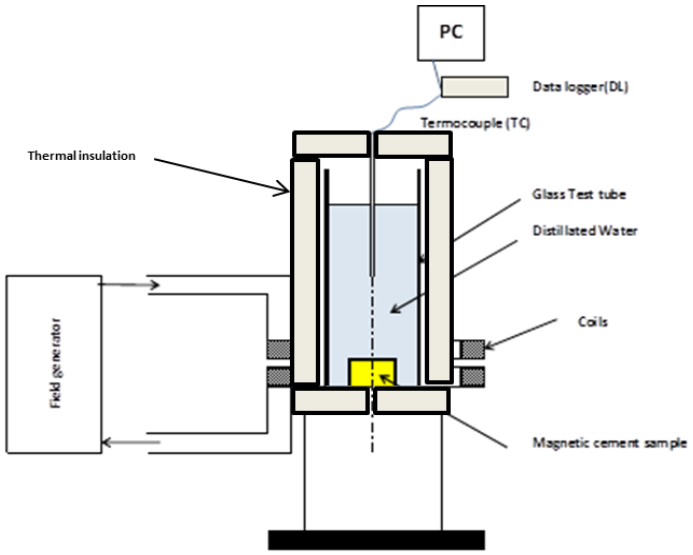

Figure 5.4: Calorimetric set up with a foam polyethylene as a thermal insulator

The system is composed of three samples, 26 ml of distillate water, the glass test tube with a diameter of 10 mm and an height of 160mm, a foam polyethylene thermal insulator (λ = 0,038 W/(m*K)) (see figure 5.4). The test was performed using two magnetic induction furnaces Egma 6 (Felmi S.r.l) generating a power up to 6 kW (39 mT) with a fixed working frequency of 220 kHz and Egma 30 (Felmi S.r.l) with a power generation up to 18 kW (132 kA/m) with a fixed frequency of 200 kHz . The measure of temperature was performed by a digital thermocouple (Datalogger Tersid S.p.A). The initial temperature (T_{in}) and final temperature (T_{fin}) was recorded at t = 0 min, t = 5 min, t = 10 min switching off the magnetic field for 1 minute between one time and another.

The proposed experimental model is based on the quantification of the energy storage in the different heated elements (sample, water, test tube) during the time of field application and on the theoretical evaluation of dispersions towards the environment.

The irradiation contribution was neglected because the thermal insulator temperature is close to the environment one.

Each component had the ability to store a specific amount of heat that has been quantified with the formula:

$$E_{st} = \sum(m_i * c_{pi}) * \Delta T \ (2) \ [8] \ (5.1.6)$$

E_{st} depends on the heat capacity (c_{pi}), the mass of the element (m_i) and the delta of temperatures between the initial and final heating period.

The dispersion term is quantified as the heat dispersion per conduction per unit heating time:

$$E_d = U * t * (T_{max} - T_{amb}) \ (3) \ [8] \ (5.1.7)$$

U transmittance coefficient between the test tube and the thermal insulator (J/(s*°C))

t heating time (s)

T_{max} medium heating temperature of the water (°C)

T_{amb} room temperature (°C)

The total amount of heat (energy stored + dispersion) is divided by the maximum heating time (10 min) and by the sample mass in order to obtain a specific power loss. The measurements were performed in duplicate.

5.1.10. Magnetic hysteresis measurements

Magnetic properties are investigated with a DC magnetometer/ AC susceptometer (Lakeshore 7225) equipped with a Cryogen-Free Magnet Frumagnet at room temperature in quasi static condition.

In particular hysteresis cycle measurements were performed both on the SC45 and on the P10, P15, P20 composite cements samples into two different magnetic field ranges: up to 800 kA/m (high field) to study the magnetic characteristics of the materials and up to 34 kA/m (low field) in order to work in a magnetic field range that can be used in clinical laboratories [5]. This test allowed the evaluation of the energy generation in one hysteresis cycle

5.1.11. Impedance measurements

These types of electromagnetic measurements had the aim of evaluation of the response of the material to an electro-magnetic stimulation.

The impedance is a physical vector which represents the opposition force to a passage of an alternate electric current in a bipol . It can be expressed as a ratio between the phasor of the voltage and the phasor of current. It is indicated with Z and it is measured in ohm [Ω].

The impedance is described by a complex number, real part represents dissipative phenomenon which correspond to an electric resistance R while the imaginary part indicates **reactance X**, associated to energy storage phenomena:

$$Z = \frac{V}{I} = R + jX \quad (5.1.8)$$

For a purely inductive or capacitive circuit, the impedance is thus reduced to pure inductive or capacitive reactance. The reactance of a capacitor and an inductor in series is the algebraic sum of their reactance. [10]

$$X = X_C + X_L \quad (5.1.9)$$

5.1.11.1. Dielectric permittivity measurement

For this measurement the polymer-based material and the composites were considered to be dielectrics between two metal copper armatures. They were excited by a radiofrequency signal, which avoids the magnetic field and only the effect of electric field contribution was evaluated.

Impedance meter resonator (HP 4192A LF Impedence Analyzer, Figure 5.5) permitted to pick up the modulus and the phase of the impedance to the current with respect to the voltage in the range of frequency 1 kHz to 10 MHz.

Figure 5.5: Impedance Analyzer

The samples used for this measurement had a disk cylindrical shape with 300 μm as a thickness and a diameter of 68 mm. Each sample was then placed into the position of maximum electric field in contact with two cylindrical copper plates in order to create a capacitor.

It was possible to measure the capacity of a dielectric with the effect of the frequency. This parameter characterizes the capacitor since it depends only on the geometry of the component and the characteristics of the dielectric interposed between the two armatures.

The measure of reactance Xc in presence of purely capacitive impedance was performed:

$$C = \frac{1}{\omega X_C} \text{ with } \omega = 2\,\pi\,f \quad (5.1.10)$$

Taking into account that the capacity of a plane capacitor with parallel faces is:

$$C = \varepsilon_0 \varepsilon_r \frac{A}{d} \quad (5.1.11)$$

It was possible to calculate the dielectric permittivity ε_r knowing all other parameter.

5.1.11.2. Magnetic permittivity measurements

This measurement involved the creation of a cylinder, with a d= 6 mm and height 8.5 mm, around which a copper coil with 100 windings was wrapped. In this case there is only the response of the magnetic field in the material which is expressed by the evaluation of the inductance L.

With the impedance meter the modulus and phase of the current with respect to the voltage were measured and the imaginary component of the impedance Z was calculated.

$$L = \frac{X_L}{\omega} \text{ with } \omega = 2\pi\,f \quad (5.1.13)$$

It gained magnetic permittivity μ, knowing all the other parameters.

$$L = \frac{\mu N^2 A}{l} \qquad (5.1.14)$$

Where :

N number of coils

A section of magnetic nucleus

l length of the nucleus around the coils

μ magnetic permittivity [10]

The goal of this test was the evaluation of the dielectric and magnetic permittivity in order to investigate if and how the magnetic glass ceramic influenced the polymer responses.

5.1.12. Mechanical tests

Mechanical characterization permitted to test the load-bearing ability of the composite material. For the polymeric bone cement both compression and four point bending tests were performed. In table 5.2 the values of compressive strength, the limits of bending strength and elastic modulus that the material must respect are reported.

Average compressive strength		Bending modulus		Bending strength	
MPa	Test method	MPa	Test method	MPa	Test method
⩾ 70	Annex E	⩾ 1 800	Annex F	⩾ 50	Annex F

Table 5.2: Inferior limit of applicability of bone cement in compression and bending [9]

The compression and the bending tests were performed with a growing static stress applied up to the sample failure. In the compression test the sample was subjected to deformation under uniaxial compression stress at a constant speed measuring the load (variable independent) necessary to provide a given compression (variable dependent).

Composites bone cements (P10, P15 and P20) and commercial composition were subjected to mechanical compression and bending test in accordance with ISO 5833 [11]. For both tests five specimens were prepared with dimensions required by the standards: cylindrical samples with, 6x12 mm, for the compression test and rectangular specimens, 75X10X3,3 mm, for the bending test. Before testing, the planarity of each sample surface was checked. Then, they were tested for the evaluation of the maximum compression strength. Compression strength was detected using a

Sintech 10/D (MTS) machine in figure 5.6, with a constant cross-head speed of 20 mm/min and a load cell of ±5 kN. The samples were prepared 24 hours before the test and they were stored at room temperature.

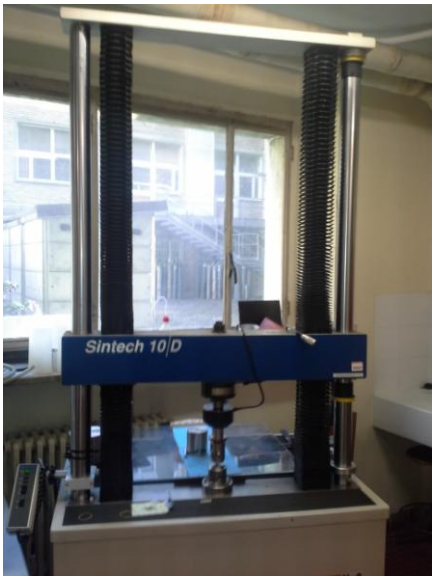

Figure 5.6 : Compression machine

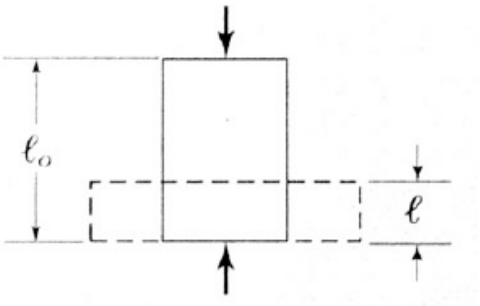

Figure 5.7: ideal compression test, following the application of a force the hight of the sample change from lo from l with a deformation of the specimen.

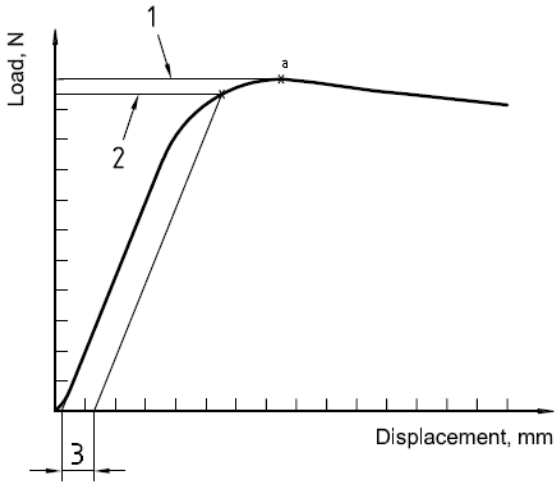

Figure 5.8 Theoretical load-displacement diagram for a cement

For each cylinder the offset load (point 2 in figure 5.8) was recorded and the value of the compressive strength was expressed in Megapascals (MPa) by dividing this force by the original cross-section area, in square millimetres, of the cylindrical sample. The average compressive strength of the five cylinders was calculated.

Bending strength and modulus were evaluated using a test machine H25KS with a load cell of ± 5kN produced by Tinius Olsen Ltd. In four points bending test the moving crosshead pushed two wedges arranged symmetrically to the centre line of the specimen. During the test the displacement of the crosshead and the applied load were measured [12].

Figure 5.9 reports a diagram of the flexural momentum during the test, demonstrating that the bending moment remains constant between the two supports.

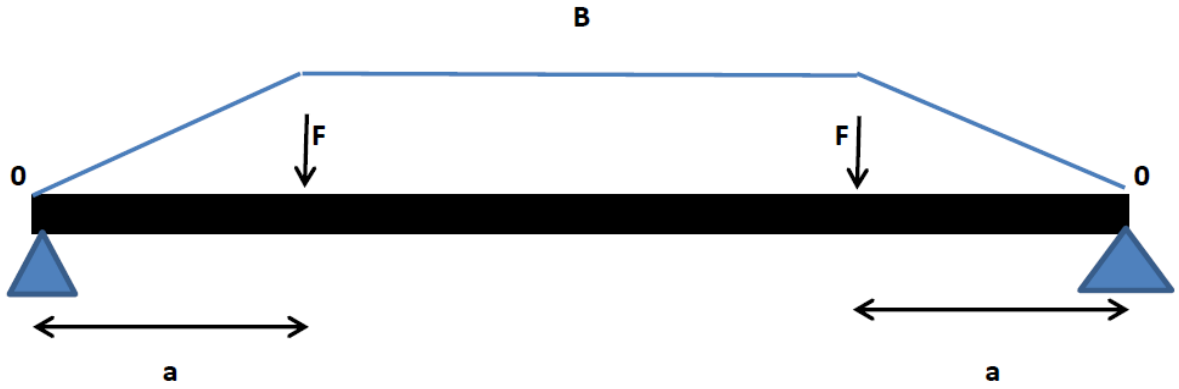

Figure 5.9: Distribution of bending moment in a 4 point flexural test

The bending strength and bending modulus were evaluated respectively according the formula:

$$B = \frac{3Fa}{bh^2} \quad (5.1.21)$$

Where

F= force at break in Newton

a = distance between the inner and outer loading points (20 mm)

b = average measured width of specimen, in millimeters

h = average measured thickness of specimen, in millimeters;

$$E = \frac{\Delta Fa}{4fbh^3} \cdot (3l^2 - 4a^2) \quad (5.1.15)$$

Where

F = force at break, in newton;

a = distance between the inner and outer loading points (20 mm)

f = difference between the deflections under the loads of 15 N and 50 N , in millimeters;

b = average measured width of specimen, in millimeters

h = average measured thickness of specimen, in millimeters;

l = distance between the outer loading points (60 mm);[11]

The fracture surfaces of samples after bending test were analyzed by SEM; three samples for each cement composition were observed: sample broken at σ maximum, σ medium and σ minimum.

5.1.13. Setting time tests

The setting time was investigated in accordance with ISO 5833-2002. All three composite cement formulations were evaluated.

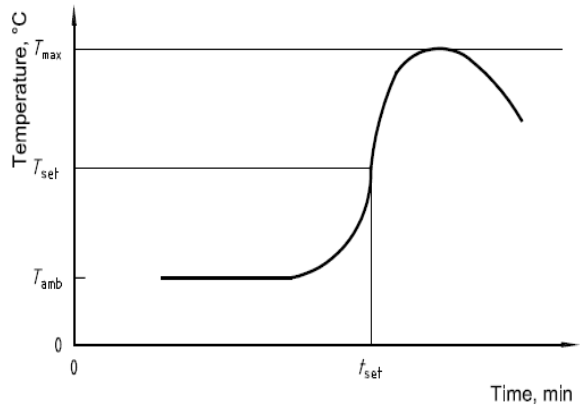

Figure 5.10: Typical setting time curve of polymeric bone cement[11]

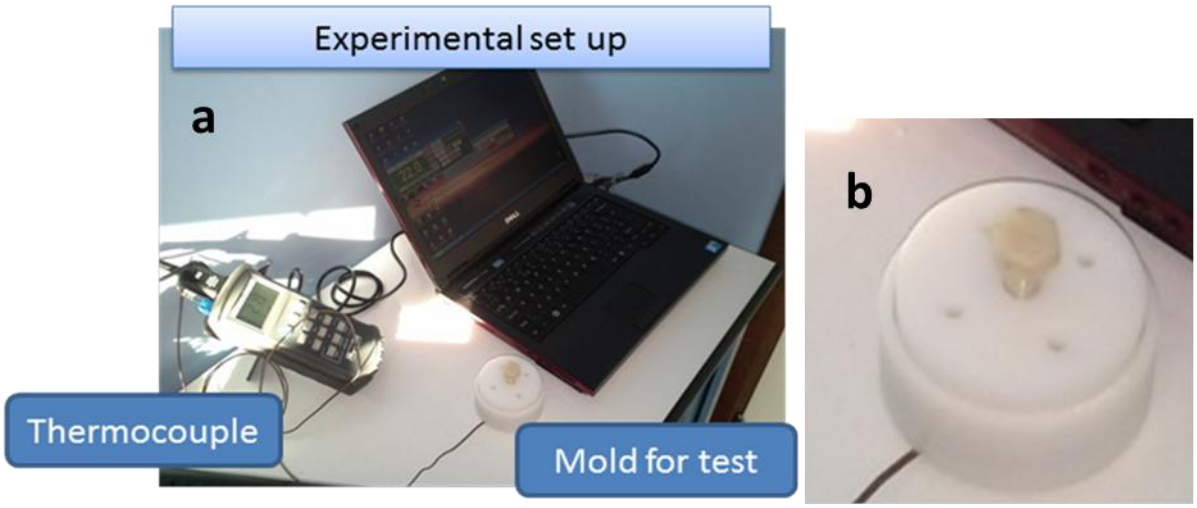

Figure 5.11: Experimental set up for setting time test in according with ISO 5822- 2008.

The powder and the liquid monomer were mixed together in a bowl. After the liquid wetted all the powder the paste was put in a teflon mould, in conformity to the standard specification (see figure 5.11b), it was covered and a temperature probe was insert and put in contact with the cement during the polymerization reaction in order to collect time/temperate data. The used temperate probe was a digital thermocouple datalogger by Tersid.

5.1.14. Micro Computed Tomography (MicroCT)

Micro computed tomography (micro-CT) is a non-destructive technique that can produce 3D sets of images. Micro-CT analyses were performed with a SkyScan1174®, using a 50 kV–800 mA x-ray source and a camera pixel size of 13,42 mm. The exposure time was 5,2 s per projection. The images were recorded on a 1024x1304 CCD detector, with the pixel size set to 6,5 mm. A 330 mm Al filter was used. The 3D structure was reconstructed by means of the Nrecon® software and for the 3D visualization of the reconstructed sample, the CTVox® software was used. For each sample a volume of interest was built; and a single voxel of reconstructed image had a size of 6,5x6,5x6,5 µm. The micro-CT analysis was carried out to evaluate the porosity of the composite cements and the dispersion of the glass ceramic in the polymeric matrix.

5.1.15. Composite bone cement: in vitro tests

5.1.15.1. Bioactivity tests

In order to evaluate the composite bioactivity, *in vitro* test by soaking samples in Simulated Body Fluid (SBF, Kokubo Protocol [17]) was performed. The bioactivity of glasses is based on their ability to induce the *in vitro* formation of a semi crystalline hydroxyapatite (HAp) rich layer through a sequence of ion exchange steps. This behavior is considered as an indication of their *in vivo* bioactivity (i.e. their bonding ability to living tissues).

The SC45 is a glass-ceramic that presents bioactive activity [3] but with a slow kinetic. Nevertheless, after one month of soaking in a simulated body fluid (SBF)(see the chemical composition in figure 5.12) a thin silica gel layer can observed on its surface together with some precipitates of a phase rich in calcium and phosphorous [4]. This glass-ceramic was already tested in a previous work for its biocompatibility showing a high degree of cytocompatibility [4].

Ion	Simulated Body Fluid (mM)	Human Blood Plasma (mM)
HCO_3^-	4.2	27
K^+	5	5
Cl^-	148.8	103
Na^+	142	142
Ca^{+2}	2.5	2.5
Mg^{+2}	1.5	1.5
HPO_4^{-2}	1	1
SO_4^{-2}	0.5	0.5
tris(hydroxymethyl) aminomethane	50	50
hydrochloric acid	45	45
Properties		
pH	7.25	7.25

Figure 5.12: SBF composition in comparison of human plasma[17]

Each composite cement (P10, P15, P20) was soaked in 25 ml of SBF and maintained at 37°C for four weeks. Every three days the solution was refreshed and the value of the pH was measured.

At the end of the treatment, samples were gently washed in distilled water, dried at room temperature and characterized by morphological and compositional analyses by Scanning Electron Microscopy (SEM– FEI, QUANTA INSPECT 200) and Energy Dispersion Spectrometry (EDS - EDAX PV 9900).

5.1.15.2. Leaching test

Composites bone cements were subjected to leaching test in order to assess if any iron release could occur, causing a potential risk of iron overloading in the fluids in future *in vivo* applications. The leaching of other ions, involved in the bioactivity mechanism, was not the object of the present work. The cement formulation containing the highest SC 45 amount (P20) was selected for the test in order to evaluate the maximum value of potential leaching. The samples were dipped in 30 ml of SBF, at 37°C, up to one month.

At determined time steps (3h, 1, 3, 7, 14 and 33 days) an aliquot of the solution was picked out and analyzed, after mineralization with nitric acid (for trace analyses, 69% w/w) and dilution with

milliQ water, by Graphite Furnace Atomic Absorption Spectrometer (GF-AAS 4100 ZL, Perkin Elmer, autosampler AS/71, Zeeman Effect background correction). The calibration curve was performed diluting a mother solution of iron in nitric acid (1g/L) in milliQ water (final concentrations: 5, 10, 25, 50 μg/l). Accuracy was determined analysing the NIST standard SRM 1643e - Trace Elements in Water.

The test was performed in triplicate and commercial cements containing 20%wt of Bioglass® (without Fe in any form) was selected as control samples.

5.1.15.3. Cytocompatibility tests

Tests were performed at University of Piemonte Orientale "A.Avogadro" with the collaboration of Prof.ssa Lia Rimondini and Dr. Andrea Cochis.

5.1.15.4. Cells cultivation

Human osteosarcoma cells (ATCC CRL-1427, Mg63) were cultivated in Dulbecco's Modification Minimal Essential Medium (DMEM, Sigma) supplemented with 10% fetal bovine serum (FBS, Sigma) and 1% antibiotics (penicillin – streptomycin) at 37°C, 5% CO_2. Cells were cultivated until 80-90% confluent, detached with a trypsin-EDTA solution and used for experiments. Mg63 cells were used as representative for osteoblasts cells since the composite cements are intended for osteointegration. This cell line is commonly used to investigate the cytocompatibility of biomaterials for bone substitutions for preliminary *in vitro* studies.

5.1.15.5. Indirect Cytocompatibility test

For the indirect test, serum free DMEM was incubated without cells for 1 week at 37°C, 5% CO_2 in direct contact with controls, Palamed®, test samples (P10, P15 and P20). Afterwards, eluates were collected, supplemented with 10% FBS and used to cultivate Mg63. Cells were seeded in a defined number ($1x10^4$ / well) into 24 wells plates (Cell Star, PBI International) and cultivated for 24, 48 and 72 hours at 37°C, 5% CO_2. Afterwards, cells viability was evaluated by the (3-(4,5-Dimethylthiazol-2-yl)-2,5-diphenyltetrazolium bromide colorimetric assay (MTT, Sigma). Briefly, 50 μl of MTT solution (3mg/ml in phosphate buffered saline (PBS), ph 7.4) were added to each sample and incubated 4 hours in the dark; afterwards, formazan crystals were solved with 100μl of

dimethyl sulphoxyde (DMSO, Sigma) and 50 μl were collected and centrifuged to remove eventually debris. Surnatant optical density (o.d.) was evaluated at 570nm with a spectrophotometer (Spectra Count, Packard Bell). Polystyrene samples o.d. were used as control and considered as 100% cells viability while coated samples viability was calculated as follow: (sample o.d. / control o.d.) *100 . Experiments were performed in triplicate for controls and test samples. Furthermore, cells morphology was visually investigated after 24, 48 and 72 hours of cultivation by light microscope (Leica AF 6500, Leica Microsystems).

5.1.15.6. Direct Contact Cytocompatibility evaluation

For the direct contact assay, cells were seeded in a defined number ($1x10^4$ / sample) directly onto the surfaces of each samples and cultivated in DMEM 10% FBS at 37°C, 5% CO_2. Cells viability was evaluated after 24, 48 and 72 hours with the MTT assay as described in the indirect assay section. Experiments were performed in triplicate.

5.1.15.7. Morphological Evaluation

The morphology of cells attached to the samples surfaces was investigated also by FESEM microscopy (FESEM - SUPRATM 40, Zeiss) equipped with Energy Dispersive Spectroscopy (EDS). Briefly, samples were removed from the media, gently washed with PBS, fixed with 2.5% glutharaldehyde for 2 h in 1 mol L21 sodium cacodylate buffer, washed with the latter, dehydrated with 70%, 80%, 90%, and 100% ethanol (10 min each), and finally treated with CO_2 at top critical point. Specimens were fixed on aluminum stubs using a conductive silver paste, covered with a chromium layer, and visualized at various magnifications.

5.1.16. Statistical analysis of data

Statistical analyses were performed using Statistical Package for Social Sciences (SPSS v20.0, IBM Co. Armonk, New York, US). The assumptions of homogeneity of variances and normal distribution of errors were checked for all the variables considered: afterwards, ANOVA one-way and post-hoc Sheffe's test were used. The significance level was set at 5%.

5.1.17. Hyperthermia on tumor cells test

On the basis of data incoming from previous test, a simplified simulation of an hyperthermia application on a culture of tumor cell was performed.

5.1.17.1. Culture Cells Preparation

The test was performed as a comparison between P10 and control PMMA . Two different types of cells have been used:

1. HFOB: fetal human osteoblast cells, non tumoral, non-tumorigenic.
2. Mg63: human osteoblast from osteosarcoma, tumoral and tumorigenic

Cells were cultivated in Dulbecco's Modified Eagle Medium (Mg63, DMEM, Sigma) or Ham's F12 mixture 0,05 mg/ml G418 salt (HFOB, Sigma) supplemented with 10% fetal bovine serum (FBS, heat-inactivated, Sigma) and 1% antibiotics (penicillin- streptomycin, Sigma). Cells were cultivated until 80-90 % confluence , detached with trypsin-EDTA solution (0,05% in PBS, Sigma) and used for experiments.

5.1.17.2. Cytocompatibility evaluation

Round 0,5 cm diameter 8mm thickness P10 and Palamed specimens were sterilized by 70% ethanol immersion overnight prior to use with cells. Afterwards, specimens were placed into the wells of a 24 multi-well plate (CellStar, PBI International , Milan , Italy) and cells (Mg63 and HFOB) were seeded in a defined number ($2x10^5$ cells/ sample, 1 ml/sample) directly onto specimens surfaces; plate was incubated 48 hours at 37°C , 5% CO_2 in a humid atmosphere. Then, cells viability was evaluated by the colorimetric metabolic assay (3-(4,5-dimethylthiazol-2-yl)-2,5diphenyltetrazolium bromide, (MTT, Sigma). Briefly, 100 µl of MTT solution (3 MG/ML IN pbs) were spotted into each well; plates were incubated for 4 hours in the dark in a 37°C incubator. Afterwards, medium was removed and formazan crystals formed on the specimens surface were solved with 100 µl of DMSO. Finally, 50 µl were collected from each well, centrifuged in order to remove eventually debris (12000 rpm, 1 minute) and the optical density was evaluated by a spectrometer (Spectra Count , Packard Bell, Chicago, USA) at a 570 nm wavelength.
Experiments were performed in triplicate and results were expressed as means and standard deviations.

5.1.17.3. Hyperthermic treatment

Specimens prepared as a previously described in the cytocompatibility assay ($2x10^5$ cells/ sample, 48 hours cultivation) were treated with a magnetic inductor (Egma 6 produced by FELMI S.r.l.) . The machine was set with a magnetic field of 22,5 mT with a fixed working frequency of 220 kHz. Specimens (Palamed and P10) were treated for 5-10-15-20-30 minutes under alternate magnetic field. For each time, three samples with tumoral (Mg63) cells and three with non tumoral (Hfob)cells were tested with the magnetic field generator. Then, cells viability was evaluated by MTT test as previously described. Non- treated samples were considered as control and their optical density (o.d.) considered as 100% ; tested samples o.d. was expressed as cells viability percentage as a function of controls. Experiments were performed in triplicate and results presented as means and standard deviations.

5.1.17.4. Cells morphology evaluation

After each assay (cytocompatibility and hyperthermic evaluations), cells morphology was visually checked by scanning electron microscopy (FESEM). Briefly , samples seeded with cells were fixed 20 minutes at room temperature with 2.5 % glutharaldehyde (Sigma , in PBS); then samples were gently washed with PBS and dehydratated with alcohol scale (70-90-100%, 10 minutes each). Finally samples were treated with hexamethyldisilazane (Sigma, 2 minutes), covered with a thin layer of chromium for 1 minute, put on a dedicated SEM stubs and observed with the instrument at various magnifications.

5.1.17.5. Hyperthermic treatment apoptosis induction

After hyperthermic treatment application, cells apoptotic induction was evaluated by Annexin-5 staining (Fitch-conjugated Annexin-5 , ImmunoTools, Germany). Cells on specimens treated surface were fixed with formaldehyde (3,7% in PBS) 20 minutes at room temperature. Then samples were gently washed with PBS and Annexin-F was added (1:200 in a 5% goat serum 1% bovine albumin in a PBS solution) at room temperature. Afterwards, cells were carefully washed three times (5 minutes each) with PBS and permeabilized 5 minutes with Triton (0,25% in PBS). The DAPI (1:250 in PBS, Sigma) was used to counter staining cells nuclei. Samples were observed

under a fluorescent microscope (Leica) and the Annexin-5 positive cells counted. Results were expressed as % of Annexin-5 positive cells towards the cells total number.
Experiment were performed in triplicate and expressed as mean and standard deviations.

5.1.17.6. Heating up to a target temperature

The effectiveness of hyperthermia treatment is closely related to the temperature that can be reached in the tumor tissue closed to bone cement insert (i.e = thermal power generator) and to maintain it for the whole required time of treatment (40-43 °C).
In order to characterize the treatment efficacy, the Cumulative Equivalent Minutes at 43°C (CEM_{43}) was calculated, using the equation derived by Stephen and Dewey [20] as a clinical means to estimate the actual thermal dose:

$$CEM_{43} = \sum R^{(43-T)}\Delta t$$

where:
R=0.5 for T>43°C
R=0.25 for 39°C<T<43°C
R=0 for T<39°C
In the foreseen applications in human body it will be difficult to control the local temperature in the treated volume because infrared-camera measures are applicable only on visible surfaces and metallic thermocouples are affected by the variable magnetic field.
For these reasons, it was necessary to perform a thermal study aimed to define the parameters of treatment. The Element Finite method allowed a good simulation of power generation. The heat was transferred by conduction and convection and it was applied to the section test used to simulate a hyperthermia treatment on tumoral cells
Using a geometry produced with Comsol Multiphysics ® (Comsol Inc.) it was outlined the experimental model which consists of a cement bone cylindrical sample (diameter 10 mm , height 5 mm) placed at the centre of a large sample holder (inner diameter 30 mm , height 10 mm, thickness 3 mm) filled by water up to 1 mm above the sample surface .
In this geometry a sufficiently fine mesh was created automatically by the software, taking into account different materials and heat transfer condition (figure 5.13).